NIST Technical Note
NIST TN 2253

NIST Outdoor Structure Separation Experiments (NOSSE) with Wind

Alexander Maranghides
Shonali Nazare
Kathryn M. Butler
Erik L. Johnsson
Eric Link
Matthew Bundy
Artur Chernovsky
William D. Walton
Steven Hawks
Frank Bigelow
William (Ruddy) Mell
Anthony Bova
Derek McNamara
Thomas Milac
Robert Raymer
Frank Frievalt

NIST | NATIONAL INSTITUTE OF STANDARDS AND TECHNOLOGY
U.S. DEPARTMENT OF COMMERCE

NIST Technical Note
NIST TN 2253

NIST Outdoor Structure Separation Experiments (NOSSE) with Wind

Alex Maranghides
Shonali Nazare
Kathryn M. Butler
Erik L. Johnsson
Eric Link
Matthew Bundy
Artur Chernovsky
Fire Research Division
Engineering Laboratory
National Institute of Standards and Technology

William D. Walton
University of Maryland

Steven Hawks
Frank Bigelow
Office of the State Fire Marshal
California Department of Forestry and Fire Protection

William (Ruddy) Mell
Anthony Bova
Derek McNamara
Thomas Milac
United States Forest Service

Robert Raymer
California Building Industry Association

Frank Frievalt
Mammoth Lakes Fire Protection District

U.S. Department of Commerce
Gina M. Raimondo, Secretary

National Institute of Standards and Technology
Laurie E. Locascio, NIST Director and Under Secretary of Commerce for Standards and Technology

NIST TN 2253
May 2023

The policy of the National Institute of Standards and Technology is to use metric units in all its published materials. Because this report is intended for the U.S. building construction industry, which uses US customary units, it is more practical and less confusing to use inch-pound units, in some cases, rather than metric units. However, in most cases, units are presented in both metric and the inch-pound system.

NIST Technical Series Policies

Publication History

How to Cite this NIST Technical Series Publication

NIST Author ORCID iDs
Alexander Maranghides: 0000-0002-3545-2475
Shonali Nazare: 0000-0002-0407-5849
Kathryn M. Butler: 0000-0001-7163-4623
Erik L. Johnsson: 0000-0003-1170-7370
Eric Link: 0000-0002-7784-5023
Matthew Bundy: 0000-0002-1138-0307

Contact Information
alexander.maranghides@nist.gov
shonali.nazare@nist.gov

Abstract

The NIST (National Institute of Standards and Technology) Outdoor Structure Separation Experiments (NOSSE) are part of the NIST Structure Separation Experiments (SSE) project, which is designed to assess structure-to-structure fire spread in the wildland-urban interface (WUI). In the first phase of this project, fire exposures from small source structures (sheds) were quantified in terms of mass loss rate (MLR) and peak heat release rate (PHRR) in the absence of wind. The performance of a target structure representing a residential façade was assessed in response to exposures from a variety of sheds (differing in construction, size, and fuel loading) and separation distances. These experiments were conducted indoors at the National Fire Research Laboratory at NIST. The knowledge gained from the indoor shed burn experiments was used to develop the outdoor shed burn experiments.

This report describes a series of outdoor shed burn experiments conducted at NIST to study the effects of applied wind on thermal (radiant and convective) exposures from sheds of various size and composition to a target structure. The results were used to determine the minimum Structure Separation Distance (SSD_{min}), which is defined as the shortest distance between the source (storage shed) and target structure (residence) to prevent ignition and flame spread. SSD_{min} is a function of both the source term and the design and fire hardening of the target structure. As defined here, $SSD_{min,}$ is aimed at reducing radiative and convective exposures to the target structure. This measure cannot be used to address ember exposures.

Experiments were conducted with three different sizes of combustible (wood) and noncombustible (steel) sheds, each containing a set of wood cribs and ignited to generate typical radiative and convective heat exposures to the target structure. The target structure was an assembly including an exterior wall with a window and a roof with a vented eave, representative of an exterior wall of a single-story residential building. Effects of shed orientation, shed size, structure separation distance, and shed type on thermal exposure to the target structure were studied. The thermal exposure was quantified in each case by measuring the peak heat flux and temperature at the target structure. Based on target structure performances due to thermal exposure from the burning of different source structures, a minimum structure separation distance was identified for each given size of combustible and noncombustible sheds.

The experiments in this study demonstrated good reproducibility of experimental data. The wind had complex effects on the burning behavior of combustible source structures, affecting flame lengths and convective heat transfer to the target structure. For combustible sheds, the peak heat flux measured at the target structure corresponded with the total amount of combustible fuel and was not affected by orientation (i.e., door opening facing downwind or upwind). In the case of noncombustible sheds with the door opening facing the target structure, the applied wind had minimal or no effect on thermal exposure to the target structure. The noncombustible steel sheds contained the fire effectively – thus reducing, but not eliminating, the thermal exposure to the target structure. For the scenarios evaluated, peak heat flux at the target structure could be reduced by half by changing the orientation of the door opening for noncombustible sheds.

Twelve out of the thirteen experiments were conducted with a fire hardened target structure. One experiment was conducted with a non-fire hardened target structure to demonstrate the effectiveness of fire hardening. The non-fire hardened structure ignited within 6 mins when exposed to a Very Small wood shed with total combustible fuel of 212 kg ± 9 kg (467 lbs ± 20

lbs) and SSD of 10 ft. With similar combustible fuel, SSD, and thermal exposure, the fire hardened target structure exhibited minimal thermal damage and significant ignition resistance.

This experimental series resulted in quantification of the SSD_{min} between a shed and a residence under the tested conditions. The SSD_{min} was identified as 10 ft for both combustible and noncombustible sheds with floor area less than 26 ft^2 in scenarios with a fire hardened target structure. For sheds with floor area between 26 ft^2 and 64 ft^2, the minimum SSD_{min} was found to be 15 ft. Because the local winds during a WUI fire are unpredictable, SSD should be omnidirectional, i.e., the same SSD in all directions.

Limitations of the experimental series include the small number of experiments, thirteen shed burn experiments. Acknowledging these limitations, implementation of the minimum separation distance identified from the experimental measurements in this study is expected to improve community resilience to WUI and structure-to-structure fire exposures.

Keywords

Table of Contents

List of Tables

List of Figures

Acknowledgments

List of Abbreviations and Acronyms

CAL FIRE	California Department of Forestry and Fire Protection
DAQ	Data Acquisition
ECS	Emissions Control System
FDS	Fire Dynamics Simulator
HDPE	High Density Polyethylene
HF	Heat Flux
HFG	Heat Flux Gauge
HMM	Hazard Mitigation Methodology
HOC	Heat of Combustion
HRR	Heat Release Rate
MIDAS	Modular In-situ Data Acquisition System
ML	Mass Loss
MLR	Mass Loss Rate
NFPA	National Fire Protection Association
NI	National Instruments
NIST	National Institute of Standards and Technology
NFRL	National Fire Research Laboratory
OSB	Oriented Strand Board
PHRR	Peak Heat Release Rate
SFM	State Fire Marshal
SI	International System of Units
SSD	Structure Separation Distance
SSE	Structure Separation Experiments
TC	Thermocouple
THR	Total Heat Released
TTPHRR	Time To Peak Heat Release Rate
USFS	United States Forest Service
WUI	Wildland-Urban Interface

Executive Summary

Structure-to-Structure Fire Spread: A WUI Problem

Structure-to-structure fire spread is of primary concern in wildland-urban interface (WUI) fires. Once ignited, a burning structure (residential or auxiliary) readily becomes a potential source of additional fire spread, often igniting nearby fuels and neighboring residential structures. This can lead to a cascade of ignitions, especially under high-wind conditions in high density housing communities. Such structure-to-structure fire spread can outpace fire control efforts, making it difficult to contain fires. Vulnerabilities related to the construction and placement of auxiliary structures and their role in structure-to-structure fire spread in the WUI have been highlighted in NIST's case studies. Small auxiliary storage sheds can be ignited from flaming fire exposures and/or by embers. Fire can reach both the shed and its contents relatively easily, since many storage sheds do not have flooring. This allows surface fire to easily get under the shed and cause ignition of the contents. Combustible shed materials, shed contents, and accumulated windblown debris adjacent to sheds are readily ignited by surface fire and embers.

Auxiliary storage sheds with footprints larger than 120 ft² are regulated under Chapter 7A of the California Building Code, as well as under the International Wildland-Urban Interface (IWUI) code. These codes require detached auxiliary structures that are located between 3 ft and 50 ft from the primary structure to be constructed of noncombustible materials or ignition-resistant materials. However, no guidance for the placement of sheds or auxiliary structures with floor area less than 120 ft^2 is currently available. Frequently used by homeowners for additional storage space, these smaller sheds can be placed against or next to residential structures. In cases of two-story buildings, these sheds may be located under second-floor windows.

This report describes a series of outdoor shed burn experiments conducted at the National Institute of Standards and Technology (NIST) to study the effects of applied wind on thermal (radiant and convective) exposures from sheds of various sizes and differing construction to a target structure. This information was used to determine the minimum Structure Separation distance (SSD$_{min}$), which is defined as the shortest distance between the source (storage shed) and target structure (residence) to prevent ignition and flame spread.

Structure Separation Distance: An Approach for Hazard Mitigation

In high density WUI communities, residential structures with nominal SSD between them of 6 ft are particularly vulnerable to exposures from parcel-level fuels, including combustible fences, decks, sheds, and vehicles. Recently, the NIST WUI Fire Hazard Mitigation Methodology (HMM)[1] addressed hazard reduction at the parcel and community levels. The HMM uses the spatial relationships among fuels, exposures, and hardening to reduce fire hazards in high density WUI communities. The rapid decrease in radiation and convection with distance is leveraged here to optimize the required level of structure hardening and establish the minimum structure separation distance. SSD$_{min}$ is a function of both the source term, such as a burning shed, and the design and fire hardening of the target structure. As defined here, SSD$_{min}$ is aimed at reducing radiative and convective exposures to the target structure. This measure cannot be used to

---

[1] A. Maranghides, E.D. Link, S. Hawks, J. McDougald, S. Quarles, D. Gorham, S. Nazaré (2022) "WUI Structure/Parcel/Community Fire Hazard Mitigation Methodology," NIST Technical Note 2205, National Institute of Standards and Technology, Gaithersburg, MD, https://doi.org/10.6028/NIST.TN.2205.

address ember exposures; structure hardening for embers is independent of SSD and is further described in the HMM.

Experimental Design

Experiments were conducted with three different sizes of combustible (wood) and noncombustible (steel) sheds, each containing a set of wood cribs and ignited to generate typical radiative and convective heat exposures to the target structure. An artificially generated wind field was applied to achieve a more realistic snapshot of what may happen during a wind-driven fire in the WUI community and to study the effects of applied wind on thermal (radiant and convective) exposures from sheds of various sizes to a target structure.

Cold Flow Experiments

The wind field applied on the source structure (shed) was provided by a dual fan wind machine operating at a variety of rotational speeds, and a flow straightener was used to remove large-scale swirl and align the applied wind parallel to the centerline axis of the experiment. The flow characterization experiments were performed without the source structure in place and in the absence of fire (thus "cold flow" measurements). The cold flow measurements were performed under imposed wind conditions perpendicular to the target structure, with maximum wind speed provided by the dual fan wind machine ranging from 13 mph to 26 mph. For all outdoor experiments, including both cold flow and shed burn experiments, the wind velocity field was measured by an array of bidirectional probes placed downwind of the wind machine. The baseline flow patterns were characterized by collecting measurements at various locations at the test site and at a range of wind speeds. The cold flow experiments generated an extensive database of wind fields as a function of distance from the dual fan wind machine and applied wind speed, providing useful insights into the wind flow patterns.

Outdoor Shed Burn Experiments

Effects of shed orientation, shed size, SSD, and shed type on thermal exposure to the target structure were studied in the presence of an applied wind field. The experimental set-up for the outdoor shed burn experiments is shown in Fig. ES-1, including the wind machine, flow straightener, bidirectional probe array, source structure (shed), and target structure.

The test matrix was developed based on the outcomes of the indoor shed burn experiments. However, the actual test sequence was dictated primarily by the availability of sheds and wood cribs on the test day. Tests were performed on dry days (no precipitation in the forecast from 5 am to noon) when wind direction and wind speed were conducive to fire tests.
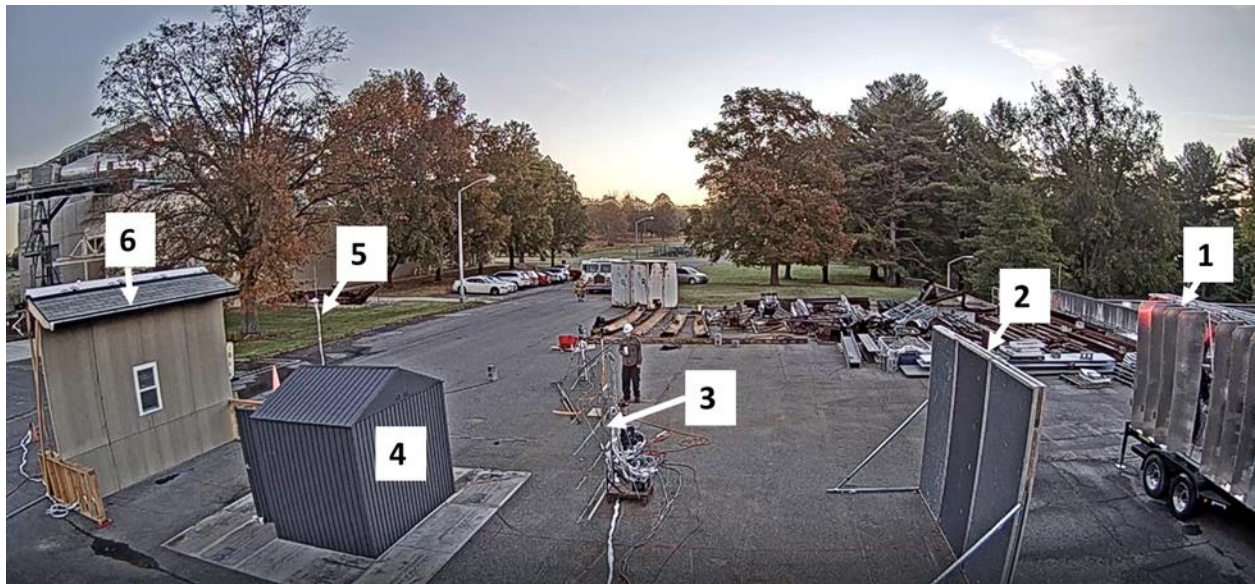
Fig. ES-1. Photograph showing experimental set-up including 1: Wind Machine, 2: Flow Straightener, 3: Array of Bidirectional Probes, 4: Shed, 5: Off-Target Heat Flux Rig, and 6: Target Structure.

The outdoor shed burn experimental series tested combustible wood sheds and noncombustible steel sheds of various sizes. Plastic sheds were excluded from this outdoor experimental test matrix due to environmental concerns associated with their combustion byproducts. Standard 1-A wood cribs were used as a substitute for combustible fuel typically stored in residential sheds. Wood cribs are commonly used in large fire experiments to limit experimental variables and provide good reproducibility.

The target structure façade was an assembly including an exterior wall with a window and a section of a roof with a vented eave, representative of an exterior wall of a single-story residential building. The target wall was constructed well above the minimum requirements specified by the WUI California Building Code. The main objective of these experiments was to assess the performance of eaves and not that of the wall. In order to achieve the main experimental objective and to prevent any potential ignition of the wall, an additional insulating layer of noncombustible gypsum panel lined with fiberglass mats was used in the construction of the target wall for these experiments.

The shed and the wood cribs were placed at pre-determined locations determined by SSD and door orientation. The wind machine was started and maintained at 'idle' speed of 760 rpm giving a nominal wind speed of 13 mph. The wood crib assembly inside the shed was ignited using 300 mL of heptane in an aluminum pan. After ignition, and as the burning of the combustible fuel developed, the speed of the wind was increased gradually until the flames leaned on to the eaves of the target structure. It is important to note here that the objective of the experiments was not to study the effects of wind speeds on plume lean. A pre-determined wind speed was not implemented; the wind was adjusted so that the flames leaned to the closest possible contact with the target structure to present worst-case scenarios. Once this condition was achieved, the speed of the wind machine was kept constant until the end of the experiment. The experiment continued until the shed and the wood cribs had collapsed and flames were no longer visible.

The thermal exposure to the target structure was quantified in each case by measuring the peak heat flux and temperature at the target structure. Twelve out of the thirteen experiments were

conducted with a fire hardened target structure. One experiment was conducted with a non-fire hardened target structure to demonstrate the effectiveness of fire hardening. Based on target structure performances due to thermal exposure from the burning of different source structures, a minimum structure separation distance was identified for each given size of combustible and noncombustible sheds.

Key Findings

The results of this limited experimental series of the NIST Outdoor Structure Separation Experiments (NOSSE) highlight the significant fire hazard presented by burning storage sheds to nearby residential structures under applied wind conditions. The experiments provide information on relative fire hazard associated with sheds of different construction materials, sizes, and fuel loadings. For a given set of target construction hardening practices, the minimum structure separation distance (SSD) is defined as the shortest distance between the source and target structures to prevent ignition and flame spread. This work demonstrated that the thermal exposure from a burning storage shed to a target structure (e.g., a house) is influenced by the construction of the latter, the separation distance between the shed and the target, the presence of wind, and the construction and orientation of the shed. As wind speed is increased, a considerable portion of the heat flux from the flame is received by the downstream target surface (house). Wind causes the flame to "tilt" towards and in some cases contact the target surface, increasing both convective and radiative heat transfer.

In this experimental series, structure separation tests involved moving the shed (source fire) from 10 ft to 15 ft. For one set of tests, this simple move led to a reduction in the heat flux measured at the target by a factor of more than three. Although there is not enough data to create a mathematical model of this trend, the data clearly shows that even small changes in the relative positions of structures can have significant effects in terms of limiting fire spread.

Because of the dramatic reduction in thermal exposure from the shed to the target structure by moving the burning shed a few feet away from the later, this work points to the idea of placing auxiliary structures no closer than the minimum SSD (SSD_{min}) to reduce fire spread in WUI communities. In scenarios where the target structure is hardened to comply with SFM standard 12-7A-1, SFM standard 12-7A-2, and ASTM E2886 (as specified in CA Chapter 7A), the SSD_{min} was determined to be 10 ft for noncombustible steel sheds with a footprint of less than 64 ft^2 and oriented so that the doors open away from the closest structures. For smaller (less than 16 ft^2) combustible (i.e., wood) sheds SSD_{min} was also determined to be no closer than 10 ft when adjacent to hardened structures. SSD_{min} for larger (footprint between 20 ft^2 and 64 ft^2) wood sheds was determined to be at least 15 ft away from any hardened residential structure or other auxiliary structure. The SSD_{min} for respective shed sizes were determined for "high" fuel loading representing "worst" case scenarios. These distances will need to be increased for non-hardened construction, as demonstrated by the experiments conducted.

While important, the influence of fuel moisture and topography (both natural and artificial) on thermal exposure of the target were beyond the scope of this experimental series and were not considered. Despite the exclusion of these parameters, the data generated in this work expands the understanding of fire spread associated with small structures. This includes the general fire hazard of a storage shed relative to structure hardening, how ignition vulnerability of the target is affected by the SSD, and the thermal exposure and expected ignition behaviors of target structures in a specific configuration.

Under the conditions of this work, a non-hardened target wall ignited and was completely engulfed in flames within six minutes of exposure from the burning shed, while no thermal damage was observed to the hardened target structure. To the extent that this work mimics potential conditions occurring in WUI fires, this is an encouraging result demonstrating the value added from hardening residential structures. The data generated from this project is unique and can be useful for WUI code development. This work may also serve for the development of computational fluid dynamics models to replicate fire spread at the parcel level in WUI communities. To facilitate easy availability of data to interested parties, an online repository has been created to store the project description, detailed test plan, test data, instrumentation, calibration and verification reports, safety documents, images, and video clips. A preliminary data management and quality assurance plan is provided in the test plan.

The experimental results are subject to uncertainties associated with parameters such as temperature, heat flux, distance, mass, and time measurements. After taking these uncertainties into account, the results demonstrate that the thermal exposure varies with the type and size of shed, the SSD, and fuel loading. Additional factors that would be expected to affect thermal exposure but were not varied in this study include fuel moisture, target structure design and orientation, and topography. While not representative of worst-case conditions, the data from these experiments should be useful for assessing the fire hazard of the storage sheds, SSD, thermal exposures, and likelihood of ignition of target structure subjected to conditions similar to those investigated here. Considering the experimental uncertainties and additional factors that could affect the thermal exposure from the source structures, it is possible to provide some general guidance on shed placement and structure hardening.

Limitations

There are a number of limitations associated with the interpretation of the NOSSE SSD data. These are listed below in two categories: limitations associated with the source structure (shed) and limitations associated with the target structure (exterior wall).

Source Structure Limitations

1. The sheds were tested with representative "high" equivalent fuel loading using standard 1-A wood cribs. Explosive fuels such as gasoline containers or propane tanks were not included for safety concerns and to avoid explosive damage to the surroundings. Such explosive items typically stored in residential sheds are likely to cause window breakages at minimum.

2. All experiments were conducted on flat ground; the effects of topography on flame spread or thermal exposures to the target structure were not considered in this study.

3. Only limited shed orientations with respect to target structure and wind direction were tested.

4. The presence of additional fuels between the source structure and the target structure including ladder fuels, vegetation, fences or vehicles were not considered in this study.

5. Non-flame retarded plastic sheds that can melt and burn as pool fires have not been studied as part of this test series but have been tested indoors under no-wind conditions. Such source structures have potential to spread fires away from the source as the polymer melt can flow and carry heat and flames with it.

6. These experiments do not reflect the ignition hazard associated with embers generated by the burning shed.

7. Limited tests were repeated to confirm the minimum identified SSD_{min}.

Target Structure Limitations

1. Assumes structure is hardened for ember exposures.

2. Fire hardened in compliance with SFM standard 12-7A-1, SFM standard 12-7A-2, and ASTM E2886 as described in Chapter 7A of the California Building Code requirement (for all but one experiment).

3. Single story target structure.

4. Normal to wind flow (limited data on various orientations).

5. Simple flat wall geometry.

6. No weathering, cracking, or any deterioration of the target structure.

Recognizing the limitations of the experiments in estimating the minimum SSDs, implementation guidance of the minimum SSD data generated from the outdoor shed burn experiments can be used for hazard assessment and for hazard mitigation.

Technical findings

The NOSSE experiments demonstrate that even a small combustible shed under 64 ft^2 can compromise a hardened residence from 10 ft away, highlighting the hazard of structure-to-structure fire spread in high density new residential construction. The technical findings from this set of experiments, based on thermal exposures to the target structure, are listed below. While these findings are associated with the auxiliary structures, they can also provide insight into structure separation distance for residential structures.

- **NOSSE TF1** – A repeat experiment showed reproducibility of the measured quantities with peak heat flux variations of ±16 % in the eaves and ±45% at the free-standing rig. The variation in temperatures recorded at the eaves was in the range of 4 % to 6 %.

- **NOSSE TF2** – Increasing the SSD by 5 ft from 10 ft to 15 ft reduced the peak heat flux registered in the eaves by roughly three times and reduced the temperatures measured at the eaves by more than a factor of two.

- **NOSSE TF3** - For combustible sheds, the peak heat flux measured at the target structure:
  - corresponded with the total combustible fuel.
  - was not affected by orientation (i.e., door opening facing downwind or upwind).

- **NOSSE TF4** - The wind had complex effects on the burning behavior of combustible source structures, causing turbulence and eddies. These affected flame lengths and enhanced convective heat transfer to the target structure, causing preheating with likely localized removal of moisture.

- **NOSSE TF5** - Combustible wood sheds were consumed in the fire, resulting in higher thermal exposure to the target structure as compared to noncombustible sheds.

- **NOSSE TF6** - In cases of noncombustible sheds with door openings facing the target structure, the applied wind had minimal or no effect on thermal exposure to the target structure.

- **NOSSE TF7** - The noncombustible steel sheds contained the fire effectively, thus reducing, but not eliminating, the thermal exposure to the target structure.

- **NOSSE TF8** – For the noncombustible shed scenarios evaluated, peak heat flux at the target structure was reduced by half by changing the orientation of the door opening 90° away from the target structure.

- **NOSSE TF9** – The minimum SSD_{min} for both combustible and noncombustible sheds with floor area less than 26 ft^2 was determined to be 10 ft. For sheds with floor area between 26 ft^2 and 64 ft^2, the minimum SSD_{min} was determined to be 15 ft. Because the local winds during a WUI fire are unpredictable, SSD is omnidirectional, i.e., the same SSD in all directions.

- **NOSSE TF9** – A non-fire hardened target structure ignited within 6 mins when exposed to a Very Small wood shed with total combustible fuel of 467 lbs $\pm$ 20 lbs (212 kg $\pm$ 9 kg) and SSD of 10 ft. With similar combustible fuel, SSD, and thermal exposure, the fire hardened target structure exhibited minimal thermal damage and significant ignition resistance.

1.   Introduction

Structure-to-structure fire spread is of primary concern in wildland-urban interface (WUI) fires. Wind is one of the dominant factors in fire spread. Estimating the ignition vulnerabilities of structures and providing guidance to prevent or decrease the ignitions caused by wind-driven fires are necessary steps for reducing structural losses in WUI areas.

The Structure Separation Experiments (SSE) project was developed at NIST to assess structure-to-structure fire spread in wildland-urban interface (WUI) communities. This report describes the NIST Outdoor Structure Separation Experiments (NOSSE), which extend a previous set of indoor experiments that quantified thermal exposures at a target structure from nearby burning sheds to outdoor shed burns in the presence of an applied wind field.

1.1.   Background

There are several ways to categorize fires and fire spread mechanisms that affect WUI communities. Generally, there are three kinds of wildfire [1, 2]:

- Ground fires move through the organic matter in the soil, beneath surface litter. Glowing combustion of available fuel pushes the ground fire forward.

- Surface fires spread with a flame front burning a variety of fuels found on the ground, including leaf litter, dry brush, branches, etc.

- Crown fires are at the top layer of the forest, in the canopy. They usually start from surface fires. Passive crown fires are isolated to a single tree or corpse. Active crown fires are very intense and spread via high wind, heavy fuel load and variable terrain. Active crown fires present a flame front, which may appear as a solid wall of flame.

The three fire spread mechanisms that are most often connected to structural ignition and fire spread include [3, 4, 5, 6]:

- direct flame impingement

- ember exposure, and

- thermal radiation and convection from flames.

Structural ignitions can occur under a variety of spatial and environmental conditions. Research is needed to illuminate the pathways by which fire spreads through a community.

A wildfire entering a WUI community is often visualized as flames from an active crown fire that ignite a flammable component on the exterior of a residential structure, leading to structure destruction. It is true that a fully developed crown fire with flame lengths in excess of 100 ft may easily ignite a structure at a distance of 50 ft. However, the full picture is more complex. External ignitions from wildfire-sourced flame exposures are dependent on the energy release (related to flame length), the residence time of the fire in the wildland fuel, the distance between the edge of the wildland fuel and the structure, and the type of structure construction [7]. Embers also contribute significantly to the ignition of structures; damage or even structure loss can occur when there is an opening (often created by architectural design and/or poor maintenance) that enables flames and/or embers to penetrate into the interior [8].

During a WUI fire, exposures from other structures (residential or auxiliary) can contribute to structure ignition and fire spread. The intense flaming exposure from a burning structure close to the neighboring structure can set the latter on fire. After an initial structure has ignited, structure-to-structure fire spread may occur quickly in moderate to high density construction in the WUI environment [9].

In a post-fire investigation, Maranghides and McNamara [10] reported that embers generated from the burning of adjacent combustibles such as fences, decks, landscape timbers, mulch beds, attached outdoor stairs, and piles of firewood contributed to the ignition of residential structures and were generally responsible for propagating fire within WUI communities. They identified secondary structures such as sheds and garages to be a major source of ember generation, exposing primary structures to increased hazardous conditions. As more structures are ignited, ember fluxes in the WUI area increase, thus furthering fire spread.

The mechanisms affecting structure ignitions in the WUI are complex and varied. Flame impingement, ember exposure, and thermal radiation and convection all play a role. The hazard posed by embers is dependent on a multitude of parameters, and hardening against embers is beyond the scope of the present work. For the other fire spread mechanisms, distance plays a central role. Flame impingement is limited by the length of the flames. Radiative heat flux decreases with the square of the distance away from the flame front [11]. Convection both transports heat from one location to another and has a cooling effect. Thus, studying structure separation distance between source structure (shed) and a target structure (primary residence) under ambient and forced wind conditions is critical for controlling structure-to-structure fire spread.

1.2. Relationship between Exposure and Hardening

The NIST WUI Fire Hazard Mitigation Methodology (HMM) [9] provides an implementable path for community members by considering the spatial relationships between fuels, exposures, and fire hardening at the structure and parcel levels. The basis for the HMM is the relationship between exposure and hardening. This is illustrated in its broadest terms in Fig. 1. The exposure level and level of structure hardening are independent variables, as represented by the two dials. By adjusting either or both, the likelihood of ignition of a structure in a WUI community can be greatly altered. The fire risk of a given structure in the WUI cannot be thought of in terms of either exposure or hardening alone but is a strong function of both. Generally, when fire and ember exposures are reduced, less hardening is required. Exposure reduction, the focus of this work, includes implementing the three 'R's: **R**emove fuels, **R**educe fuels, and **R**elocate fuels.

Fig. 1. Input dials for optimizing WUI fire hazard mitigation methodology **[9]**.

Understanding the role of structure separation distance (SSD) in wind-driven fires via experimentation is an effective way to improve community resilience to WUI and structure-to-structure fire exposures. Identifying minimum SSDs to reduce fire spread will enable the refinement of best practice guidelines described in the HMM document with respect to the 'Relocate fuels' aspect of reducing exposure.

1.3.   Structure-to-Structure Fire Spread Studies

Post-fire investigations [3, 12, 13, 14] of structural fires that occurred during WUI fires within the US and Australia have shown that the chance of a residential structure surviving during a wildland fire is determined by several factors, including defensive actions [10, 15, 16], defensible space, the distance between structures, noncombustible roofing and siding, type of roof constructions, types of soffit, presence of deck/balcony, exterior cladding, percent wood exterior, and environmental conditions. Additionally, Papalou and Baros [14]concluded that the behavior of structures exposed to fire depends on the duration of the fire exposure and the temperatures.

Wind is one of the main controlling parameters that specifies the direction, spread rate and configuration of a fire. Several researchers [17, 18, 19, 20] investigated wind-driven structure-to-structure fire spread in WUI settings. Himoto et al. [18] studied fire spread within multiple houses in an urban area. They concluded that the major contributing factor during wind-driven fire spread between the model houses was thermal radiative heat transfer and that burned-through roof vents resulted in structure-to-structure fire spread. Edalati-nejad et al. [19] investigated the effect of the fire intensity from a wind-driven wildfire on an idealized structure located downstream from the fire source. Using numerical simulations, they found that increasing fire intensity from 10 MW/m to 18 MW/m raised the integrated temperature on the ground near the building and on the surface of the building by 26%, and 69%, respectively. Ghodrat et al. [20] studied the impact of the wind-driven fire on structural integrity. They concluded that the exposure of structural materials to fire and wind resulted in significant heating of the material, often leading to mechanical failure as the material properties were weakened. This can happen due to various thermal decomposition processes such as ignition and pyrolysis, or to mechanical weakening of the part exposed to extreme heat. The wind becomes instrumental in displacing the weakened parts.

A set of experiments with a shed near a target structure representing the wall of a residence was performed indoors and without wind at the NIST National Fire Research Laboratory (NFRL) [21]. The indoor shed burn experiments quantified thermal exposures at a target structure in terms of peak heat release rate (PHRR) and mass loss rate (MLR). They provided information on relative hazards associated with sheds of different construction materials, sizes, and fuel loadings. For the wood and plastic sheds in the study (Closets and Very Small sheds), the construction material contributed approximately 40% of the total combustible mass, greatly increasing the PHRR and fire hazard to the target structure. Steel sheds are not combustible; however, the experiments showed that they may still increase fire risk to the target structure, depending on fuel loading, door orientation, and structure separation distance (SSD). The information from this study was intended to inform the recommendations of the NIST HMM document to 'Remove fuel' and 'Reduce fuel'.

1.4. Approach

The NIST Outdoor Structure Separation Experiments (NOSSE) project was developed to study structure-to-structure fire spread in wildland-urban interface (WUI) communities in the presence of an applied wind field. This experimental series is part of the larger Structure Separation Experiments (SSE) project and complements the indoor shed burn experiments previously conducted at NIST.

By introducing an artificially generated wind field during the outdoor shed burn experiments, a more realistic snapshot of what may happen during a wind-driven fire in the WUI community can be taken. This information can be used to determine the minimum Structure Separation distance (SSD_{min}) to prevent fire spread. The SSD_{min} is defined as the shortest distance between the source and target structures to prevent ignition and flame spread. SSD_{min} is a function of both the source term – in this case the shed – and the design and fire hardening of the target structure. As defined here, SSD_{min} is aimed at reducing radiative and convective exposures to the target structure. This measure cannot be used to address ember exposures; structure hardening for embers is independent of SSD and is further described in the HMM [9].

In this study, thermal exposures from the source structures are quantified by measuring temperatures and incident heat fluxes at the target structure. These outdoor full-scale shed burn experiments are conducted in the presence of an artificially generated wind field. Full-scale, outdoor shed burn experiments with wind better represent the physical environment associated with spreading fires and provide greater understanding of fire spread in WUI communities. The thermal exposure data is fundamental in determining SSD_{min} between storage sheds and the target structure in this (limited) experimental series. Further, the data obtained from these experiments will feed computational modelling efforts and can also be used for model validation.

The experimental design [22] includes a variety of sizes of combustible (wood) and noncombustible (steel) sheds. These sheds are filled with wood cribs and ignited to generate typical radiative and convective heat exposures to the target structure. The target structure is an assembly including an exterior wall with a window and a roof with a vented eave, representative of an exterior wall of a single-story residential building. The spacing between the source and target structures is varied to identify safe structure separation distance (SSD_{min}), defined as the shortest distance between the source and the target structure. The safe SSD for combustible (wood) and noncombustible (steel) sheds with combustible contents is identified under forced wind conditions. All the outdoor experiments are conducted at NIST. The test area is approximately 50 ft × 100 ft. A photograph of the test site is shown in Fig. 2, and a typical set-up for the outdoor shed burn experiments is shown in Fig. 3.
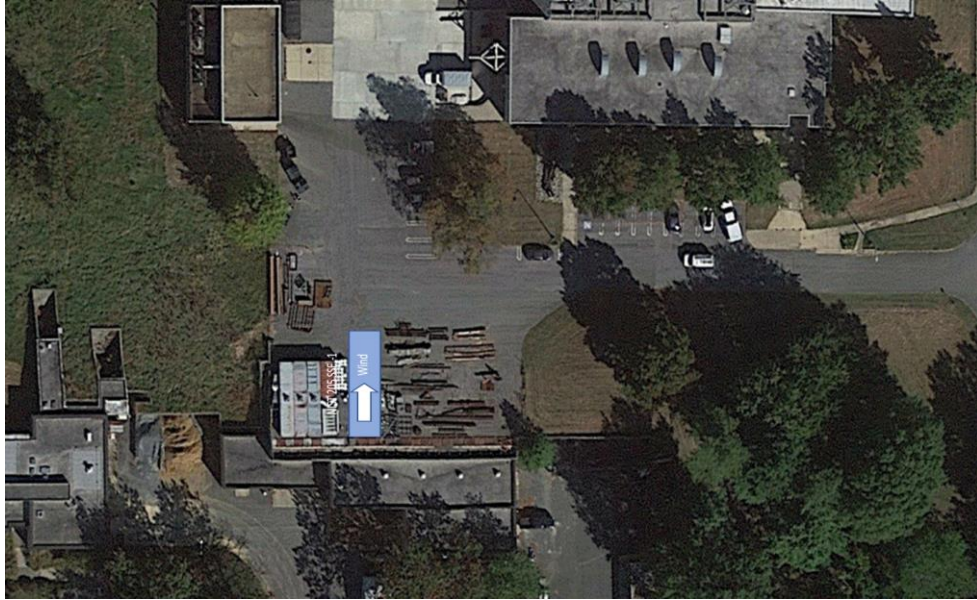
Fig. 2. Aerial view of NIST NFRL. Blue rectangle is 50 ft × 100 ft and represents the maximum extent of the test area to be used. Imagery: Google, Landsat/ Copernicus. Overlays: NIST
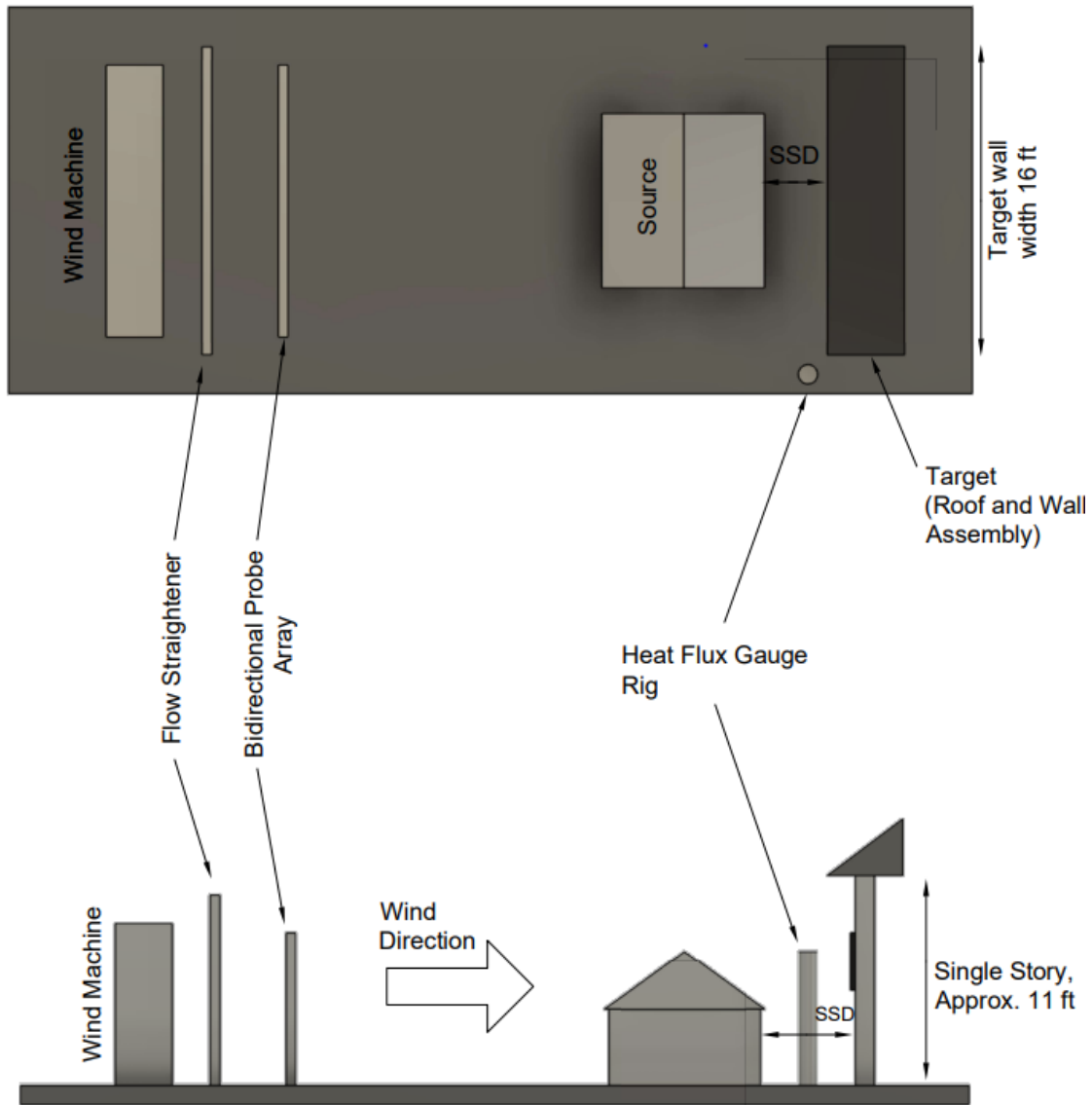
Fig. 3. Typical experimental set-up for shed burn experiments with applied wind (top: plan view, bottom: side view). Figure not to scale.

The policy of NIST is to use SI units in its published materials. However, this report is primarily directed to communities and the building construction industry in the U.S., which use U.S. customary units. As a result, at times it is more practical and less confusing to use U.S. customary units for the purpose of this report. Most engineering drawings, experimental specifications, and dimensions are presented in SI units.

2. NIST Cold Flow Wind Measurements

The outdoor structure separation experiments required a controlled wind source to lay the flames from a burning shed (the source structure) against the eaves of the target structure in order to generate maximum fire exposures for a given source at a specific distance from the target. The wind field was provided by a dual fan wind machine operating at a variety of rotational speeds. This section discusses the wind flow experiments that were conducted to characterize flow patterns over the test site. The flow characterization the experiments were performed without the source structure and in the absence of fire (thus "cold flow" measurements). The baseline flow patterns were characterized by collecting measurements at various locations at the test site and at a range of wind speeds that encompassed the rotational speeds to be used in the structure separation experiments.

2.1. Experimental Set-up

The experimental set-up for the cold flow experiments is shown in Fig. 4 from two points of view. In a photo taken from slightly forward of the wind machine, Fig. 4(a) shows the target structure, bidirectional probe array, controller and dual fan synchronizer, and the flow straightener. In a photo taken from the side of the target structure, Fig. 4(b) shows the dual propeller wind machine at the far-right, behind the flow straightener. The bidirectional probe array for collecting data on the applied wind was situated downwind from the flow straightener. Figure 5, also taken from the side of the target structure, shows the sea container housing the data acquisition system, location of the thermocouple outside of the sea container, anemometer 1, and bidirectional probe array.

Descriptions of individual components of the cold flow experimental set-up are provided below.
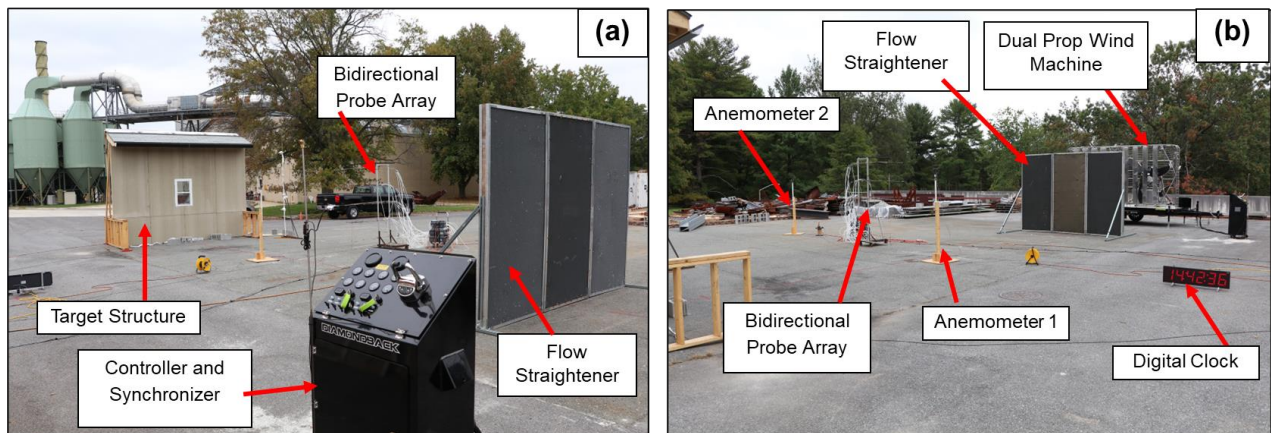
Fig. 4. Photo of test site from (a) wind machine and (b) target structure showing target structure, bidirectional probe array, flow straightener, anemometers, controller and synchronizer, digital clock, and dual prop wind machine.
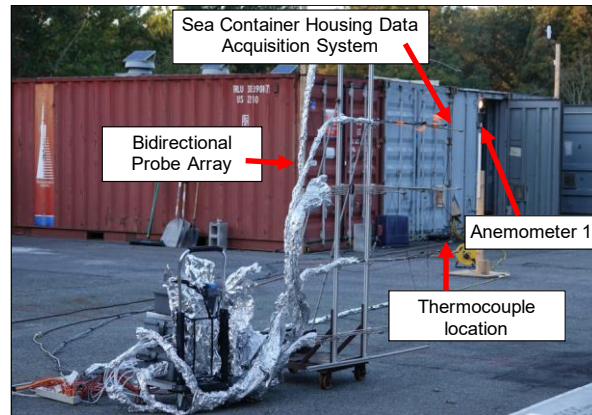
Fig. 5. Photo of test site from target structure showing sea container, bidirectional probe array, anemometers, and thermocouple location.

2.1.1. Imposed Wind Field

The wind field applied to the test site was generated by a dual fan wind machine. A flow straightener was positioned downwind to help align the wind perpendicular to the target structure.

2.1.2. Wind Machine Specifications

The wind machine shown in Fig. 6 was used to impose a wind field on the source structure. It was assembled and mounted on a trailer by Diamondback Airboat. Power was provided by two 6.0 L displacement, 450 HP-rated PCM marine engines with multi-port fuel injection. The wind machine utilized a pair (right- and left-handed sets for opposite rotation) of Whirlwind Propellers model Whisper Tip CarbonMax EX 83, each of which had three quiet-design, graphite composite blades with a width of 13 in and a sweep diameter of 83 in. The wind machine incorporated a high-performance positive drive belt with 2.3:1 reduction for one prop and a gear reduction for the other to provide reverse rotation direction. two propellers were counterrotating to limit flow vorticity. The baffles seen in front of the fans in Fig. 6(b) helped to direct the wind in the forward direction.

Fig. 6. Dual fan wind machine, a) rear view, and b) front view.

Physical distances were measured manually. The distance between the hub centers was 85 13/16 in ± 1/8 in, for a separation between the propeller sweeps of 2 13/16 in ± 1/8 in. The hub centers were 46 in ± ¼ in above the deck sitting on the trailer, allowing the propellers to clear the deck surface by 4 ½ in. The distance of the deck surface from the ground was 27 ¼ in on the left side and 28 in on the right, both with uncertainties of 1/8 in, for an average deck height of 27 5/8 in ± ½ in.

From these measurements, the lowest sweep extent of the wind machine propellers was calculated as approximately 32 in above the ground, and the highest extent was 115 in, or about 9 ½ ft above the ground. The column of air moved horizontally by the wind machine was thus focused on the fire plume extending vertically from the shed vents rather than near the ground. This allowed the imposed wind to fully impact the fire plume from its base a few feet above the ground to the top of the target wall.

The wind machine included a Glendinning CH2001 ProGrade digital control system. In addition, a Glendinning Automatic Synchronizer was employed to match the engine speeds. The control system and synchronizer allowed the operator to start the engines independently, synchronize them through the push of a button, and then increase or decrease the engine speed by 80 rpm at a time through increment or decrement buttons. Manual binnacle-style throttle controls also enabled fast increase or decrease of the individual engine speeds. The operator could monitor the engine rpms with a digital tachometer, and a webcam was utilized to send 30 Hz digital video of the control panel readouts to the data acquisition system.

2.1.2.1. Flow Straightener

A flow straightener was used to remove large-scale swirl and align the applied wind parallel to the centerline axis of the experiment. The flow straightener consisted of three framed sections of Plascore Aluminum Honeycomb model PCGA-XR2-1.8-3/4 30-N-3000 Series that were 6 in thick with 3/4 in cells. The three framed sections, each measuring 4 ft × 8 ft, were erected on end and connected together horizontally as shown in Fig. 7, with the center plane of the flow straightener positioned 12 ft in front (downwind) of the rotational planes of the propellers. Steel u-channels were used as feet and angle braces for the flow straightener assembly. The u-channels used as feet were weighed down for stability with large I-beams as shown in Fig. 7(a). For the experiments, however, the I-beams were moved as far to the sides as possible.

A view of the flow straightener from the downwind side is shown in Fig. 7(b). The bidirectional probe array also appearing in this photo is described in Section 2.1.3.1.
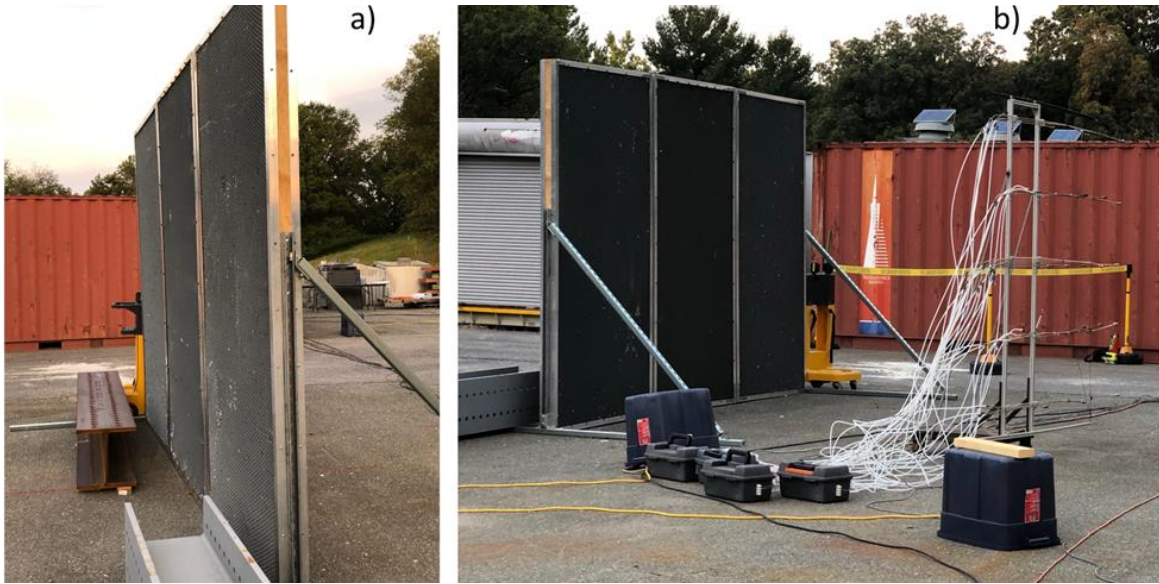
Fig. 7. Flow straightener a) from upwind side and b) from downwind side, also showing the bidirectional probe array. Wind direction is left to right.

2.1.3. Instrumentation and Data Acquisition

For the cold flow experiments, data was collected for the wind applied by the dual fan wind machine and for ambient temperature and wind conditions.

2.1.3.1. Bidirectional Probe Array

This location was selected to capture the wind field close to the shed without influencing the upwind measurement. Bidirectional pressure probes measure the difference between the total pressure on the windward side of the probe and the static pressure on the leeward side. The difference is the dynamic pressure caused by the wind, which can be combined with temperature and a probe factor to calculate the wind speed [23]. The leads of the probes were connected with polyethylene tubing (1/4" OD) to Setra Model 264 bidirectional pressure transducers, which have a pressure range of ±373.6 Pa. Each transducer produced a voltage output from 0 V to 5 V, with 2.5 V output indicating zero pressure differential. Combining the pressure measurement with ambient temperature gave a corresponding velocity range of about ±52 mph. Immediately prior to the experimental series, the transducer calibrations were checked against a recently calibrated, high accuracy pressure transducer, and their sensitivities were applied to the data from this series. Voltage outputs measured during pneumatic zeroing prior to each experiment were used to account for any voltage offsets. The pneumatic zeroing procedure is described in Section 2.1.5.

A photograph of the bidirectional probe array in front of a shed and target wall is shown in Fig. 8. The blowup images in Fig. 8 show the tubing connections for the upper row of bidirectional probes (A) and on probes #2 and #3 (B). The diagram in Fig. 9 indicates the locations of the probes. The array contained a total of 17 bidirectional probes attached to five rods extended

horizontally from two vertical posts attached to a heavy cart, with supports to maintain stability in a heavy wind. The rods supported rows of three to five probes at heights from 1 ft to 7 ft above the ground at 1.5 ft intervals. The set of five probes arranged vertically at the ends of the rods enabled the collection of data for a vertical profile along the side of the probe array, and the set of five probes at 1 ft intervals along the center rod provided data for a horizontal velocity profile 4 ft above the ground. Velocity measurements from the additional probes in the array filled in the top and bottom and gave a more complete picture of the velocity field generated by the dual propeller wind machine. Repositioning the probe array under repeated cold flow wind conditions allowed it to cover the full width of the velocity field seen by the shed in the absence of fire.
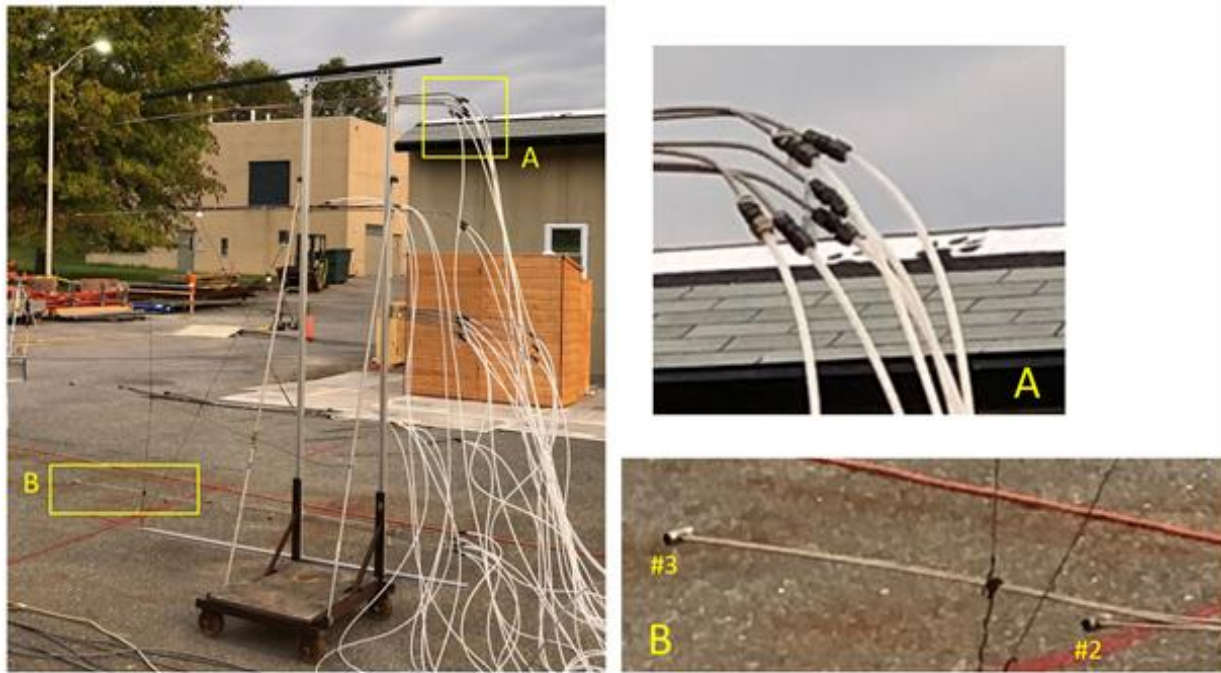
Fig. 8. Bidirectional probe array holding 17 probes. A wood shed and the target structure appear in the background to the right. The blowup images show the tubing connections for the upper row of bidirectional probes (A) and on probes #2 and #3 (B).
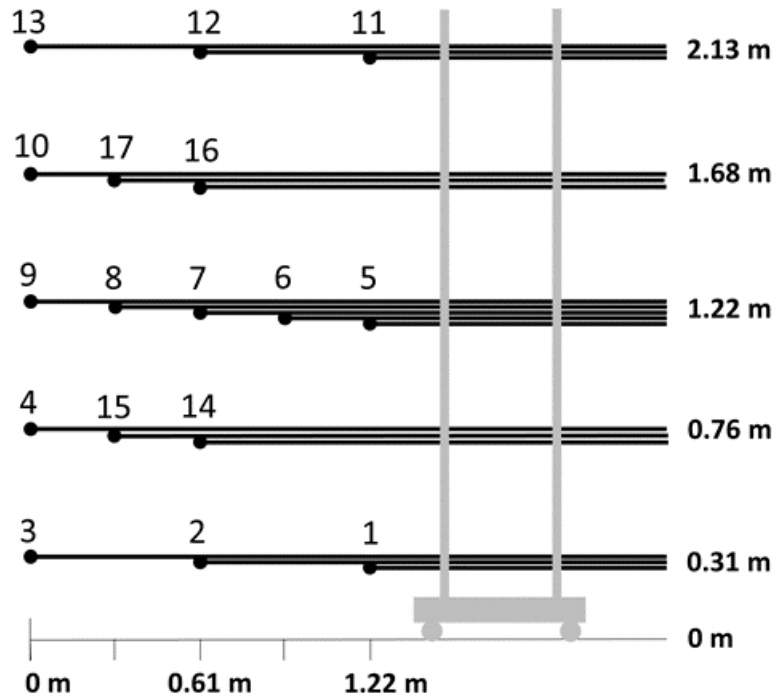
Fig. 9. Diagram of the bidirectional probe array used to measure the velocity field. Numbers are used to label and identify particular probes. The array is oriented perpendicular to the wind.

2.1.3.2. Ambient Conditions

The calculation of wind speed from the differential probe pressures also required measurements of the ambient temperature. Temperature was measured with a type K thermocouple bead made from 24 AWG wire (0.0201 in diameter). Ambient temperature measurement was taken at the front of the sea container as shown in Fig. 5(c).

The ambient wind speed and direction were measured by two anemometers mounted on separate 6 ft poles in two locations (see Fig. 5(b)). One anemometer was 15 ft west of the centerline axis of the experiments and the other was 15 ft east. Both were located 24 ft south of the target wall. The instruments were Young model 86000 Ultrasonic Anemometers [24] with 5 V output and 0.25 s response time for both wind speed and horizontal (two dimensional) wind direction. Wind speed was measured with 0.01 m/s resolution and ± 2 % or 0.1 m/s accuracy, as stated by the manufacturer, and wind direction was measured with 0.1° resolution and ± 2° accuracy. Wind direction accuracy may have degraded to about ± 5° due to the estimation of true north during installation and slight positional drift due to high winds. The ambient wind measurements provided the approximate wind environment in the vicinity of the experiments but not exactly at their location, so some focused wind gusts may have been located at the experiment and not at either of the anemometers or vice versa.

2.1.3.3. Data Acquisition System

For the cold flow and NOSSE experiments, a separate data acquisition system was required to collect and process data from 22 channels of wind-related measurements: 17 pressure transducer

voltage outputs from the bidirectional probe array located in front of the shed, a millivolt signal from the ambient temperature thermocouple, and voltages generated from the two sonic anemometers representing the local ambient wind speed and direction for each. Voltage and thermocouple data from the sensors were collected using two National Instruments input modules, NI-9205 and NI-9213, respectively, inserted into a National Instruments cDAQ-9174 Compact DAQ USB 4-slot chassis. The thermocouple data were collected at 90 Hz, the pressure and anemometer data were collected at 50 kHz, and all channels were averaged over every second. The program saved to output files the average values and standard deviations of the samples collected from each channel. The Labview MIDAS program [25] used to collect the data was also used to monitor data quality and spot-check for sensor malfunctions.

2.1.4. Cold Flow Test Matrix

To characterize the wind field directed toward the target structure, the flow was measured across several cross-sectional planes downstream from the dual wind machine and flow straightener. The variables for the cold flow testing included distance from the target wall, position of the bidirectional probe array sideways along the test plane, and wind speed, as shown in the test matrix in Table 1.

The wind field was measured along the plane at four separation distances between the bidirectional probe array and the wall of the target structure, as shown in the first column of Table 1. With a fixed distance between the wind machine and the target wall of 57 ft, smaller distances from the target wall corresponded to larger distances from the wind machine as listed in column 2. The wind field is expected to become more diffuse with distance downstream from the wind machine, a characteristic that is expected to show up in the measurement results.

Table 1. Cold flow test matrix. (1ft = 0.305 m)

Probe Array Position			Wind Machine Setting	
Distance from Target Wall (ft)	Distance from Wind Machine (ft)	Lateral Positions East from Center (ft)	Wind Speed Classification	Rotation (rpm)
41	16	-8, -4, 0, 4	High, Medium	1280, 1020
36	21	-8, -4, 0, 4	High, Medium	1280, 1020
28	29	-8, -4, 0, 4	Medium, Low, Idle	1080, 830, 760
23	34	-8, -4, 0, 4	Medium, Low, Idle	1080, 830, 760

Data was collected by moving the bidirectional probe array back and forth along each test plane, with the same wind conditions at each location. The bidirectional probe array was 4 ft wide and 7 ft tall, as shown in Fig. 9. Repositioning was therefore required in order to measure the wind field along the plane over a 16 ft width. As indicated in Fig. 10, the probe array was repositioned four times for each set of conditions. The array positions were identified as (-8, -4, 0, and 4) ft east of the centerline of the wind machine, as measured from the leftmost column of five probes.

The positions of bidirectional probes are shown in Fig. 10 for the probe array position at 0 ft from the centerline. Note that the three probes on the right in this position (probes #1, #5, and #11) are at the same points as probes #3, #9, and #13 when the probe array is repositioned 4 ft from the centerline. These overlapping probe pairs provided a check on the repeatability of wind data under identical conditions.

Positioning the array at four consecutive locations enabled measurement of wind speeds over a total area 16 ft wide by 7 ft high. This is the same width as the target structure, 4 ft lower than the 11 ft height of the target, and within 3 ft above and 6 in below the highest points of the source sheds (see shed specifications in Section 3.1.4).

Wind speeds were studied for wind machine settings ranging from Idle, at a rotational speed of 760 rpm and giving a maximum wind speed measured by the bidirectional probes of about 13 mph, to High, with rotational speed of 1280 rpm and maximum wind speed of about 26 mph. The four wind speed classifications studied during the cold flow tests are listed along with the corresponding fan rotation speeds and maximum measured wind speeds in Table 2.
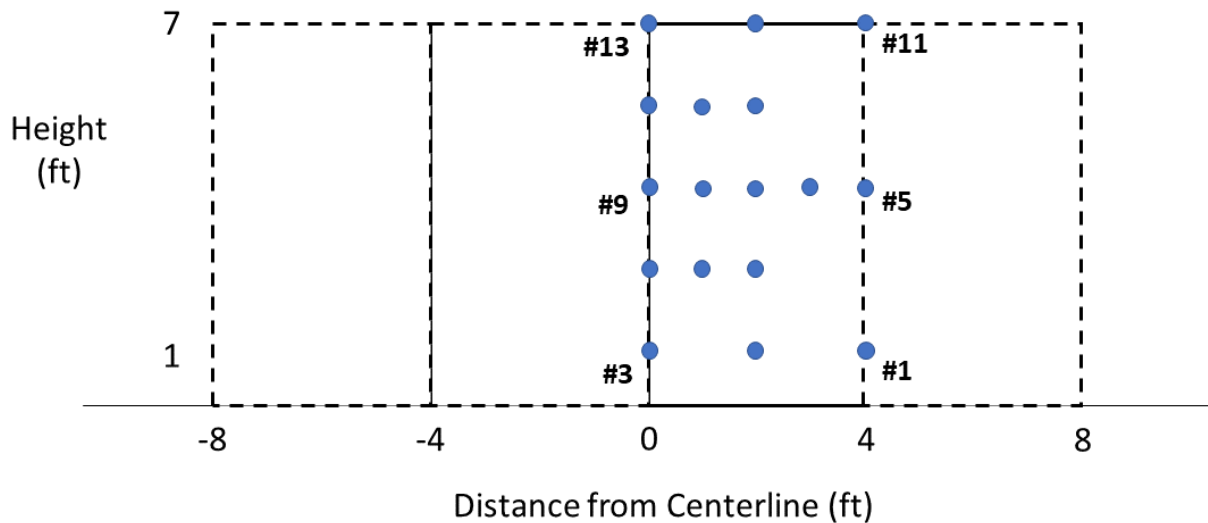
Fig. 10. Four positions of bidirectional probe to measure wind field in plane 16 ft wide, 7 ft high. Locations of probes are shown for probe array position 0 ft east from center. (1ft = 0.305 m)

Table 2. Wind machine settings

Wind Speed Classification	Nominal Wind Speed (mph)	Rotation Speed (rpm)
High	26	1280
Medium	20	1020-1080
Low	16	830
Idle	13	760

The test matrix in Table 3 shows the positions of the probe array and wind machine settings for the set of cold flow experiments. The wind field was measured across planes at four distances

between the wind machine and the target wall for two or three wind speeds at each distance, for a total of ten unique combinations of separation distance and applied wind speed. Four lateral probe array positions were required for each of the ten combinations in order to cover the entire cross-sectional plane. During each of these 40 tests, data were collected at the rate of one measurement per second for 90 s for each of the 17 bidirectional probes and for the instruments measuring ambient wind and temperature.

Table 3. Cold flow test matrix. (1ft = 0.305 m)

Probe Array Position		Wind Machine Setting
Distance from Target Wall (ft)	Lateral Positions East from Center (ft)	Rotation (rpm)
41	-8, -4, 0, 4	1280, 1020
36	-8, -4, 0, 4	1280, 1020
28	-8, -4, 0, 4	1080, 830, 760
23	-8, -4, 0, 4	1080, 830, 760

2.1.5. Test Procedure

The cold flow tests were carried out on a single day at NIST Gaithersburg in mid-October 2021. Before the first cold flow test, data was collected with short lengths of rubber tubing connected to each side of the bidirectional probes as shown in Fig. 11 . This enabled pneumatic zeroing of the pressure transducers under conditions of zero wind. It also enabled observation of the pressure transducer voltages being read by the data acquisition system to troubleshoot measurement problems with the probes. Voltages that were drifting indicated a poor connection, and voltages offset significantly from 2.5 V indicated a plumbing leak. These issues were resolved before taking cold flow measurements.

Fig. 11. Photograph showing pneumatic zeroing of the bidirectional probes using rubber tubing.

The bidirectional probe array was then arranged at the closest separation distance from the target wall (the farthest position to the fan), in the lateral position 4 ft east of the centerline. The fan was set to the lowest rotational speed being measured at that position and allowed to equilibrate for about 30 s. Data was collected for 90 s, after which the fan was set to the next highest rotational speed and the process was repeated.

When all of the applied wind speeds had been measured, the probe array was moved 4 ft to the west to its next lateral position, the fan was reset to the lowest rotational speed, and the data was collected for every wind speed at the second position. This was repeated for the final two lateral positions, until all data had been collected for that separation distance. Then the probe array was moved to the position 4 ft east from the centerline at the next separation distance from the target wall.

In this way, data was systematically collected for cold flow tests at each wind speed, each of the four lateral probe array positions across the wind field, and each downwind distance from the wind machine listed in Table 3.

2.1.6. Data Analysis

The goals for the data analysis were to calculate the mean wind speed at each probe site for each case of applied wind speed and distance from the target wall, to assemble the data from the four lateral probe array positions into a single wind field, and to evaluate the uncertainty of the wind speed measurements. This section also describes the use of measurements from overlapping probe pairs (probes collecting data at the same location and wind speed during different experiments) to assess the repeatability of these measurements.

2.1.6.1. Wind Field Along Plane

The process for analyzing the data for each wind speed and downwind location listed in Table 3 took three steps.

First, the mean wind speed values were calculated for each probe at each of the four lateral positions of the probe array, at (-8, -4, 0, 4) ft east of the wind machine centerline. An example of the resulting data from one cold flow test is displayed in a pseudocolor plot in Fig. 12. In this plot, a matrix of colored cells on a gray background represents the mean wind speed value at each of the 17 probes in the array. The data are scaled based on the highest and lowest mean probe values, as shown in the color scale to the right of the plot. The locations of bidirectional probes are marked by dots.

Figure 13 shows a set of four pseudocolor plots for the case of high wind speed and 41 ft distance from the target wall. The plots are arranged in order of lateral position along the cross-sectional plane.
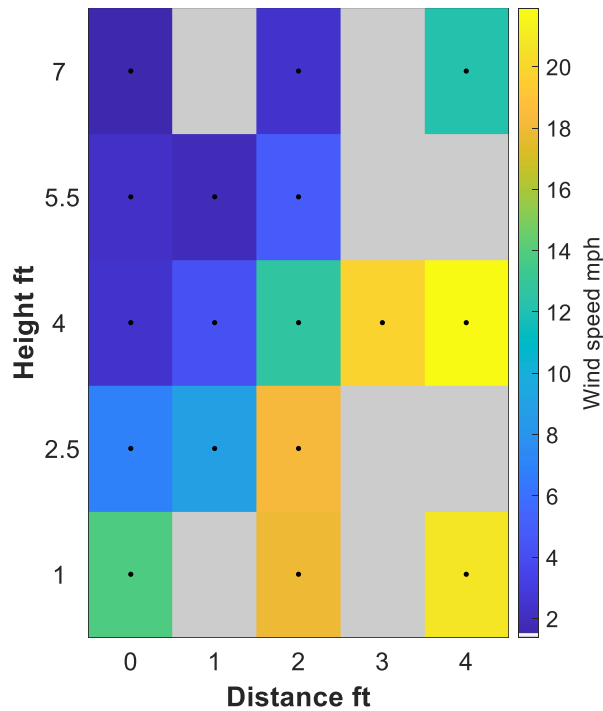
Fig. 12. Plot of mean wind speed data from bidirectional probes. (1ft = 0.305 m)
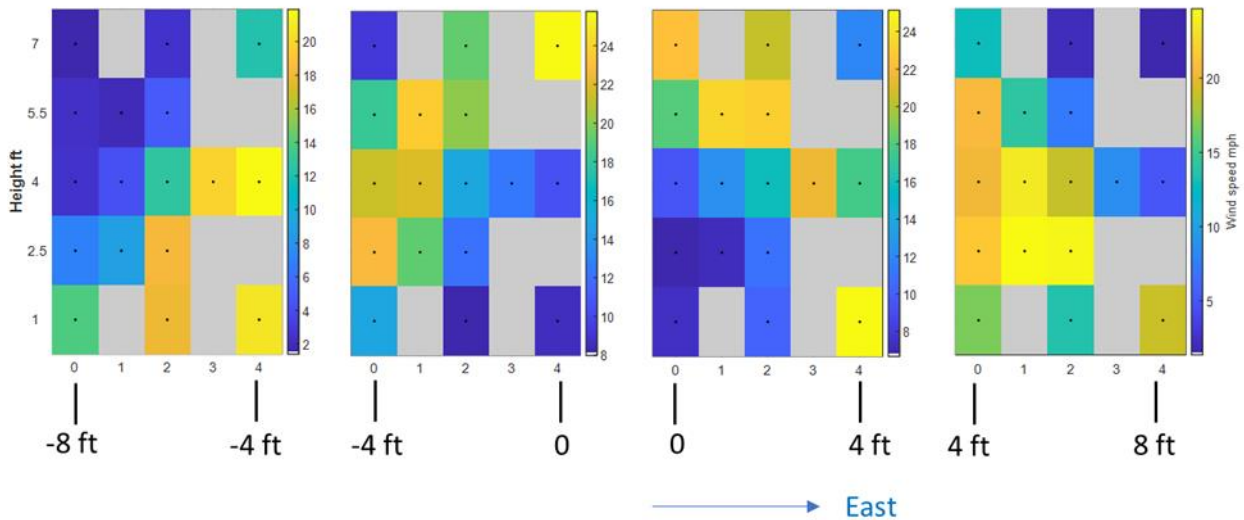
Fig. 13. Mean wind speed values for each probe at the four lateral positions of the probe array. (1ft = 0.305 m)

Second, the same sets of data were replotted using identical color scales for all four images. An example of synchronizing the color scales is shown in Fig. 14 for the same case discussed above. The identical color scale for each image appears to its right.

This allowed a direct comparison of the values along the entire plane, including the probes at 1 ft, 4 ft, and 7 ft heights that overlapped at -4 ft, 0 ft, and 4 ft east of the centerline when the

probe array was repositioned. The nine positions of these overlapping probes, shown in Fig. 15, played an important role in the uncertainty analysis, as will be described in the next section.
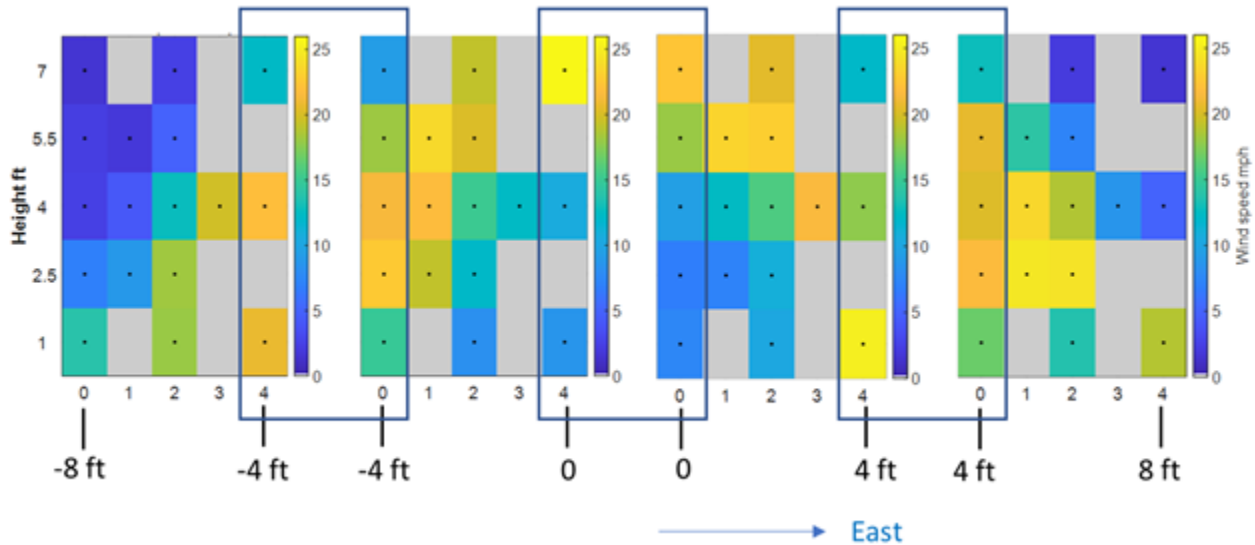
Fig. 14. Mean wind speed values for each probe at the four lateral positions of the probe array, using the same scale for all plots. (1ft = 0.305 m)
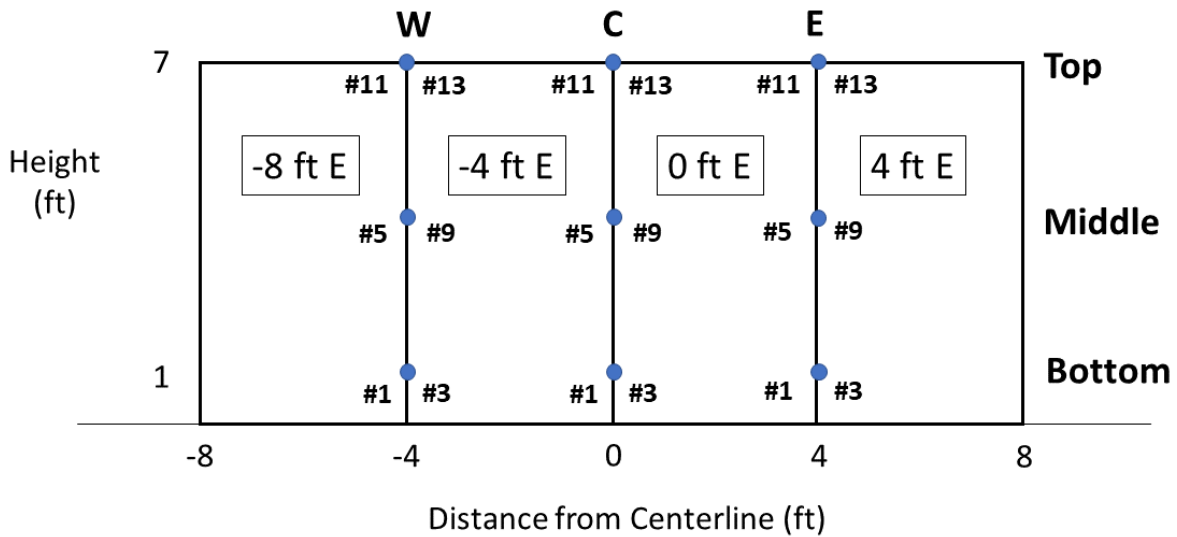
Fig. 15. Overlapping probes at nine locations for the four lateral positions of the bidirectional probe array. (1ft = 0.305 m)

Third, the values from the nine pairs of overlapping probes were averaged and a pseudo color plot was assembled from all four lateral plots in the same plane at the same wind speed. This shows the entire wind pattern across the plane for this set of conditions. Fig. 16 shows this final plot resulting from assembling the plots in Fig. 14, with the common color scale on the right.
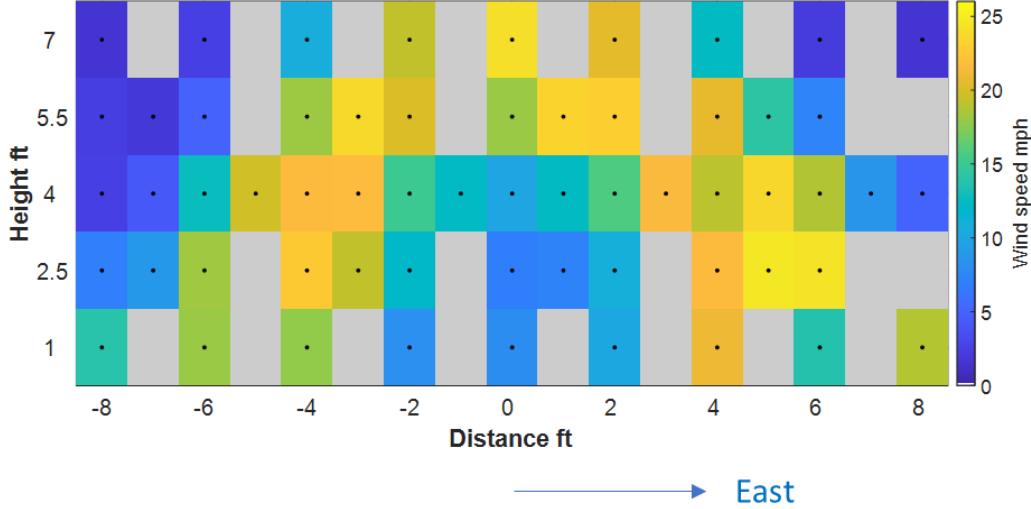
Fig. 16. Assembled wind speed plot showing mean values across the full plane. (1ft = 0.305 m)

2.1.6.2. Evaluation of Wind Speed Uncertainties

The uncertainty of a measurement result can be determined by combining uncertainty components due to various factors. The components are classified as Type A, those evaluated using statistical methods, and Type B, those evaluated by other means [26].

Bidirectional probes are simple tubular devices that calculate the wind speed from the pressure difference between front and back openings. They have the advantages of being robust in a fire environment and insensitive to flow angle. A probe array similar to the one used in this cold flow study, but with thirteen bidirectional probes rather than seventeen, was deployed for a NIST study of fire spread over fences and mulch [27]. The analysis of uncertainty inherent to these probes found that the only significant source of error was the relative standard uncertainty of $u_{r,BP} = 0.07$ for the probe constant. This finding was based on an analysis by Bryant [28] and on work by McCaffrey and Heskestad [23]. This is a Type B uncertainty, based on scientific judgment.

A Type A uncertainty resulting from measurements of the wind speed quantifies the variation in wind speed due to fluctuations caused by the fan, the ambient wind, vibrations in the probe position, and other influences that are picked up during data collection. The uncertainty in the mean of the measured value is given by the standard deviation of the mean $\sigma_{\overline{V}}$, also known as the standard error, and is equal to the standard deviation of the measurements σ divided by the square root of the number of measurements N:

$$\sigma_{\overline{V}} = \frac{\sigma}{\sqrt{N}} \tag{1}$$

The relative standard error is equal to the standard error divided by the mean wind speed $\overline{V}$,

$$\sigma_{r,\overline{V}} = \frac{\sigma_{\overline{V}}}{\overline{V}} \tag{2}$$

The relative combined uncertainty $u_{r,c}(\overline{V})$ for a bidirectional probe during an experiment is the combination of Type A and Type B uncertainties using the root sum square (RSS) method:

$$u_{r,c}(\overline{V}) = \sqrt{u_{r,BP}^2 + \sigma_{r,\overline{V}}^2} \qquad (3)$$

Finally, the relative expanded uncertainty,

$$U_r = k u_{r,c}(\overline{V}) \qquad (4)$$

describes an interval around the mean value, $\overline{V} \pm U_r\overline{V}$ within which the value of the wind speed is confidently expected to lie. For a normal distribution, a coverage factor of $k = 2$ defines an interval with a level of confidence of approximately 95 %.

2.1.6.3. Evaluation of Wind Speed Repeatability

The cold flow experiments provided a ready check on the repeatability of the applied wind field generated by the dual fan wind machine. As the probe array was moved laterally to cover each cross-sectional plane, the mean wind speed values were measured twice at each applied wind speed at 1 ft, 4 ft, and 7 ft high (Bottom, Middle, and Top, respectively) and 4 ft, 0 ft, and 4 ft east of the centerline (W, C, and E respectively), as shown in Fig. 15. Ideally, although the data were collected at different times, the mean wind speeds measured by these probes should be identical, within the uncertainty bounds. Therefore, comparing the relative differences in mean wind speed values for these overlapping probe pairs to the relative expanded uncertainty allows an assessment of measurement repeatability.

For each of the probe pairs (#1–#3, #5–#9, or #11–#13), the mean wind speeds are averaged. For example, for the probe pair #1–#3,

$$V_{av,1-3} = \frac{\overline{V}_1 + \overline{V}_3}{2} \qquad (5)$$

The difference of the mean wind speed of either probe from this average value is then given by

$$\Delta V_{1-3} = \left| V_{av,1-3} - \overline{V}_1 \right| = \left| V_{av,1-3} - \overline{V}_3 \right| \qquad (6)$$

and the relative difference is the difference divided by the average wind speed value,

$$\Delta V_{r,1-3} = \frac{\Delta V_{1-3}}{V_{av,1-3}} \qquad (7)$$

The set of relative differences from the nine overlapping probe pairs can now be compared to the relative expanded uncertainty for the combined set of probes,

$$U_{r,1-3} = k \sqrt{u_{r,c}^2(\overline{V}_1) + u_{r,c}^2(\overline{V}_3)} = k \sqrt{2u_{r,BP}^2 + \sigma_{r,\overline{V}_1}^2 + \sigma_{r,\overline{V}_3}^2} \qquad (8)$$

using the relative combined uncertainty for each probe defined in Eq. 3, to assess the repeatability of the measurement of the applied wind speed from the dual fan wind machine.

2.2. Results

2.2.1. Wind Fields

Wind field plots were assembled for cross-sectional planes at each separation distance and each applied wind speed, as described in Section 2.1.6.1. Figure 17 shows the wind fields in a matrix as a function of wind speed and distance from the wind machine. Velocity scales on the right are identical within each family of nominal applied wind speeds.

The overall pattern in the wind field from the dual fan wind machine was consistent. In each case, the highest wind speeds describe an arc from one side of the cross-sectional plane to the other. Within about ± 2 ft from the centerline, high winds extend from 5 ½ ft to at least 7 ft high. Closer to the ground, the maximum winds are found between 3 ft and 6 ft away from the centerline, with low winds within ± 2 ft from the centerline. The implication for the structure separation experiments (SSE) is that high winds directed toward the target wall surround the shed and reach the eaves in the central area where the flames are located. The winds directly impinging on the shed are lower. The differences between this wind field and a more uniform wind field are not expected to significantly affect the results of the SSE, which requires only that the applied winds provide the worst-case condition of flames impacting the eaves.

The matrix in Fig. 17 shows that the trend is toward increasing uniformity of the wind field as the distance from the wind machine increases and the applied wind speed decreases. This is consistent with the expected effects of diffusion downwind from the wind machine.
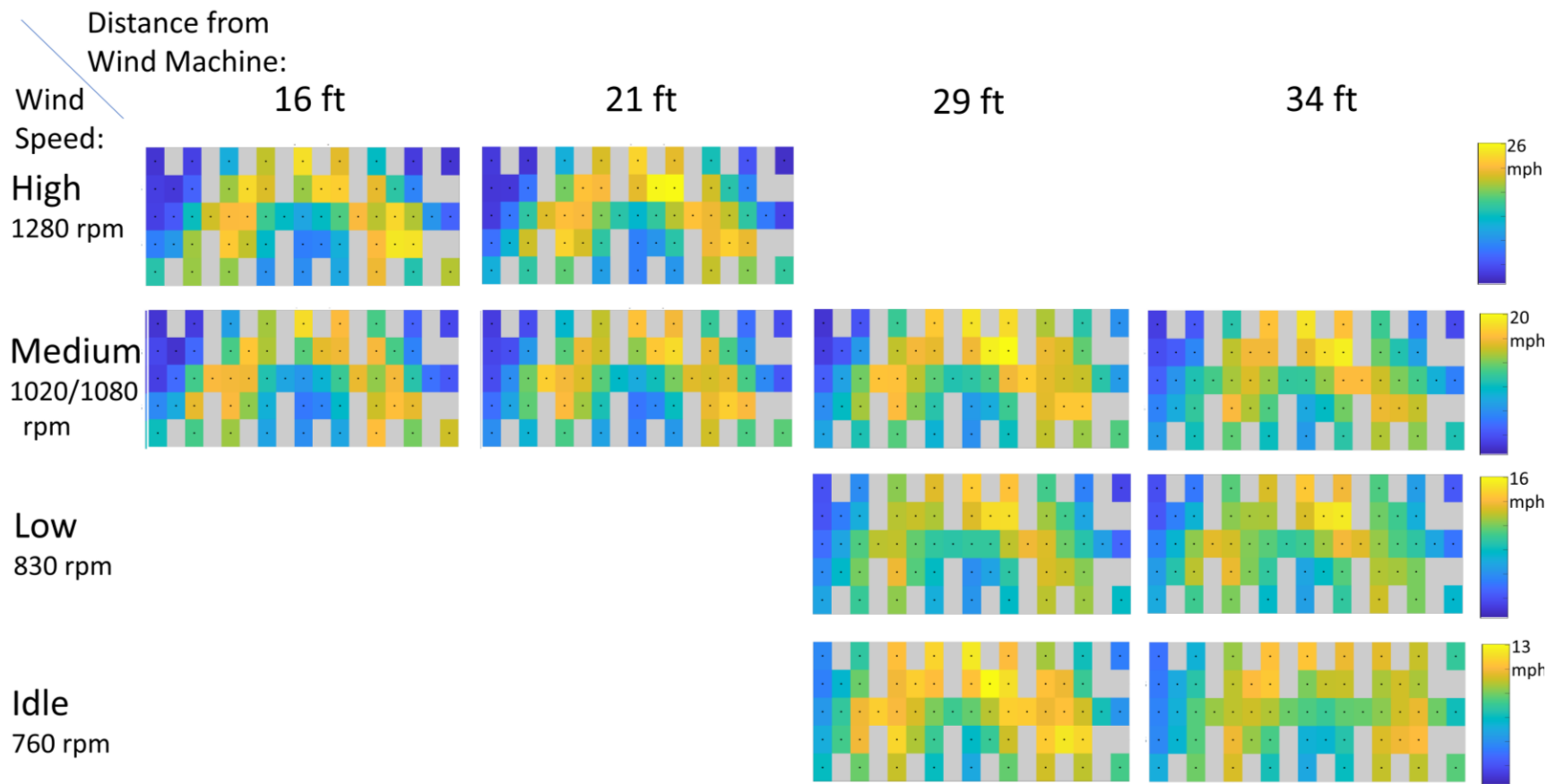
Fig. 17. Matrix showing wind fields as a function of wind speed and distance from wind machine. (1ft = 0.305 m)

2.2.2. Wind Field Uncertainties

As discussed in Section 2.1.6.2, the uncertainties in mean wind speed measured for each probe are expected to be dominated by the Type B contribution from the probe constant, inherent to the bidirectional probe design, and the Type A contribution of data variations due to wind variability and other factors. The relative expanded uncertainty U_r (confidence factor of 95 %) was calculated from Eq. 4 for all 680 probe measurements. This includes all 17 probes in the probe array in 4 lateral positions for each of 10 combinations of applied wind speed and separation distance from the target wall. The median value of U_r was found to be 0.144, or 14.4 % of the mean wind speed value, and the maximum value was 0.215. Seventy-five percent of the values of U_r were between 0.14 and 0.15. This indicates that the dominant uncertainty factor was the probe constant, which contributed a base value of 0.14 to the relative expanded uncertainty.

2.2.3. Wind Field Repeatability

The repeatability of measurements of the applied wind field was tested by comparing the overlapping probe pairs that measured the same conditions at the same positions at different times. For each of the nine probe pairs illustrated in Fig. 15 there were ten cases, corresponding to the tests at different applied wind speed and separation distance. In addition to the sources of uncertainty listed in Sections 2.1.6.2 and 2.2.2, changing the position of the probe array may introduce errors due to mispositioning of the base of the array or misalignment of the upper probes.

Following the procedure discussed in Section 2.1.6.3, the mean wind speeds from the probe pairs were averaged. Equation 7 was then used to calculate the relative difference between the mean wind speed measured by either probe and the averaged value. The resulting statistics for the relative differences for each of the 9 probe pairs under the 10 test conditions are shown in the box plot in Fig. 18. The data does not reveal any patterns that might indicate systematic issues with misalignment of the probes, such as higher relative differences for the probes at the top of the array.
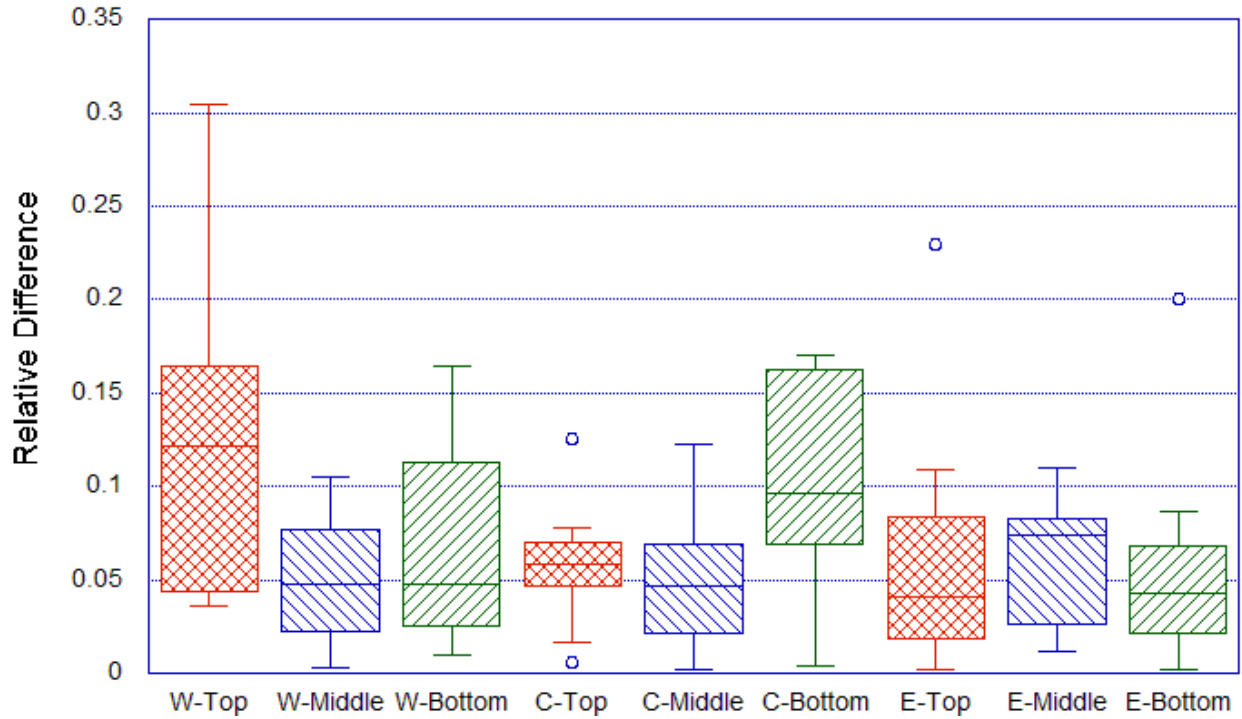
Fig. 18. Relative differences in wind speed for overlapping pairs of bidirectional probes.

The repeatability was assessed by a comparison of the relative difference for each overlapping probe pair to the relative expanded uncertainty for the combination of two probes, as calculated in Eq. 8. Out of a total of ninety probe pairs, the relative difference exceeded the relative expanded uncertainty in only two cases: for the W-Top location with wind speed classified as Idle and distance from the wind machine of 29 ft, and for the E-Top location with wind speed classified as Medium and distance from the wind machine of 34 ft. The measurement of the wind field generated by the dual fan wind machine can therefore be considered repeatable within the uncertainty inherent in the bidirectional probe and the variability of the winds being measured.

2.2.4. Ambient Conditions

The mean ambient temperature measured during the 40 cold flow tests was 23.6 °C ± 0.6 °C. This was well within the Type B accuracy limits of ± 2.2 °C for the Type-K thermocouple instrument.

The mean ambient wind speeds measured during the tests were 0.73 m/s ± 0.44 m/s. The Type B accuracy limits for the anemometer were given by the manufacturer as ± 0.1 m/s. If this range is taken as a standard uncertainty, then the extended standard uncertainty is ± 0.2 m/s for a confidence level of 95 %. The measured mean ambient wind speed is well outside of these limits, indicating that the variability of the ambient wind was the dominant factor in the uncertainty of the wind speed measurement.

2.3. Technical Outcomes

The cold flow experiments generated an extensive database of wind fields as a function of distance from the dual fan wind machine and applied wind speed, providing useful insights into the wind flow patterns. The data consistently showed that the wind speed was highest in an arch extending downstream from the wind machine. The maximum wind speeds were found about 5 ft to either side of the centerline at ground level and extended to roughly 6-7 ft in height in the center. The region of highest wind speed expanded in width with distance downstream due to diffusion.

Although the wind field generated by the dual fan wind machine was not uniform, the cold flow measurements showed that the area of highest wind speeds surrounds the shed and extends above it, providing strong winds for the flames in the areas of greatest interest to the structure separation experiments.

3. NIST Outdoor Shed Burn Experiments

The primary objective of the outdoor shed burn experiments was to determine the safe structure separation distance (SSD_{min}) to prevent fire spread from a burning shed (the source) to a nearby target structure in the presence of wind for various parameters:

- Size of source structure (Closet, Very Small shed, and Small shed) with high fuel loadings,

- Construction material for source structure (combustible and noncombustible), and

- Fire resistance of target structure (fire hardened and non-fire hardened).

Thermal exposure from the source structure (storage shed) was quantified by measuring temperatures and incident heat fluxes at and near the target structure. This experimental series did not include effects of moisture or topography or variations in target design. The presence of additional fuels between the source structure and the target structure, which may include landscaping components such as shrubs, mulch, and railroad ties, were also not considered. Inclusion of these more complex conditions was beyond the scope of the current work.

The experimental set-up, details of the sheds and fuel loading, and descriptions of the instrumentation and data collection system are provided in the following subsections. The results section includes analysis and discussion of measured thermal exposure quantities for the various experimental configurations. Finally, minimum SSDs for combustible and noncombustible sheds are suggested based on technical findings derived from the results of this test series.

3.1. Experimental Set-up

The experimental set-up for the outdoor shed burn experiments is shown in Fig. 19, including the wind machine, flow straightener, bidirectional probe array, and target structure. This is consistent with the cold flow measurements described in Section 2. The shed (fire source) and a free-standing heat flux gauge rig were placed within the wind field according to the desired SSD and shed configuration.
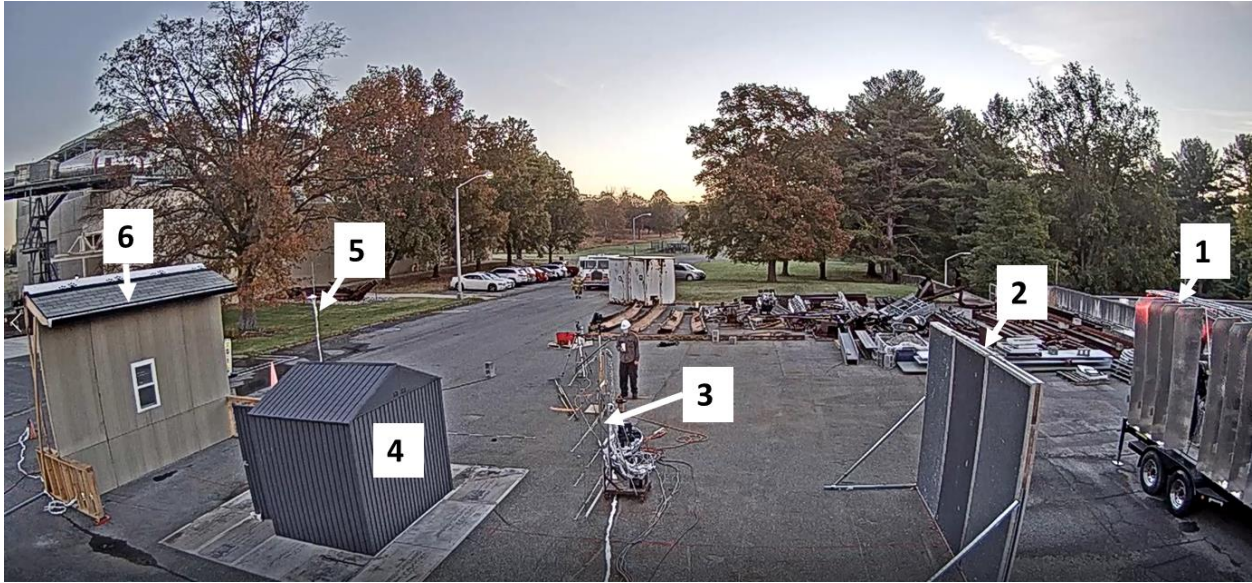
Fig. 19. Photograph taken from site camera # 6 showing experimental set-up including 1: Wind Machine, 2: Flow Straightener, 3: Array of Bidirectional Probes, 4: Shed, 5: Off-Target Heat Flux Rig, and 6: Target Structure.

3.1.1. Target Structure Specifications

The target structure (i.e., a single-story residential structure façade) shown in Fig. 20 comprised a wall-roof assembly with a centered double-pane window, open eaves, and an eave vent. The target wall was designed to have nominal dimensions of 13 ft × 16 ft (height × width), similar to the target used in previous indoor shed burn experiments [21]. A support assembly anchored the target wall to the hard asphalt surface at both the front and the back. The front supports were not enclosed in order to limit the impact on local wind fields.

The target wall was constructed to standards exceeding the minimum fire protection requirements specified by the California Building Code. Chapter 7A of the California Building Code specifies a test method (SFM-12-7A-1) for assessing the performance of exterior wall assemblies exposed to direct flames. According to test method SFM-12-7A-1, a wall assembly meets these test requirements if no flame penetration is observed through the assembly and there is no evidence of glowing combustion on the unexposed side.

The asphalt shingle roof had a pitch of 5:12 and an open-eave configuration. The wall was constructed with nominal 2×4 wood studs. The central section of the wall, within the red square highlighted in Fig. 20(b), was constructed as a complete exterior wall assembly, with a 5/8-in drywall interior layer, 1-in-thick mineral fiber cavity insulation, and an exterior layer of oriented strand board (OSB) covered with noncombustible cement board. Outside of the highlighted red square, the wall was not fitted with insulation or the interior layer of drywall. The central section of the wall was interchangeable, saving the effort of re-building the entire target structure in case of excessive thermal damage or wall burn through. This approach also simplified construction, facilitated faster cooling for the re-use of the target structure, and resulted in light-weight wall assembly.

One experiment tested the effects of thermal exposure from a burning shed on a combustible (non-fire hardened) exterior wall. For this experiment, the exterior cement boards were removed

from the area surrounding the window, thereby exposing the OSB layer. The painted brown area surrounding the window in Fig. 21 is the combustible section of the target structure. This target wall represents a situation where the exterior vinyl siding has melted away due to thermal exposure and exposed the OSB.

Fig. 20. Photograph showing (a) front view and (b) rear view of the target structure. The area highlighted by the red outline denotes the portion of the replaceable complete wall assembly.
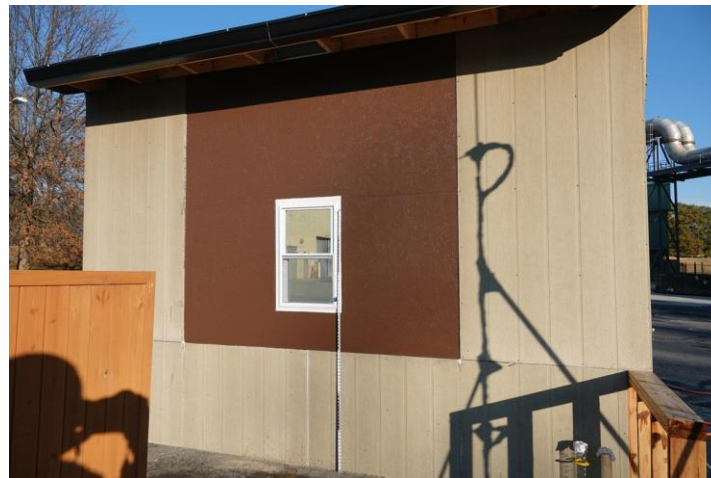
Fig. 21. Photograph showing the target structure with exposed OSB (painted in brown) without the outer layer of noncombustible cement board.

A commercially-available fire-resistant eave vent with an intumescent coating was installed in the central rafter bay above the window. The front and rear views of the eave vent are shown in Fig. 22. The core of the vent was made of aluminum honeycomb coated with a proprietary intumescent coating and encased within a galvanized metal casing. This eave vent is listed as conforming to Chapter 7A of the California Building Code for residential construction in WUI areas. Also in compliance with Chapter 7A of the California Building Code, the underside of the roof rafters on the unexposed side was fire hardened using noncombustible drywall lining. This fire hardening is necessary to resist structure ignition from the intrusion of flames through the vent.
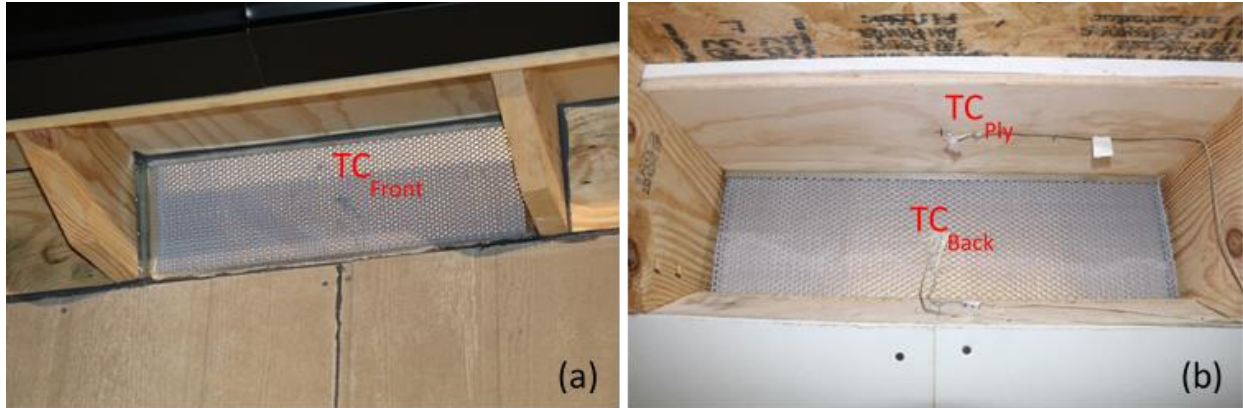
Fig. 22. Photographs showing eave vents with (a) front and (b) rear TCs.

A vertical double-pane window with a vinyl frame and fiberglass screen had dimensions of 3 ft (high) × 2 ft (wide). Similar window configurations are commonly used in bathrooms, for example. Exterior window screens are typically required for WUI construction compliance; metal or fiberglass screens are used to resist ember entry, and they are also known to reduce the amount of radiant heat transmitted to the glass [29].

3.1.2. Source Structures (Storage Sheds)

The outdoor shed burn experimental series tested combustible wood sheds and noncombustible steel sheds of various sizes. Plastic sheds were excluded from this outdoor experimental test matrix due to environmental concerns associated with combustion products released by burning plastic. The shed sizes tested included closet (C), very small (VS), and small (S). The photographs of the sheds tested are shown in Fig. 23. The shed dimensions and dimensions of the door openings are provided in Table 4.

Fig. 23. Photographs of combustible and noncombustible sheds of different sizes. (Images not to scale)

Table 4. Shed dimensions and storage capacity. (1ft = 0.305 m)

Shed Type	Measured shed dimensions, inches			Measured door dimensions, inches		Area of door opening, ft²	Measured footprint, ft²	Nominal shed storage capacity, ft³
	Height, minimum/ maximum	Width	Depth	Height	Width			
Wood Closet	52/53	63	36	47	60	20	16	68
Wood Very Small Shed	60/64	67	56	52	63	23	26	128
Wood Small Shed	74/92	100	97	70	56	27	67	405
Steel Closet	45/53	58	37	47	53	17	15	54
Steel Very Small Shed	45/52	55	51	49	59	20	20	73
Steel Small Shed	74/92	96	72	63	63	23	48	296

3.1.3. Instrumentation Data and Acquisition

Measurements from thermocouples, heat flux gauges, velocity and bidirectional probes were collected using National Instruments (NI) hardware. An NIcDAQ-9184 data acquisition (DAQ) chassis populated with NI-9213 I/O-Modules for thermocouples and NI-9219 modules for sensors with voltage outputs were used to sample the output from the heat flux sensors and thermocouples at a frequency of 1 Hz.

Ambient temperature was recorded at an average frequency of 1 Hz using an NI PXI-Chassis, populated with a PXIe-4353 module. Anemometer, bidirectional probe, and reference pressure outputs were sampled with an NI 8-slot compact DAQ chassis NI cDAQ-9188, populated with NI-9205 modules. Analog outputs from probes digitized as voltage signals with range set to ±10 V RSE (referenced single-ended mode) were recorded at an average frequency of 1 Hz. The mean and standard deviation values were also recorded.

Experiments were recorded by five video cameras. Three high definition (HD) video cameras (Cameras 1-3) were used to record the shed burning from different side views, while one sacrificial webcam (Camera 5) was placed on the ground facing upward to monitor eave ignition. An IR camera (Camera 4) facing the unexposed side of the target was used to monitor thermal heating of the wall. However, the data from the IR camera are not reported or discussed in this report. A 360° camera (Camera 6) was used to capture video of the entire test site during the shed burning. The locations of the video cameras are as shown in Fig. 24. Not shown in Fig. 24 is the camera under the roof, facing the eaves above.

Synchronization of the video data and instrument data was enabled through a central timing capability. A coordinate system was used to identify the location of instrumentation in the test set-up. The global origin of the coordinate system is marked at the front center of the target structure as shown in Fig. 24. The specific locations and orientations of the instrumentation for these experiments are provided in Table 5.
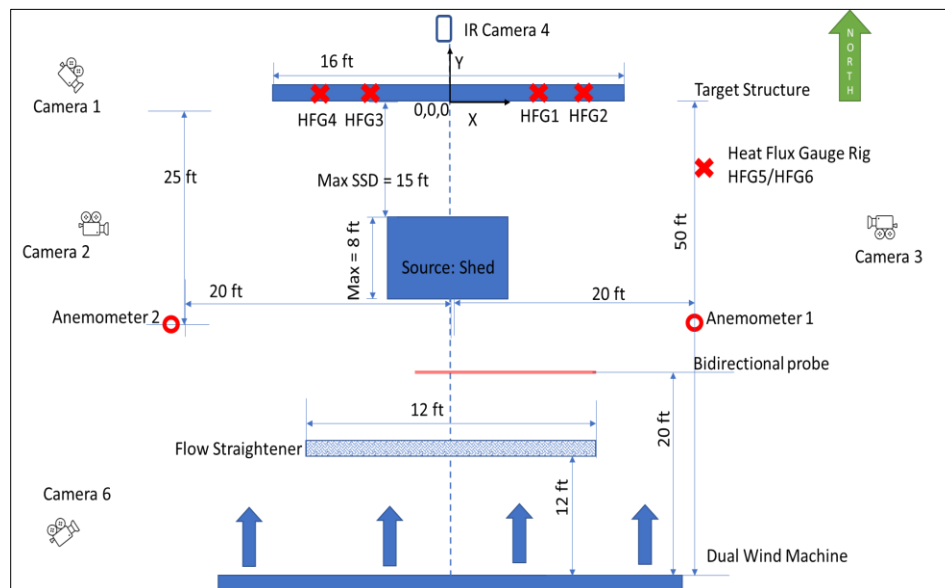
Fig. 24. Test set-up and instrumentation schematic for outdoor shed burn experiments. (Figure not to scale) (1ft = 0.305 m)

Table 5: Locations and orientation of instrumentation with reference to the global origin (front center of the target structure). (1ft = 0.305 m)

Device	ID	X, East+ (cm)	Y, North+ (cm)	Z, Up + (cm)	Orientation
Heat flux gauge	HF1	122	0	340	Facing shed
Heat flux gauge	HF2	183	0	340	Facing shed
Heat flux gauge	HF3	-122	0	340	Facing shed
Heat flux gauge	HF4	-183	0	340	Facing shed
Heat flux gauge	HF5	-500	=SSD/2	100	Facing plume between shed and target wall
Heat flux gauge	HF6	-500	-152	300	Facing plume between shed and target wall
Thermocouple	TCventF	-4	0	416	-
Thermocouple	TCventR	0	0	416	-
Thermocouple	TCply	10	0	427	-
Thermocouple	TCeave1	122	0	340	-
Thermocouple	TCeave2	183	0	340	-
Thermocouple	TCeave3	-122	0	340	-
Thermocouple	TCeave4	-183	0	340	-
Anemometer	Anemometer 1	762	-609	183	-
Anemometer	Anemometer 2	-760	-609	183	-
HDMI Camera	Camera 1	-747	480	115	Rear northwest (facing shed)
HDMI Camera	Camera 2	-716	-343	118	Side west (facing shed)
HDMI Camera	Camera 3	924	-610	145	Side east (facing shed)
IR Camera	Camera 4	0	-633	38	Facing target wall rear
Web Camera	Camera 5	0	0	0	Facing up toward eave
Site Camera	Camera 6	762	-1128	396	Facing target wall

3.1.3.1. Heat Flux Measurements

Commercially available (manufactured by Medtherm) 25 mm diameter, water-cooled Schmidt-Boelter heat flux gauges were used to measure the total incident heat flux (combined radiative and convective) at the eaves of the target structure. A total of six heat flux gauges were used. The viewing angle of 150° was similar for all gauges used in this study. Four heat flux gauges (HF1, HF2, HF3, and HF4) were placed in the eave rafter bays, two on each side of the centrally located eave vent. Two heat flux gauges were mounted on a rig at a height of 3 ft (HF5) and 10 ft (HF6) above the ground. The heat flux gauge rig was located between the target structure and the shed to view the fire plume. The locations and orientations of the heat flux gauges are provided in Table 5.

3.1.3.2. Temperature Measurements

Type-K thermocouples were placed in the eaves near each heat flux gauge. The thermocouples were embedded into the wood by drilling small holes in the eaves. Additionally, three thermocouples were used to measure temperatures in the eave vent: one in the front of the vent measuring temperature of fire gases on the exposed side (exterior) and one on the unexposed (interior) side of the vent, as shown in Fig. 22 as TC_{front} and TC_{back}, respectively. The third thermocouple (TC_{ply}) was placed on the plywood at the unexposed side of the vent. All thermocouples had a full range value of 1250 °C, and the standard relative uncertainty in temperature measurements reported by the manufacturer was ± 0.75 %.

3.1.3.3. Moisture Measurement

The moisture content of the wood cribs and of the wood in the eaves was measured on a dry basis using a hand-held moisture meter for solid wood. To operate the hand-held moisture meter, two probes about 3 cm apart were pressed into the wood to measure the conductivity of an electrical circuit including the pins and the wood. The principle of electrical resistance works because moisture conducts electricity well and dry wood is an effective insulator. Resistance-type meters express moisture content as a percentage of the oven-dry weight of the wood.

These instruments work well for wood moisture content between the saturation point of wood fiber (25 % to 30 %) down to around 6 %. Typical wood moisture content is usually within this range. Below 6 %, the accuracy is uncertain due to the high electrical resistance in dry wood [30].

3.1.4. Test Matrix

The outcomes of the indoor shed burn experiments [21] provided guidance for the selection of structure separation distances (SSDs) for the testing of combustible and noncombustible sheds in the presence of wind. The possible test space, the tentative sequence of tests, and the rationale for each experiment were outlined in the preliminary test plan published earlier [22]. The flow charts showing hypothetical logical test sequences for noncombustible and combustible sheds are provided in Fig. 25 and Fig. 26, respectively. However, given the limited test days and logistic constraints, the actual test sequence was dictated primarily by the availability of sheds and wood cribs on the test day. The test matrix and the actual test sequence for the outdoor shed burns are provided in Table 6. The comments column in Table 6 describes the logical progression between tests. The test naming convention in Table 6 is similar to the one used for indoor shed burn experiments [21] and is as follows:

•   *Outdoor* (O) - *Material* [Wood (W), Steel (S)] - *Size* [Closet (C), Very Small (VS), and Small (S)] – *Fuel Loading* (h) - *Wind* (w) –*SSD* [# (ft)].

•   The letter "R" followed by a number at the end of the test name indicates a test replicate. For example, the first repeat for a Very Small wooden shed with high fuel loading, wind, and 10 ft SSD will have test number O-WVShw-10-R1.

Note that the orientation of the shed door opening, which forms part of the test naming convention in Fig. 25 and Fig. 26, is listed under Test ID in Table 6.
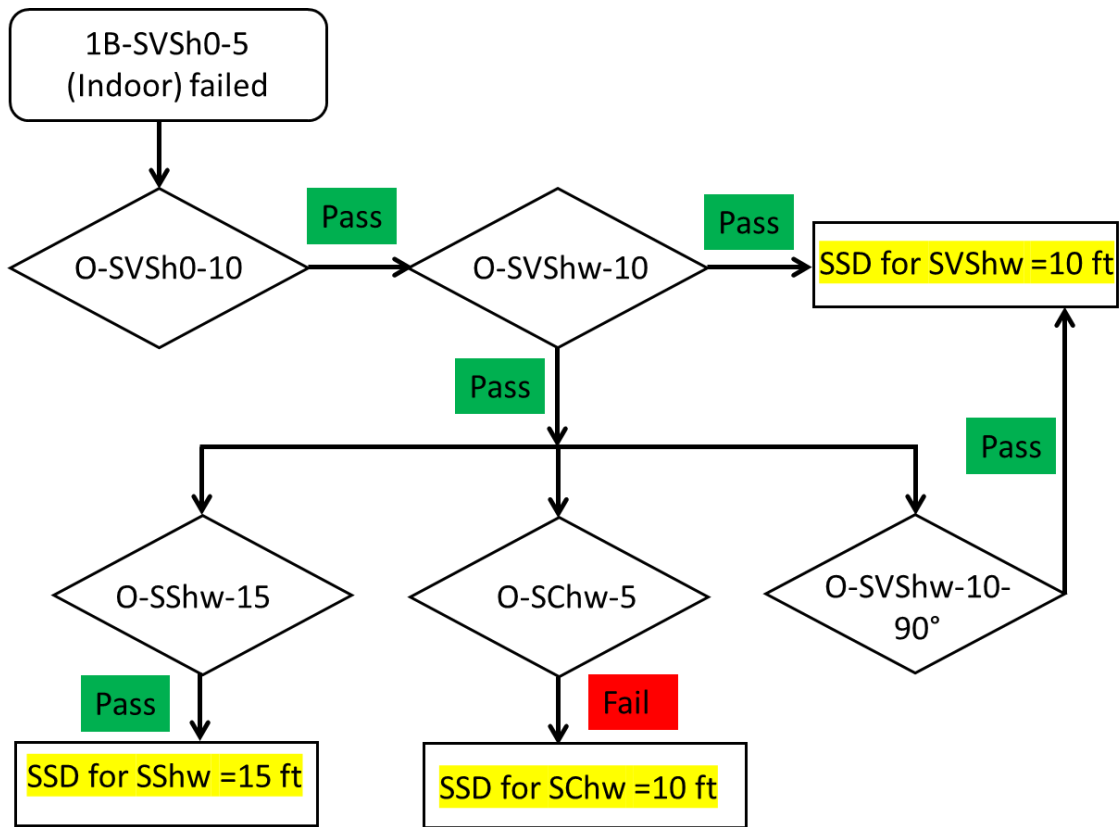
Fig. 25. Logical flowchart for noncombustible shed burns.
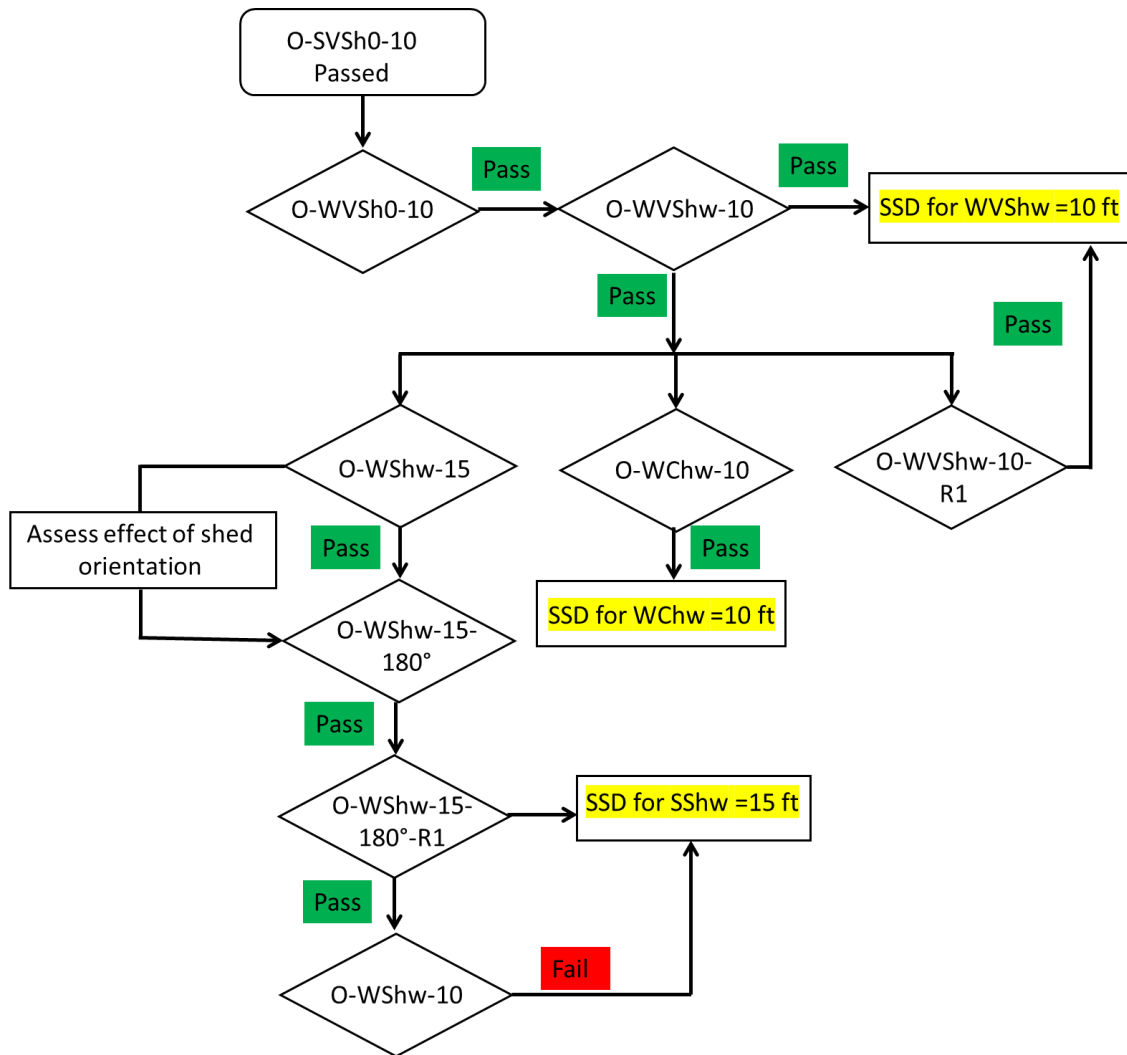
Fig. 26. Logical flowchart for combustible shed burns.

Table 6. Test matrix and sequence of outdoor shed burn experiments. (1ft = 0.305 m)

Serial number	Test ID	Shed Type	Shed Construction Material	Fuel Loading, (number of 1-A cribs)	SSD, ft	Wind	Comments
NOSSE 1	O-WVSh0-10	Very Small	Wood	6	10	No	Determine SSD_min for VS combustible shed in absence of applied wind field
NOSSE 2	O-SVSh0-10	Very Small	Steel	6	10	No	Determine SSD_min for VS noncombustible shed in absence of applied wind field
NOSSE 3	O-WVShw-10	Very Small	Wood	6	10	Yes	Determine SSD_min for VS combustible shed in presence of applied wind field and compare effects of wind on thermal exposure from combustible shed
NOSSE 4	O-SVShw-10	Very Small	Steel	6	10	Yes	Determine SSD_min for VS noncombustible shed in presence of applied wind field and compare effects of wind on thermal exposure
NOSSE 5	O-SChw-5	Closet	Steel	4	5	Yes	Determine SSD_min for noncombustible closet in presence of applied wind field
NOSSE 6	O-WChw-10	Closet	Wood	4	10	Yes	Determine SSD_min for combustible closet in presence of applied wind field
NOSSE 7	O-SShw-15	Small	Steel	12	15	Yes	Determine SSD_min for Small noncombustible shed in presence of applied wind field
NOSSE 8	O-WShw-15	Small	Wood	12	15	Yes	Determine SSD_min for Small combustible shed in presence of applied wind field
NOSSE 9	O-SVShw-10-90º Door opening:90º	Very Small	Steel	6	10	Yes	Study effect of shed orientation (door opening) on thermal exposure to the target structure
NOSSE 10	O-WVShw-10-R1	Very Small	Wood	6	10	Yes	Establish reproducibility of experimental set-up (Repeat of NOSSE 3)
NOSSE 11	O-WShw-15-R1 Door opening:180°	Small	Wood	12	15	Yes	Establish reproducibility of experimental set-up (door opening upwind)
NOSSE 12	O-WShw-10 Door opening: 180°	Small	Wood	12	10	Yes	Study effect of smaller SSD on thermal exposure to the target structure
NOSSE 13	O-WVShw-10-R2	Very Small	Wood	6	10	Yes	Study effect of thermal exposure on non-fire hardened target structure

1-A wood cribs were placed within the shed to simulate reasonable anticipated fuel loadings of various combustible items stored in residential storage sheds. The shed and fuel loading specifications for all shed burn experiments are provided in Table 7. A variety of combustible items that would have fuel loading equivalent to that used in Closet, Very Small, and Small sheds are listed in Table 8. The estimation method to determine equivalent fuel loading of various combustible items stored in various shed types is described in Appendix A. The fuel loadings presented in Table 8 are based on total fuel energy. The fuel geometry, oxygen availability, and fire growth will collectively impact the actual energy release (heat release rate), and therefore the contents presented are provided for illustration purposes and not as an actual energy release equivalent to the wood cribs used.

Table 7. Shed and fuel loading specifications for the sheds tested at NIST. (1ft = 0.305 m, 1 kg = 2.2 lbs)

Serial number	Test ID	Shed Type	Fuel Loading, (number of 1-A cribs)	Mass, kg			Fuel Density*, (MJ/ft²)
				Shed	Cribs	Total combustible	
NOSSE1	O-WVSh0-10	Very Small	6	76	128	203	151
NOSSE2	O-SVSh0-10	Very Small	6	42	131	131	126
NOSSE 3	O-WVShw-10	Very Small	6	72	131	203	150
NOSSE 4	O-SVShw-10	Very Small	6	42	138	138	132
NOSSE 5	O-SChw-5	Closet	4	24	95	95	122
NOSSE 6	O-WChw-10	Closet	4	50	96	146	175
NOSSE 7	O-SShw-15	Small	12	110	287	287	112
NOSSE 8	O-WShw-15	Small	12	261	283	544	156
NOSSE 9	O-SVShw-10-90º Door opening:90º	Very Small	6	42	140	140	134
NOSSE 10	O-WVShw-10-R1	Very Small	6	47	144	191	141
NOSSE 11	O-WShw-15-R1 Door opening:180°	Small	12	268	290	558	160
NOSSE 12	O-WShw-10 Door opening: 180°	Small	12	261	285	546	156
NOSSE 13[§]	O-WVShw-10-R2	Very Small	6	47	147	194	143

[§] Non-fire hardened target structure was used for this test.
* Fuel density is defined as energy per unit area of shed floor space and has units of MJ/ft².

Table 8. Fuel loading specifications and equivalent combustible items in storage sheds. (1 kg = 2.2 lbs)

Source Shed	Crib Mass, kg	Crib HOC, MJ	Estimated combustible items in storage sheds (count of items)
Closet	95±1	1830±10	Pine wood 2 × 4 (8), Plywood 3/8 sq ft (32), 4 tier Plastic shelving (1), Motor oil qt (2), Rubber garden hose (0) , Plastic garden hose reel (1), Plastic watering can (1), Rake handle (1), Plastic rake (1), Plastic bucket w/top (1), Garden tool handle (3), Plastic flower pots (6), Wooden croquet set (1), Plastic milk crate (2) , Plastic frisbee (1), Black plastic tote w/top (1), Small plastic lawn spreader (1), Can liner (1), Plastic trash can w/lid (1)
Very Small Shed	140±10	2458-2822	Pine wood 2 × 4 (18), Plywood 3/8 sq ft (48), 4 tier Plastic shelving (1), Motor oil qt (2), Rubber garden hose (1) , Plastic garden hose reel (1), Plastic watering can (1), Rake handle (1), Plastic rake (1), Plastic bucket w/top (1), Garden tool handle (4), Plastic flower pots (9), Plastic milk crate (1), Black plastic tote w/top (1), Small plastic lawn spreader (1), Can liner (1), Plastic trash can w/lid (1), Propane tank (1), Paper leaf bags (1), Plastic planter (1), Plastic flower pot base (2)
Small Shed	270±10	5434-5568	Pine wood 2 × 4 (32), Plywood 3/8 sq ft (96), 4 tier Plastic shelving (2), Motor oil qt (2), Rubber garden hose (0) , Plastic garden hose reel (1), Plastic watering can (1), Rake handle (1), Plastic rake (1), Plastic bucket w/top (1), Garden tool handle (4), Plastic flower pots (6), Wooden croquet set (1), Plastic milk crate (2) , Plastic frisbee (1), Black plastic tote w/top (1), Large plastic lawn spreader (1), Can liner (1), Plastic trash can w/lid (1), Automobile tire (2), Propane cylinder (1), Plastic rake (large), Plastic bucket (2), Plastic recliner (2), Plastic kid's water table (1), Plastic patio chair (1), Gasoline can (1)

3.1.5. Test Procedure

The shed and wood crib masses were measured and recorded at the start of each test. Measured moisture content for wood cribs was below 8 %. The moisture content of the wood in the eaves and the underside of the roof was also measured. The moisture content of wood in these areas varied between 7 % and 15 %.

The shed and the wood cribs were placed at pre-determined locations determined by SSD and door orientation. The door opening faced the target structure unless indicated otherwise. In all the tests, the shed door was kept fully open to represent worst case fire growth and exposure scenarios and to minimize complexities in fire growth rate arising from reduced ventilation. Closed doors would significantly alter the fire spread within the shed and hence the thermal exposure. The wind machine was started and maintained at 'idle' speed of 760 rpm. When the test preparatory tasks were completed, the wood crib assembly inside the shed was ignited using 300 mL of heptane in an aluminum pan of nominal dimensions 90 mm × 130 mm × 30 mm. This method of wood crib ignition is known to be reproducible [31]. The heptane in the aluminum pan was ignited using a propane burner, and ignition time was manually entered in the data acquisition system. At the same time, a digital display clock was started.

After ignition, and as the burning of the combustible fuel developed, the speed of the wind was increased gradually until the flames leaned into the eaves of the target structure. It is important to note here that the objective of the experiments was not to study the effects of wind speeds on plume lean. A pre-determined wind speed was not implemented; the wind was adjusted so that the flames leaned into the closest possible contact with the target structure to present worst-case scenarios. Once this condition was achieved, the speed of the wind machine was kept constant until the end of the experiment. The experiment continued until the shed and the wood cribs had collapsed and flames were no longer visible. In the case of the noncombustible steel sheds, the experiment ended after the wood cribs had collapsed and flames were no longer visible. At this point, the experiment was terminated and the data acquisition was stopped.

Digital still cameras were used to take images from several directions and distances during each experiment to visually document the exposure conditions, and after the burn to document the damaged parts of the target structure.

Tests were performed on dry days (no precipitation in forecast from 5 am to noon) when wind direction and wind speed were conducive to fire tests. The criterion for wind coming from the south (in-line with the wind machine) was 10 mi/h or less. From other directions, wind speed of less than 5 mi/h was considered acceptable for conducting the tests.

3.1.6. Effects of Combustible Shed Size on Thermal Exposure

Comparison of heat flux profiles for O-WChw-10 (NOSSE6), O-WVShw-10 (NOSSE3), and O-WShw-10 (NOSSE12) shows the effects of combustible shed size on thermal exposure on the target structure. In these three tests, the combustible sheds (Closet, Very Small and Small shed) were located 10 ft away from the target structure (SSD = 10 ft). The sheds had high fuel loadings of 1-A wood cribs, and the total combustible fuel (shed plus wood cribs) for O-WChw-10, O-WVShw-10, and O-WShw-10 was 146 kg, 203 kg, and 825 kg, respectively.

Heat flux profiles of measurements taken at HF1 for these three different sizes of wooden source structures are shown in Fig. 27. The heat fluxes at the target structure peaked at 30 kW/m² ±

5 kW/m², 20 kW/m² ± 5 kW/m², and 10 kW/m² ± 5 kW/m² for the Small shed, Very Small shed and Closet, respectively. The peak heat flux recorded at the target structure (HF1) was the highest for test O-WShw-10, corresponding to the highest amount of combustible fuel. The delayed and rapid increase in heat flux for the Small shed (O-WShw-10) shown in Fig. 27 is attributed to a different door orientation, facing upwind away from the target. The door openings of the Closet and the Very Small sheds were facing the target structure. The more gradual increase in heat flux in these two tests was due to direct exposure of the wood crib burning to the target structure throughout. Due to the limited number of tests, a direct comparison with the Small shed door opening facing the target structure was not possible. However, some inferences can be drawn from tests comparing effects of shed size on thermal exposures.
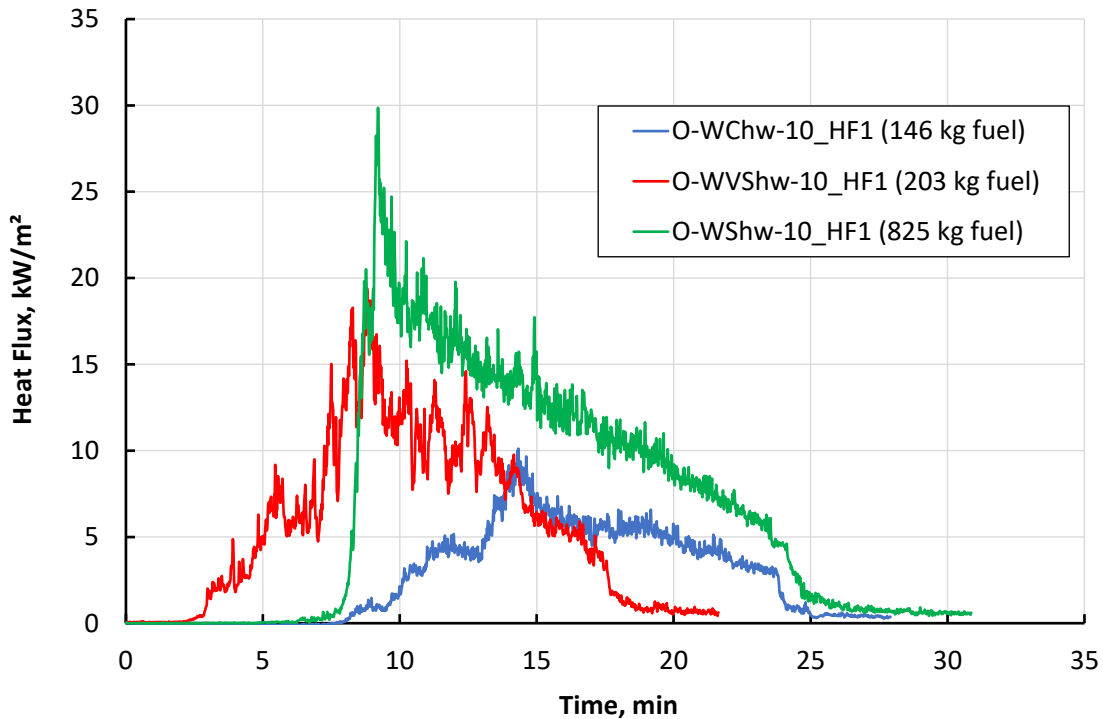
Fig. 27. Temporal profiles of heat flux data showing effects of shed size on heat flux measurement in the eave (HF1) for combustible source structures in tests O-WChw-10, O-WVShw-10, and O-WShw-10.

The incident heat flux at the target structure with the Very Small shed grew faster than that with the Closet. The fire growth rate for the wood Very Small shed in test O-WVShw-10 is faster than that for the Closet (test O-WChw-10). This could be attributed to the higher combustible mass of the Very Small shed, its higher fuel loading, or its lower fuel per unit area. The lower fuel density, shown in Table 7, could result in more re-radiation between the burning wood cribs and shed structure, thereby causing faster pyrolysis. Additionally, the Very Small shed is taller than the Closet as shown in Fig. 28. This configuration of fuel resulted in flames reaching higher to the eaves and increasing the heat flux compared to the shorter fuel arrangement in test O-WChw-10. The flames in O-WChw-10 only reached slightly above the window height, thereby registering lower heat fluxes in the eaves.
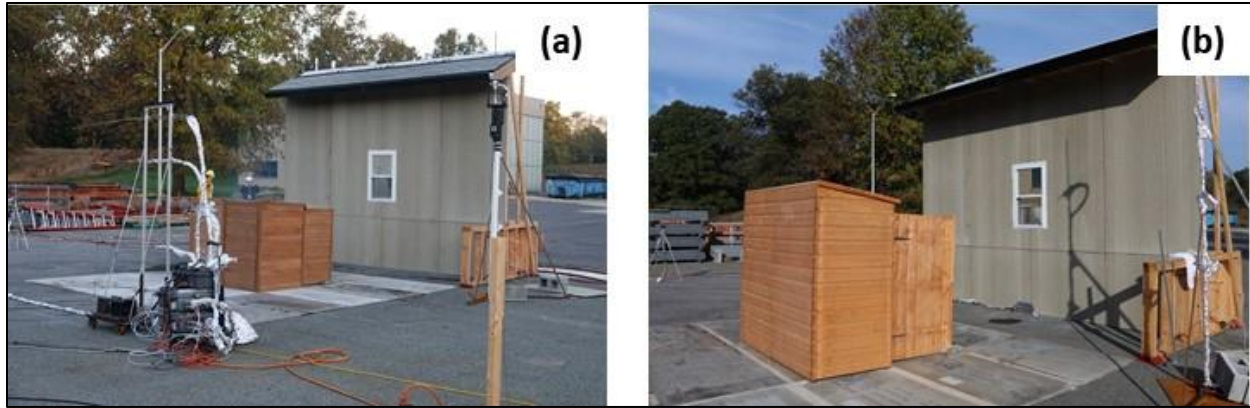
Fig. 28. Photographs showing shed configurations with respect to the target structure for wood (a) Closet in Test O-WChw-10 and (b) Very Small shed in Test O-WVShw-10.

The delayed thermal exposure from the Small shed was due to its orientation with respect to the target structure. The door opening of the Small shed in test O-WShw-10 was facing away from the target structure, resulting in a delay in radiant and convective exposure to the target structure. Photographs of the three burning source structures are shown in Fig. 29. While the measured peak heat flux corresponded to the amount of total combustible fuel, the orientation of the source structure with respect to the target structure had a significant effect on the measured temporal profiles of heat fluxes. The effect of shed orientation on the thermal exposure is further examined in the following section.
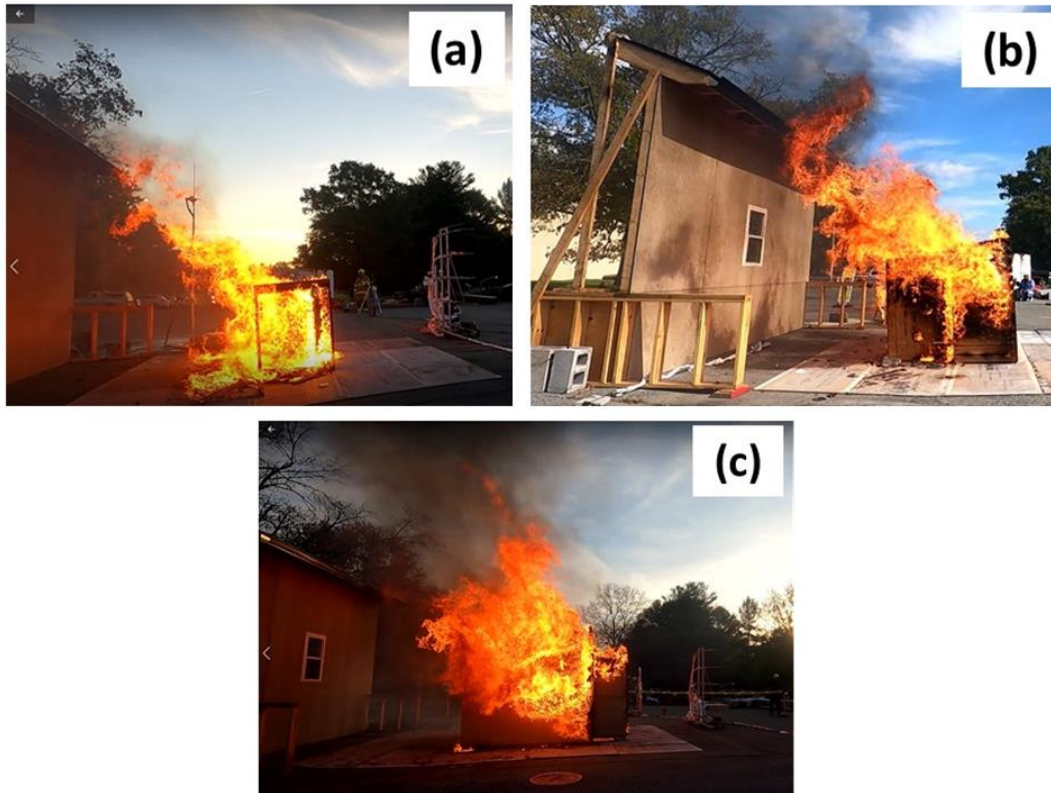
Fig. 29. Photographs showing thermal exposures from burning of wood (a) Closet in Test O-WChw-10 (door opening downwind), (b) Very Small shed in Test O-WVShw-10 (door opening downwind), and (c) Small shed in Test O-WShw-10 (door opening upwind).

3.2. Thermal Exposure Results

In this study, total heat flux, temperature measurements, visual observations of direct flame exposure, and examinations of post-exposure damage were used to characterize thermal exposure to the target structure from burning sheds.

Images captured from video cameras were used to provide an overview of each shed burn experiment. The experimental data for each experiment, including the test and shed specifications, are provided in Appendix B. The experimental data includes temporal plots of heat fluxes at the eaves and on the free-standing heat flux gauge rig. Temporal plots of temperature data collected at the eaves and at the eave vent are also included. The overview photograph shows the shed orientation with respect to the target structure at the time when peak heat fluxes were recorded.

The incident heat flux at the eaves was a function of shed size, shed construction, door opening, fuel loading, and SSD. The heat flux gauges in the center (on either sides of the eave vent), located closer to the fire plume, registered higher heat fluxes as compared to the gauges situated farther away from the eave vent. Peak heat flux values and temperatures are tabulated for each experiment in Table 9. The heat fluxes at the eave-rafter bays and at the rig are plotted as a function of time for each experiment in Appendix B. Due to the position (see Table 5) of the lower gauge near the constant flaming base of the fuels compared to the upper flux gauge near the intermittent flame and plume, the lower positioned heat flux gauge recorded greater heat fluxes.

The measured temperatures at the eaves began to rise from the ambient temperature and increased to a maximum of 214 ºC, which is significantly lower than the typical ignition temperature of wood (260 ºC).[2] Consequently, thermal degradation of the wood was not observed in any test except the last, for which the target structure was not fire hardened. The performance of vents based on temperature measurements is discussed in detail in Section 3.3.4.

The heat flux data presented in the subsections below have not been smoothed. Similarly, high fluctuations in the temperature-time curves, likely due to flame pulsations and the applied wind field, have not been smoothed. Table 9 provides a summary of peak heat flux and temperature measurements for all shed burn experiments, along with the times at which the peaks occurred.

The reproducibility of the measured quantities for repeated tests is reported in Section 3.2.1. The qualitative performance of the target structure, including the wall, window, and vent are discussed below in Section 3.3. Finally, depending on the thermal damage of the target structure, the minimum SSD_{min} for the source structures in this study are identified in Section 3.4.

---

[2] Ignition temperature of wood as measured by ASTM D1929.

Table 9. Peak heat flux and peak temperature measurements during outdoor shed burns. (1ft = 0.305 m, 1 kg = 2.2 lbs)

Serial number	Test ID	Shed Type	Fuel Loading, (number of 1-A cribs)	Total Combustible Mass, kg	Wind	SSD, ft	Peak HF, kW/m² (min)		Peak Temp, ºC (min)	
							Eaves	HF Rig	Eaves	Vent
NOSSE1	O-WVSh0-10	Very Small	6	204	NO	10	5 (11)	7 (11)	135 (5)	148 (5)
NOSSE2	O-SVSh0-10	Very Small	6	131	NO	10	5 (22)	6 (21)	112 (18)	169 (18)
NOSSE 3	O-WVShw-10	Very Small	6	203	YES	10	19 (9)	29 (9)	160 (8)	166 (8)
NOSSE 4	O-SVShw-10	Very Small	6	138	YES	10	7 (21)	5 (21)	76 (20)	80 (17)
NOSSE 5	O-SChw-5	Closet	4	95	YES	5	17 (15)	5 (15)	214 (15)	319 (16)
NOSSE 6	O-WChw-10	Closet	4	146	YES	10	10 (14)	11 (14)	113 (14)	136 (14)
NOSSE 7	O-SShw-15	Small	12	287	YES	15	3 (30)	5 (27)	56 (32)	50 (27)
NOSSE 8	O-WShw-15	Small	12	805	YES	15	10 (17)	15 (12)	100 (17)	95 (17)
NOSSE 9	O-SVShw-10-90º Door opening:90º	Very Small	6	140	YES	10	3 (23)	4 (27)	35 (23)	35 (23)
NOSSE 10	O-WVShw-10-R1	Very Small	6	190	YES	10	16 (10)	16 (10)	150 (10)	160 (10)
NOSSE 11	O-WShw-15-R1 Door opening:180°	Small	12	826	YES	15	8 (15)	15 (10)	100 (17)	85 (16)
NOSSE 12	O-WShw-10 Door opening: 180°	Small	12	825	YES	10	27 (9)	40 (9)	237 (9)	269 (9)
NOSSE 13	O-WVShw-10-R2	Very Small	6	241	YES	10	159 (7)	35 (7)	853 (7)	1029 (7)

### 3.2.1. Reproducibility of Outdoor Shed Burns with Wind

The reproducibility of outdoor shed burns was assessed by comparing the temporal profiles of heat flux and temperature measurements. Comparisons of the heat flux and temperature profiles for tests O-WVShw-10 (NOSSE3) and O-WVShw-10-R1 (NOSSE10) in Fig. 30, Fig. 31, and Fig. 32 show that the data for repeated tests had similar shapes, magnitudes, and burning periods. The growth and peak heat flux for O-WVShw-10-R1 in Fig. 30 are slightly delayed relative to the test O-WVShw-10. This can be attributed to lower ambient temperatures (< 10 °C) on the day of test O-WVShw-10-R1 (shown in Fig. 32(d)) as compared to 25 °C to 30 °C for test O-WVShw-10. These data show reproducibility of the measured quantities, with peak heat flux variation of 16 % in the eaves and variation of 45 % at the rig. The variation in temperatures recorded at the eaves was in the range of 4 % to 6 %. The data from this repeat experiment confirmed the experimental set-up, operating procedure, and repeatability of the experiments.
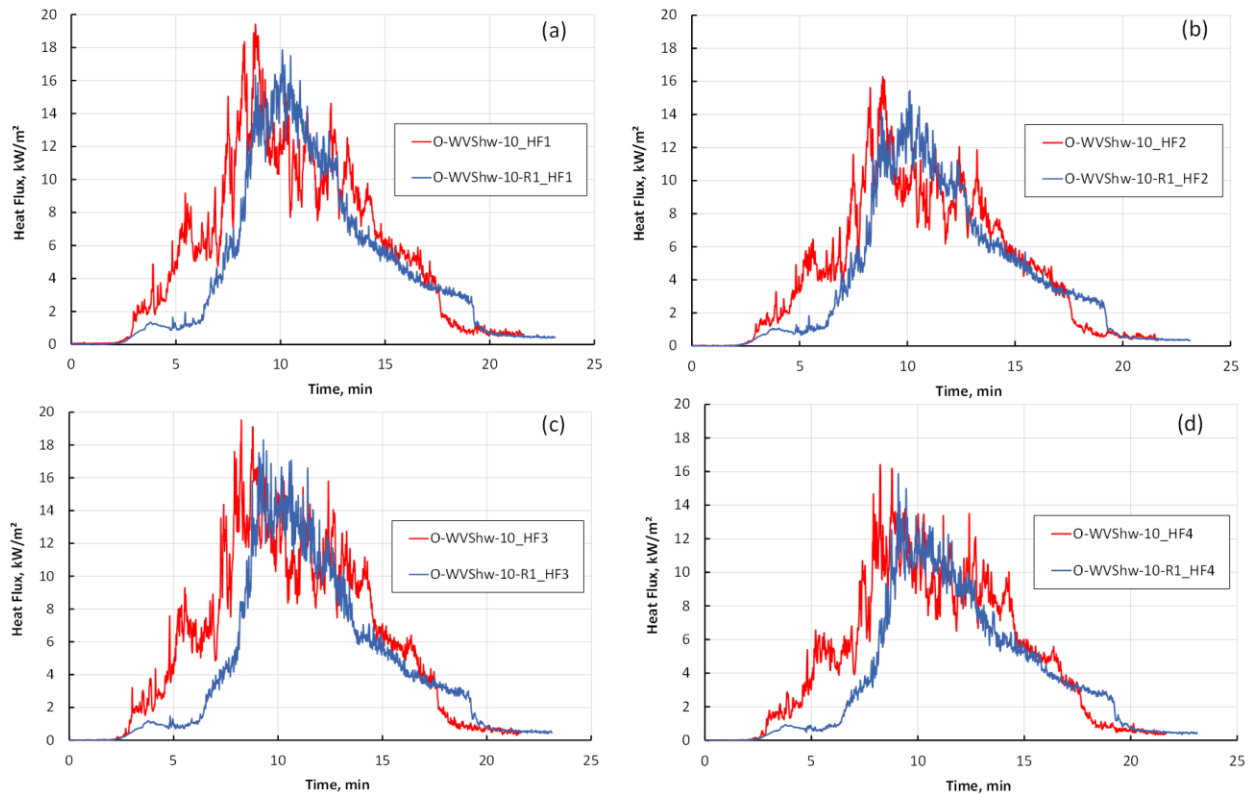
Fig. 30. Reproducibility of heat flux data recorded in the eaves at (a) HF1, (b) HF2, (c) HF3, and (d) HF4 for tests O-WVShw-10 and O-WVShw-10-R1.
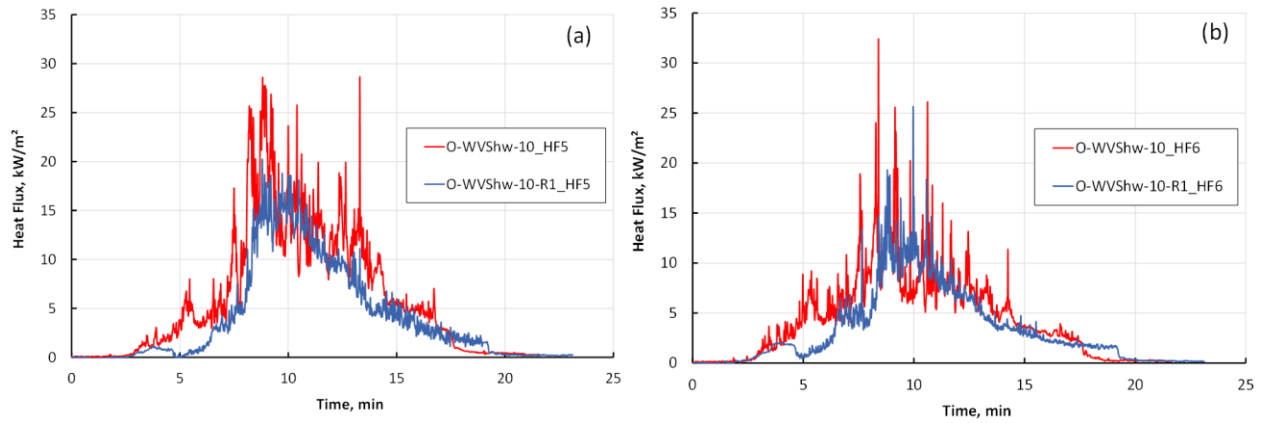
Fig. 31. Reproducibility of heat flux data recorded at the rig at (a) HF5 and (b) HF6 for tests O-WVShw-10 and O-WVShw-10-R1.
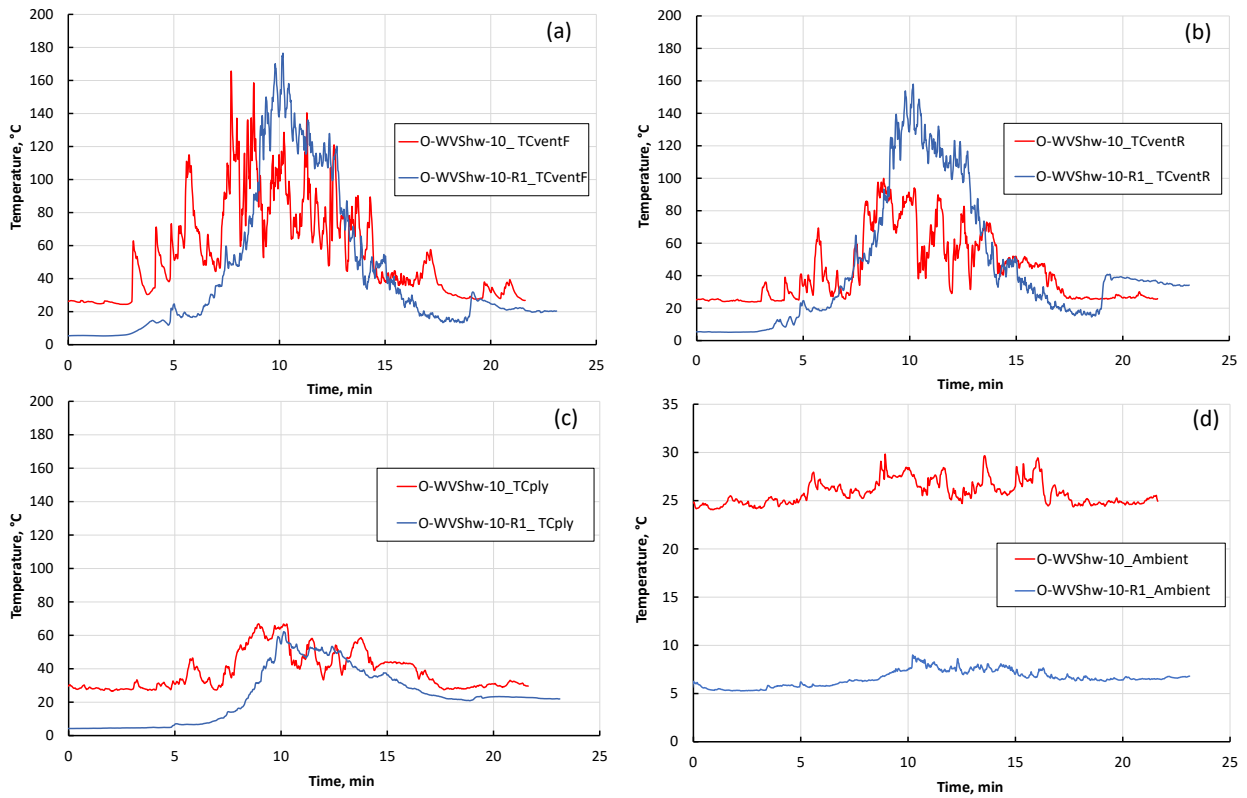
Fig. 32. Reproducibility of temperature data recorded by TCs (a) in front of the vent (TCventF), (b) behind the vent (TCventR), (c) on the plywood (TCply) behind the vent, and (d) ambient for tests O-WVShw-10 and O-WVShw-10-R1.

51
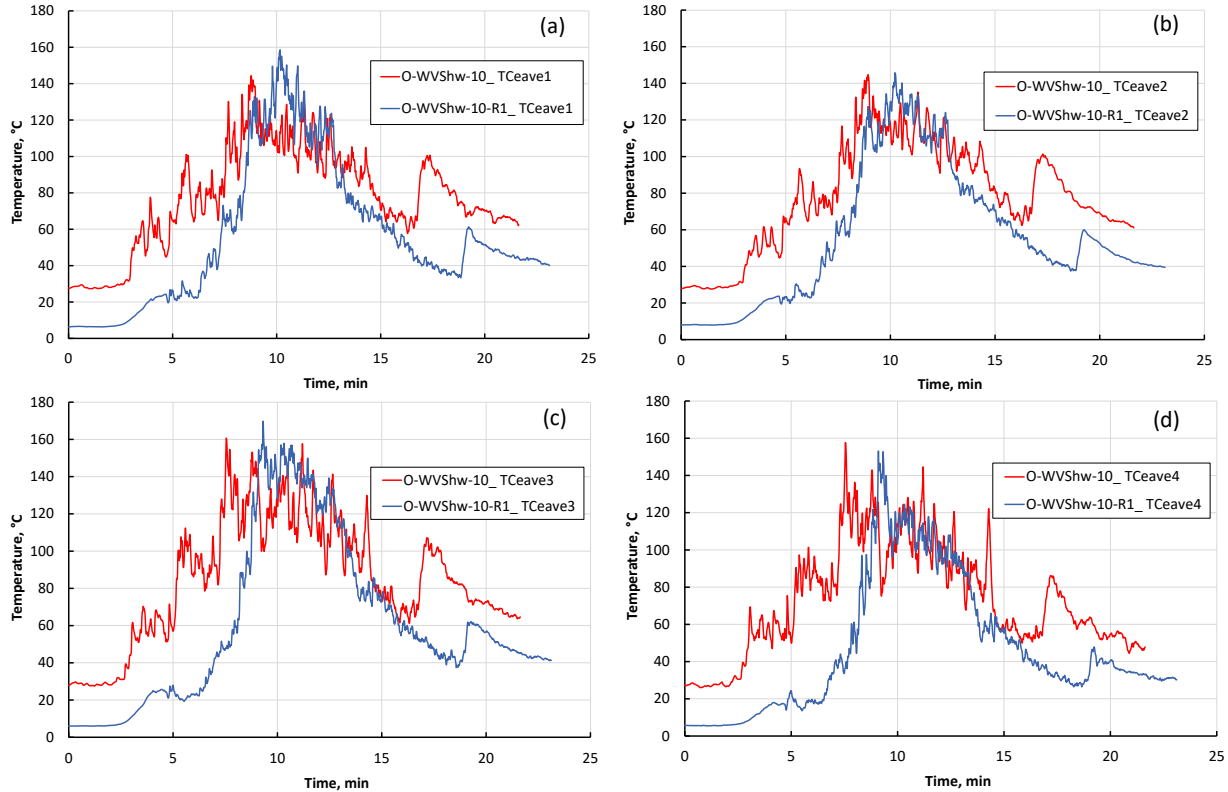
Fig. 33. Reproducibility of temperature data recorded by (a) TCeave1 (b) TCeave2, (c) TCeave3, and (d) TCeave4 for tests O-WVShw-10 and O-WVShw-10-R1.

3.2.2. Effects of Wind on Thermal Exposure

The wind has complex effects on the burning behavior of source structures as well as on the fire spread to the target structure. For the combustible source structures, the wind can cause turbulence and eddies, thus tilting the flames and affecting flame lengths. At the target structure, the wind entrainment provides excess oxygen that can accelerate piloted ignitions in presence of embers. The wind may preheat and remove the fuel moisture, thereby facilitating ignitability and flame spread on the target structure. For plume-dominated fires, the flame flow strongly responds to the buoyancy force generated by the fire, guiding the fire plume upward. For wind-driven fires, the flow is governed by inertial forces due to the wind, and the fire plume is strongly tilted in the direction of the wind [32]. If wind is blowing in the same direction as the fire front advance, flames are tilted forward and are brought closer to the unburned fuel, increasing the radiation impinging on the target structure, the preheating range (leading to faster release of volatiles), and thus the rate of spread.

The effects of forced wind on the burning behavior of combustible and noncombustible source structures are shown in Fig. 34 and Fig. 35, respectively. The burning behavior of the combustible shed in calm wind conditions is primarily driven by the buoyancy force. The upward fire plume generated by the buoyancy force in the absence of applied wind can be noted for test O-WVSh0-10 (NOSSE1) in Fig. 34 (a). In the presence of an applied wind field in test O-WVShw-10 (NOSSE3), the fire plume is tilted towards the target structure, as shown in

Fig. 34 (b). In this case, the wind inertia forces exceed buoyancy forces, thereby tilting the flames in the direction of the wind.

The heat flux measurements for Test O-WVSh0-10 and Test O-WVShw-10 are plotted as a function of time in Fig. 36 (a). The source structure for both tests included a wood Very Small shed with high fuel loading of six 1-A cribs. While all other test specifications were the same, an artificial wind field was applied during Test O-WVShw-10. The SSD for both outdoor tests was 10 ft. Outdoor Test O-WVSh0-10 is a repeat experiment of indoor test 1B-WVSh0 [21]. The indoor experiment with wood Very Small shed with fuel loading of six 1-A cribs generated a fire with peak heat release rate (PHRR) of 4.8 MW.

The heat flux measurements in the eaves recorded less than 5 kW/m² for the full duration of the shed burn in Test O-WVSh0-10 in the absence of an applied wind field. With wind applied, the temporal profile of the heat flux measurements at HF1 for Test O-WVShw-10 in Fig. 36 (a) shows significantly higher heat fluxes. In this case, the heat fluxes in the eave remained above 5 kW/m² for nearly the full duration of the shed burn. A peak heat flux of 19 kW/m² was registered for Test O-WVShw-10. The wind affects flame lengths and enhances convective heat transfer to the target structure, causing preheating with likely localized removal of moisture.

Visual observations during the noncombustible shed burn experiments, Test O-SVSh0-10 (NOSSE2) and Test O-SVShw-10 (NOSSE4), indicated that the fire plume was primarily dominated by the dimensions of the door opening. The plume tilt towards the target structure in Fig. 35 (a) and Fig. 35 (b) are similar except that the wind eddies seem to cause a thinning effect on the fire plume, thereby stretching the flame longer for Test O-SVShw-10. However, Fig. 32 (b) shows that the heat flux measurements for both experiments, with and without wind, are similar, with peak heat flux of approximately 5 kW/m².
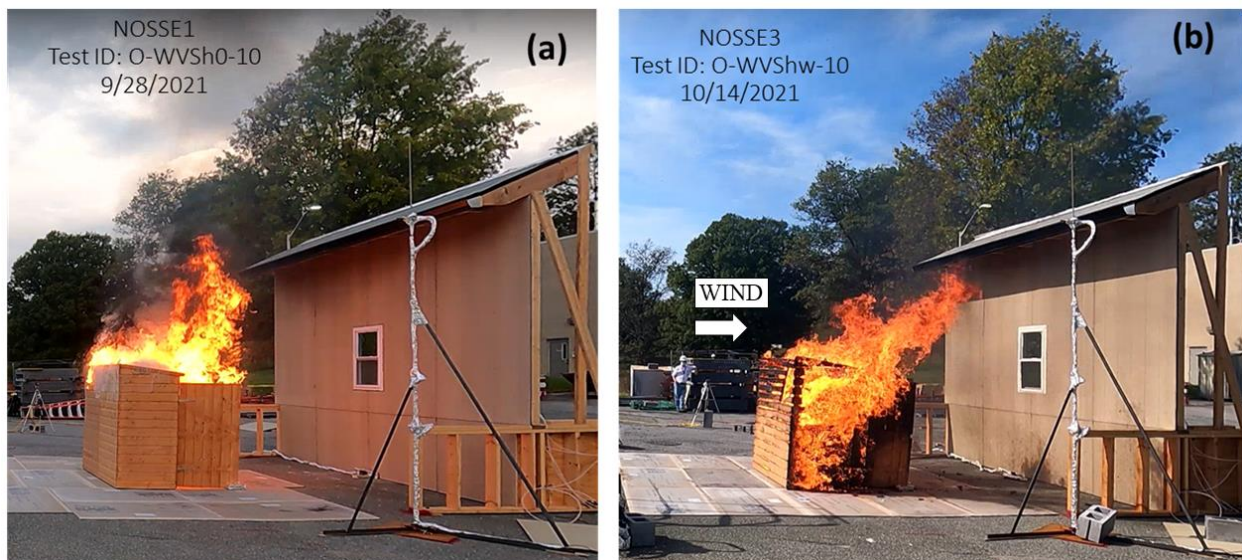
Fig. 34. Photograph captured from videos recorded by Camera #3 showing effects of wind on the fire plume from combustible source structures in (a) Test: O-WVSh0-10 and (b) Test: O-WVShw-10.
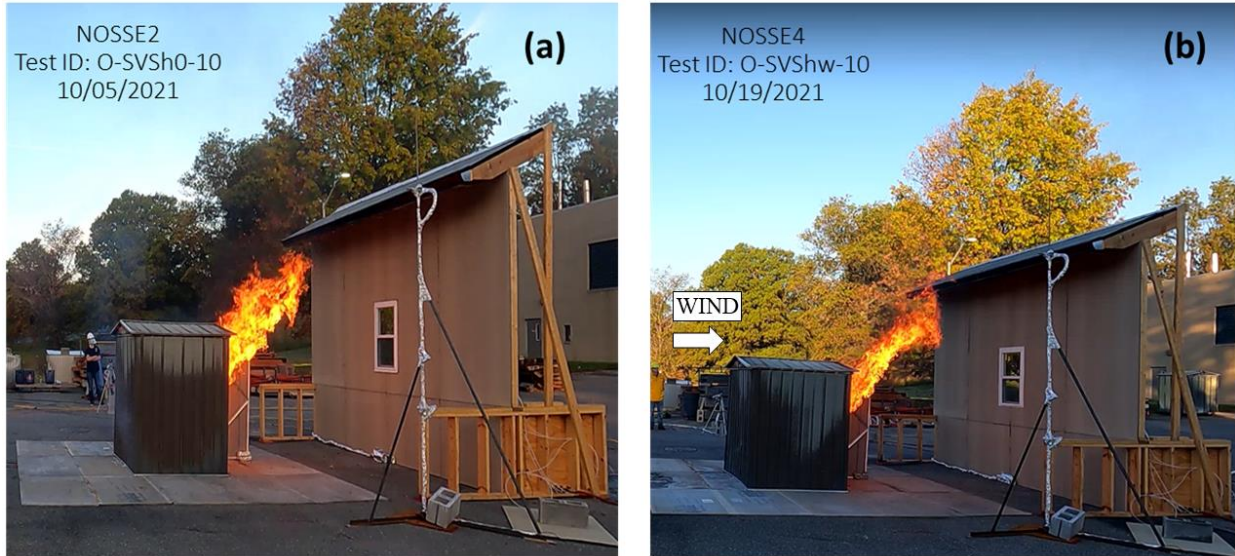
Fig. 35. Photograph captured from videos recorded by Camera #3 showing effects of wind on the fire plume from noncombustible source structures in (a) Test: O-SVSh0-10 and (b) Test: O-SVShw-10.
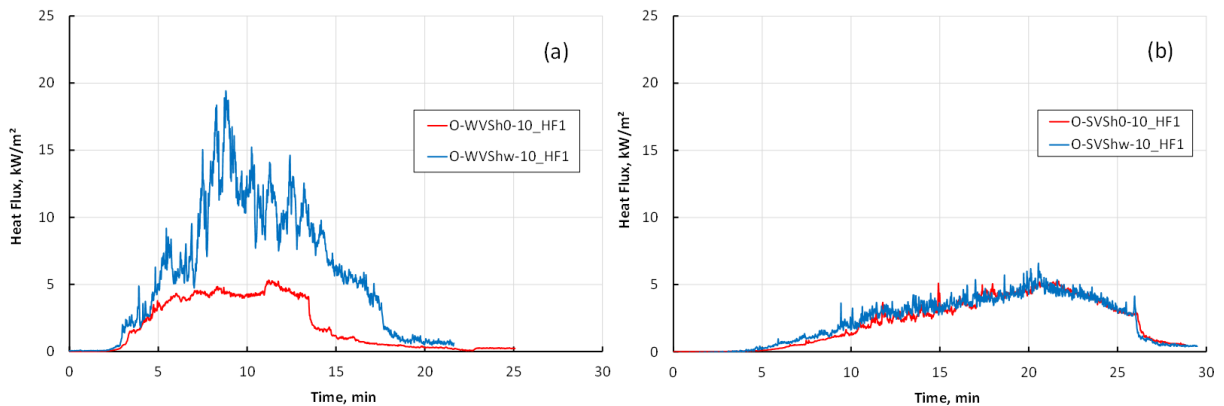
**Fig. 36.** Temporal profiles of heat flux data showing effects of wind on heat flux measurements in the eave (HF1) for (a) wood sheds in tests O-WVSh0-10 and O-WVShw-10, and (b) steel sheds in tests O-SVSh0-10 and O-SVShw-10.

3.2.3. Effects of Shed Orientation on Thermal Exposure

The effects of shed orientation on the thermal exposure to the target structure were studied for both noncombustible and combustible sheds. The photographs in Fig. 37 show two different orientations of the steel Very Small shed with respect to the target structure. Fig. 37(a) shows the door opening of the steel Very Small shed in test O-SVShw-10 (NOSSE4) facing downwind and toward the target structure, while Fig. 37(b) shows the door opening in O-SVShw-10-90° (NOSSE9) facing the heat flux gauge rig, perpendicular to the target structure. For combustible wood sheds, the effects of orientation were studied using Small sheds. The photographs in Fig. 38 (a) and Fig. 38 (b) show the door opening facing downwind (facing the target structure) in test O-WShw-15 (NOSSE8) and upwind in test O-WShw-15-R1 (NOSSE11), respectively. The

54

effects of orientation on thermal exposures to the target structure can be assessed by comparing heat flux data recorded for these four cases.
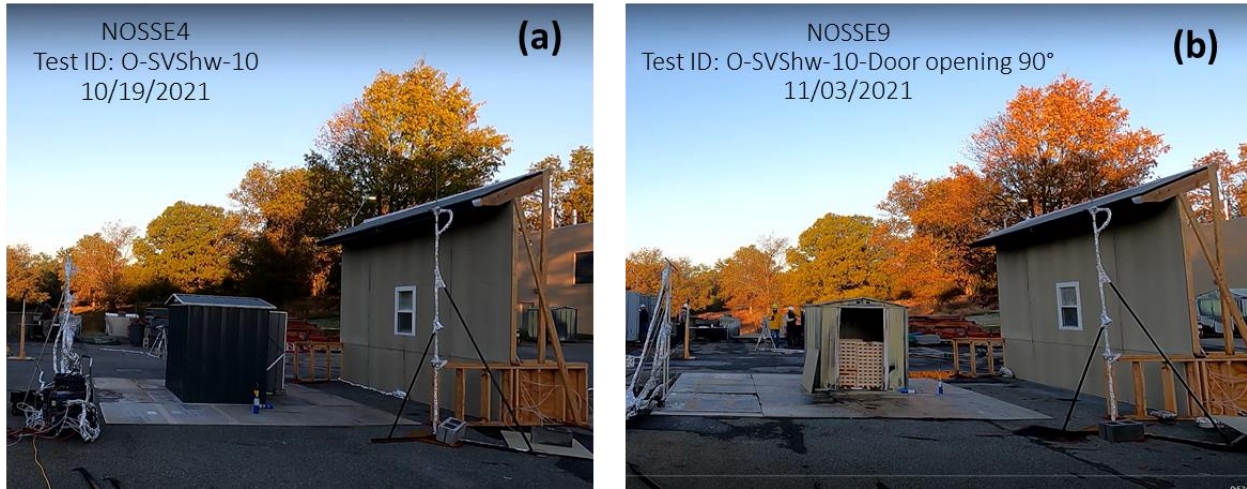

Fig. 37. Photograph captured from videos recorded by Camera #3 showing noncombustible source structure (a) facing downwind (0°) in Test: O-SVShw-10 and (b) Test: O-SVShw-10-90°.
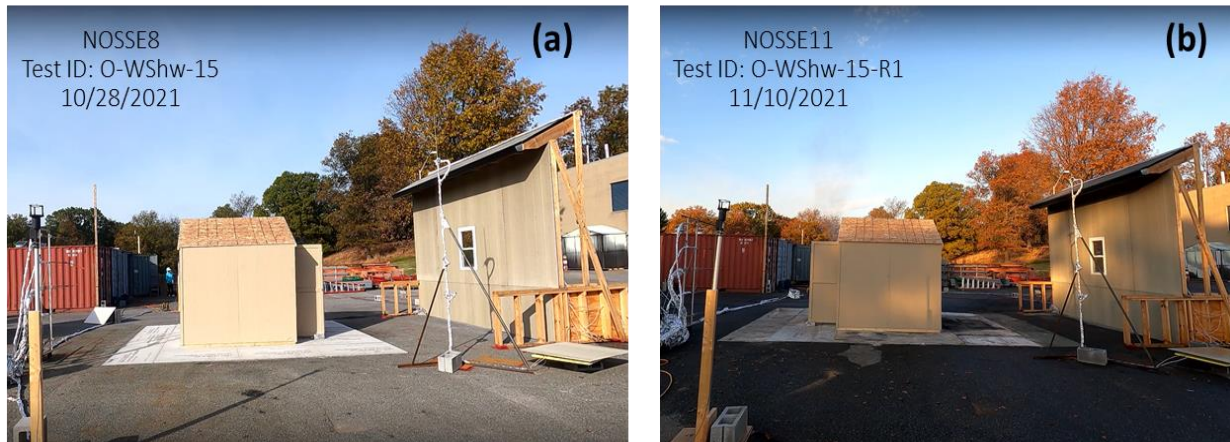
Fig. 38. Photograph captured from videos recorded by Camera #3 showing combustible source structure (a) facing downwind (0°) in Test: O-WShw-15 and (b) upwind (180°) Test: O-WShw-15-R1.

For noncombustible sheds, comparison of heat flux profiles recorded by HF1 (under eaves) in Fig. 39 indicate that changing the orientation of the door opening from 0° to 90° had a noticeable effect on the thermal exposure to the target structure. The incident peak heat flux on the target structure was reduced by half by changing the orientation of the door opening (see Fig. 39(a)). This is attributed to the shielding of the burning wood cribs provided by the noncombustible steel shed, which reduced the thermal exposure to the target structure. The orientation of the door opening may thus be seen as a potential approach for mitigating the exposure from burning fuel in a noncombustible shed. In reorienting the door, however, care should be taken to see that the exposure is not redirected toward other targets, including structures on neighboring parcels.

In contrast to the noncombustible shed, the effect of shed orientation for combustible source structures was marginal. The temporal profiles of heat flux data in Fig. 39(b) indicate that the peak heat flux exposure to the target structure is comparable for both upwind and downwind orientation of door opening in combustible wood sheds. This result suggests that the door orientation of the combustible sheds does not significantly affect the thermal exposure to the target structure. The combustible wood structure is consumed in the fire, thereby exposing the burning wood cribs to the target structure. The slight delay and fast rise in thermal exposure to the target structure in test O-WShw-15-R1 may be due to the upwind orientation of the door opening, as discussed for test O-WShw-10 in the previous section. While the door opening facing upwind increases the burning intensity of the wood cribs due to the fanning effect, the thermal exposure to the target structure begins to rise only when the roof of the source structure is consumed in fire.
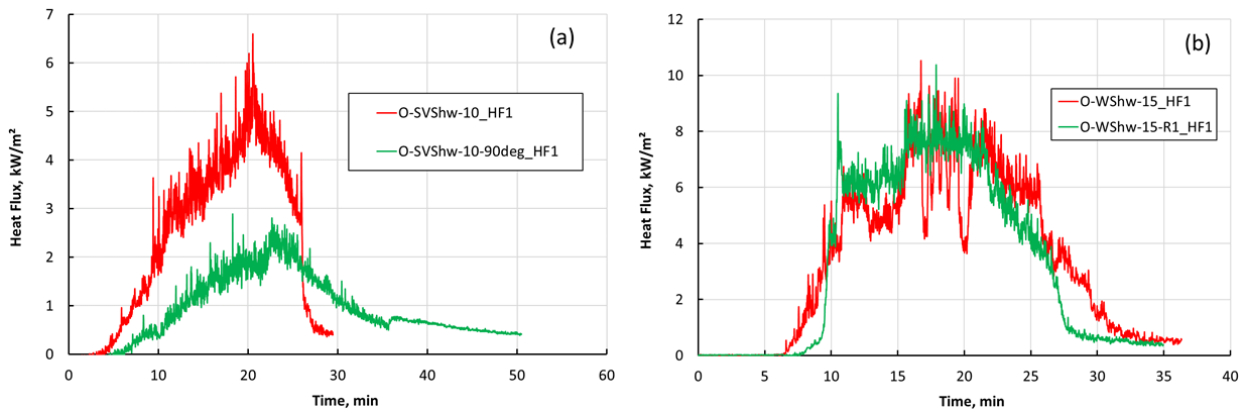
Fig. 39. Temporal profiles of heat flux data showing effects of shed orientation on heat flux measurement in the eave (HF1) for (a) noncombustible source structure in Test: O-SVShw-10 and Test: O-SVShw-10-90° and (b) combustible source structure in Test: WShw-15 and Test: O-WShw-15-R1.
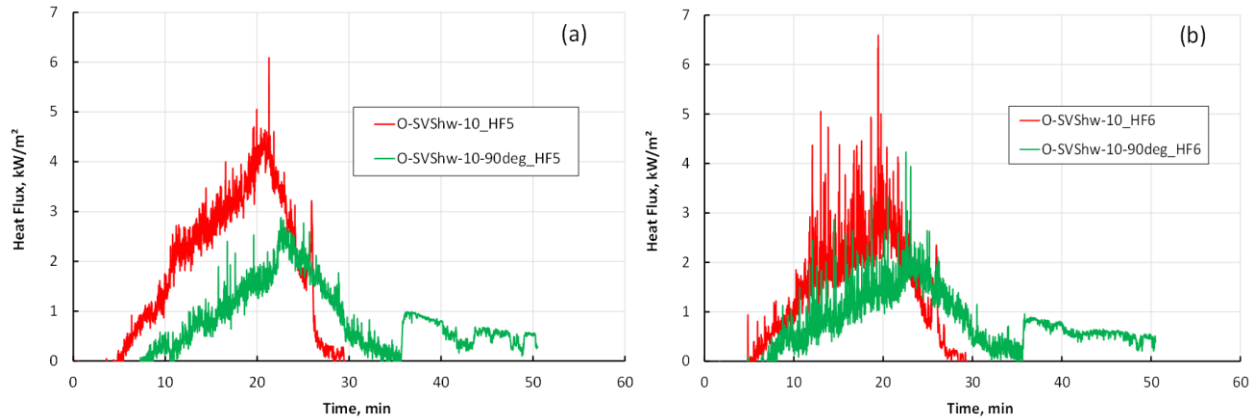
Fig. 40. Temporal profiles of heat flux data showing effects of shed orientation for noncombustible source structure in Test: O-SVShw-10 and Test: O-SVShw-10-90° on heat flux measurement at the Rig (a) HF5 and (b) HF6.

Comparison of heat fluxes recorded by HF5 and HF6 on the heat flux gauge rig (Fig.36) for test O-SVShw-10 and test O-SVShw-10-90° suggests that HF5 and HF6 recorded lower heat fluxes

when the shed door opening was facing the heat flux gauge rig. Visual observations indicated significant thinning of flames coming out from the door opening in test O-SVShw-10-90° while the effect of wind on the flames coming out from the door opening downwind was minimal. The possibility of cooling the flames emerging from the door facing the rig is much higher than those emerging from the door facing downwind in test O-SVShw-10.

3.2.4. Effects of Fuel Containment and Orientation on Thermal Exposure

This section examines the effects of fuel containment and orientation with respect to the target structure. A comparison of heat flux profiles for source structures with similar total combustible fuel located at a distance of 10 ft from the target structure is shown in Fig. 41. The total mass of combustible fuel in tests O-WChw-10 (NOSSE6), O-SVShw-10 (NOSSE4), and O-SVShw-10-90° (NOSSE9) is similar (145 kg ±73 kg, see Table 5). However, the thermal exposure to the target structure was a function of fuel containment and orientation of the door opening with respect to the target structure. In test O-WChw-10, the combustible wood Closet was consumed in the fire and exposed the burning wood cribs. In test O-SVShw-10, the Very Small steel shed had similar amount of combustible fuel, but the burning was contained within the noncombustible steel shed thereby limiting the intensity of exposure to the target structure. Changing the orientation of the Very Small steel shed such that the door opening was facing perpendicular to the target structure reduced the thermal exposure to the target wall significantly as seen in Fig. 41.

The effects of fuel containment can be noted clearly in Fig. 42. Temporal profiles of heat flux data in Fig. 42(a) and(b) shows effects of fuel containment i.e., heat flux reduction in the eave (HF1) for Very Small and Small source structures, respectively. The noncombustible steel sheds contain the fire effectively, thus reducing the thermal exposure to the target structure while combustible shed is consumed in the fire resulting in higher thermal exposure to the target structure. Comparison of plots in Fig. 42(a) and Fig. 42(b) reveals that increasing the SSD from 10 ft to 15 ft significantly reduces the thermal exposure despite higher combustible fuel in tests O-WShw-15 (NOSSE8) and O-SShw-15 (NOSSE7). This finding is further discussed and confirmed in the section below.
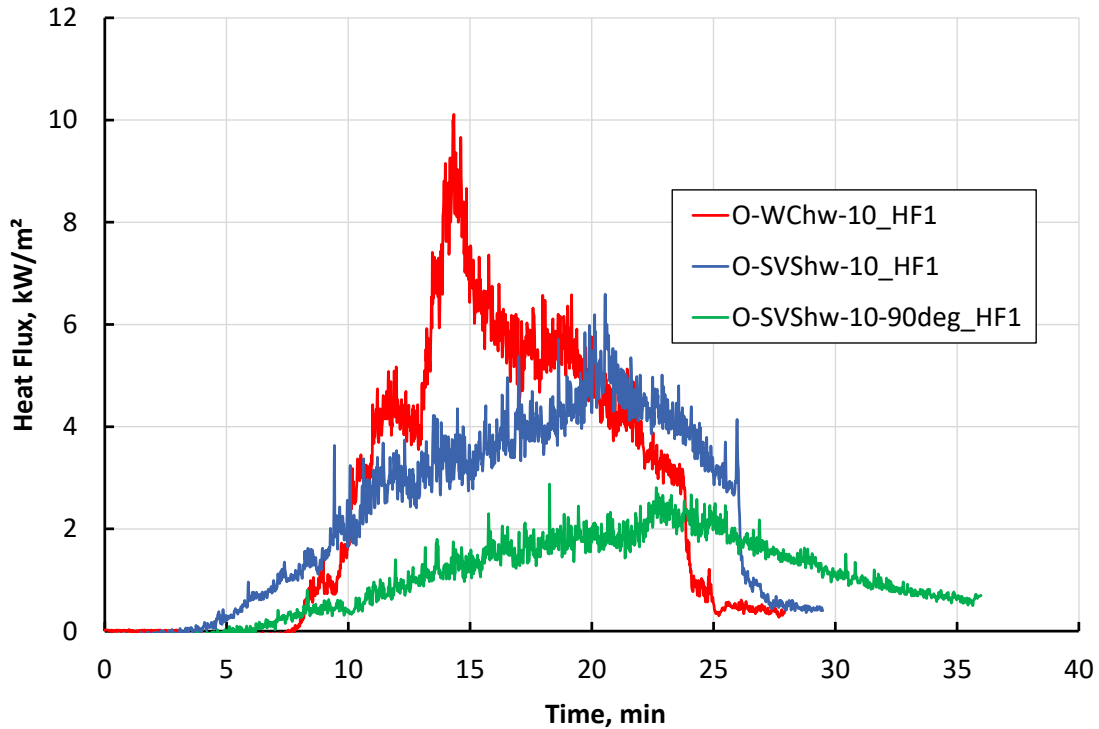
Fig. 41. Temporal profiles of heat flux data showing effects of fuel containment and orientation on heat flux measurement in the eave (HF1) for source structures with similar amounts of total fuel.
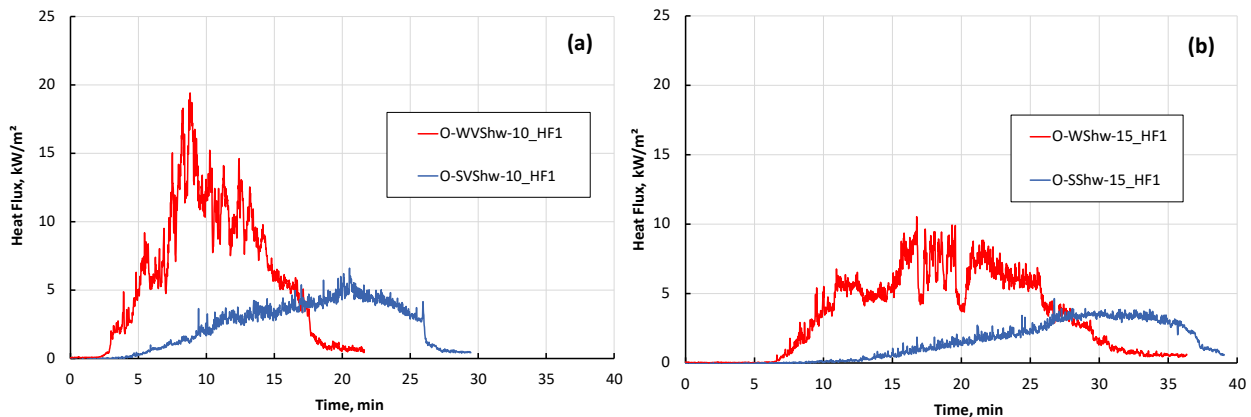
Fig. 42. Temporal profiles of heat flux data showing effects of fuel containment i.e., heat flux reduction in the eave (HF1) for (a) Very Small and (b) Small source structures.

3.2.5. Effects of Structure Separation Distance on Thermal Exposure

The effect of increased structure separation distance on the incident heat flux measured in the eaves is shown in Fig. 43, below, for combustible wood shed (Small shed) with high fuel loading of 12 1-A wood cribs. The door opening in both the tests was facing upwind, away from the target structure. A sudden rise in the heat flux curves is typical of a door opening facing upwind as opposed to a gradual increase in heat flux for door opening facing downwind (facing the target structure) as discussed in the previous section. The peak heat flux (27 kW/m²) registered at HF1

58

in eaves for test O-WShw-10 (NOSSE12) is roughly three times higher than the peak of 8 kW/m² registered for test O-WShw-15-R1 (NOSSE11). The temperatures measured at the eaves reduced by more than a factor of two with an increased SSD of 15 ft in test O-WShw-15-R1.
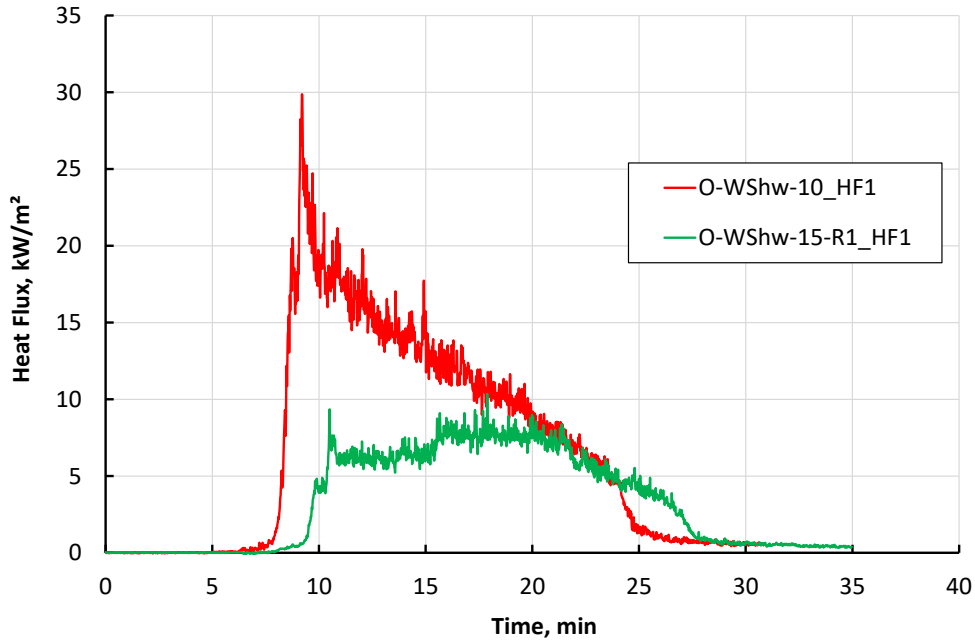
Fig. 43. Temporal profiles of heat flux data showing effects of SSD on heat flux measurement in the eave (HF1) for combustible source structures in Test: O-WShw-10 and Test: O-WShw-15-R1.

The effects of SSD on the thermal exposure to the target wall can be noted from Fig. 44. The fire plume in Test O-WShw-10 is seen impinging on the target structure while the fire plume in Test O-WShw-15-R1 is hardly reaching the target structure.
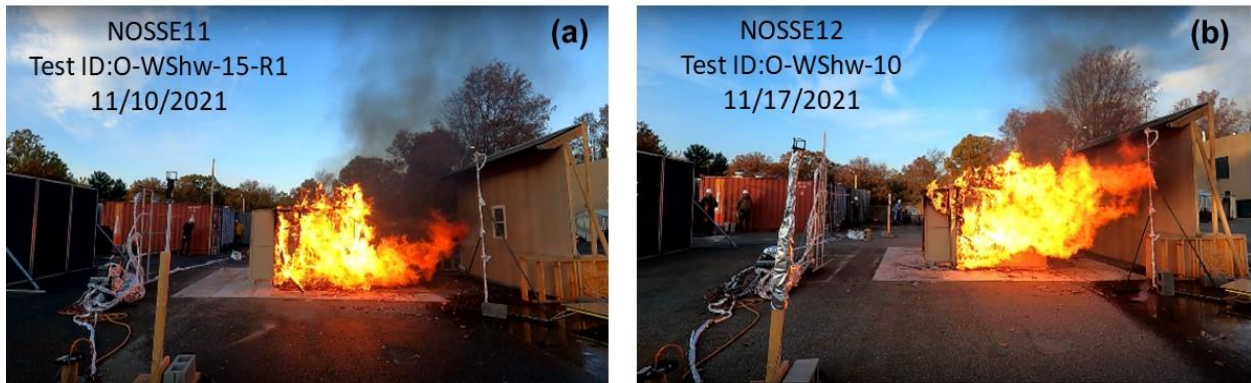
Fig. 44. Photograph captured from videos recorded by Camera #3 showing effects of SSD on fire plume from combustible source structures in (a) Test: O-WShw-15-R1 and (b) Test: O-WShw-10.

3.2.6. Effect of Target Structure Construction Materials on Ignitability

The effects of fire-hardened and non-fire-hardened target structures were examined for similar thermal exposures in tests O-WVShw-10 (NOSSE3) and O-WVShw-10-R2 (NOSSE13). A combustible wood Very Small shed with high fuel loading of six 1-A wood cribs was used as a source structure with an SSD of 10 ft. Nominal thermal damage to the vinyl window frame was noted for the fire-hardened target structure. The window screen fell off as shown in Fig. 45(a). The shed and wood cribs had a total combustible fuel of 212 kg ± 9 kg. The non-fire hardened target structure ignited within 6 min from ignition of the wood cribs. Ignition occurred simultaneously at the window frame and of the exposed OSB as shown in Fig. 45(b). These two experiments illustrate the enhanced ignition resistance provided by the fire-hardening.
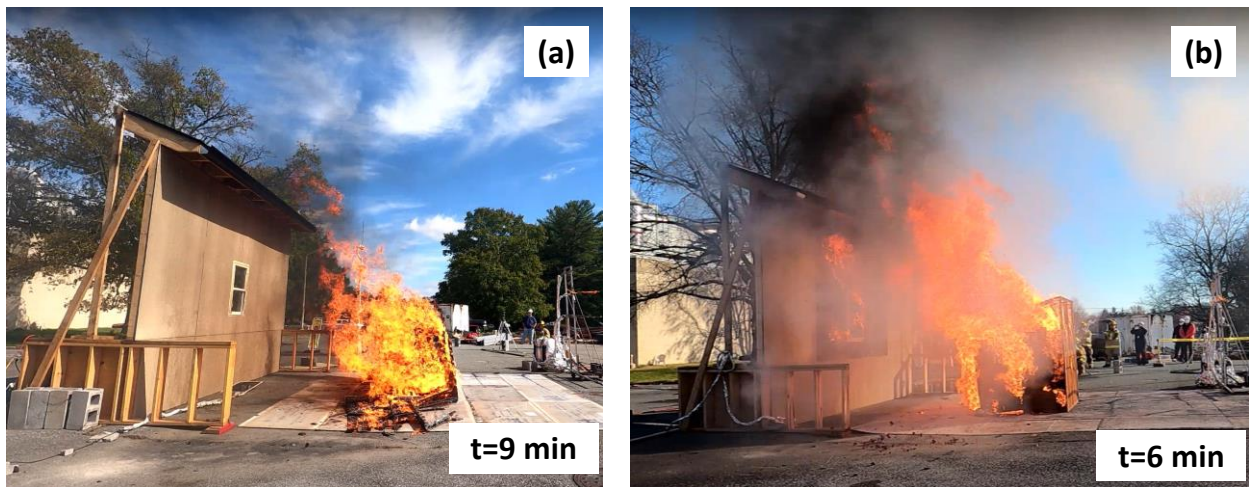
Fig. 45. Photograph showing (a) peak thermal exposure to fire hardened target structure in test O-WVShw-10 and (b) ignition of non-fire hardened target structure in test O-WVShw-10-R2.

3.3. Target Structure Performance

The associated target structure performances due to thermal exposure from the burning of different source structures are summarized in Table 10 below. Tests O-SChw-5 (NOSSE5) and O-WShw-10 (NOSSE12) are notable for cracking of the cement board wall. Test O-WVShw-10-R2 (NOSSE13) is notable for ignition of the exposed OSB wall and eaves and failure of the vents.

The performance of the windows, walls, eaves, and vents listed in Table 10 is discussed in the subsections below.

Table 10. Summary of target structure performance for various exposures.

| Serial number	Test ID	Shed Type	Target Structure Performance			
			Window	**Wall**	**Eaves**	**Vent**
NOSSE1	O-WVSh0-10	Very Small	Thermal deformation of vinyl frame, screen fell off	ND	ND	ND
NOSSE2	O-SVSh0-10	Very Small	ND	ND	ND	ND
NOSSE 3	O-WVShw-10	Very Small	Thermal deformation of vinyl frame, screen fell off	ND	ND	ND
NOSSE 4	O-SVShw-10	Very Small	ND	ND	ND	ND
NOSSE 5	O-SChw-5	Closet	Melting and charring of vinyl frame, screen fell off, cracking of window pane forming an opening	Cracking of cement board	ND	ND
NOSSE 6	O-WChw-10	Closet	ND	ND	ND	ND
NOSSE 7	O-SShw-15	Small	ND	ND	ND	ND
NOSSE 8	O-WShw-15	Small	ND	ND	ND	ND
NOSSE 9	O-SVShw-10-90º Door opening: 90º	Very Small	Thermal deformation of vinyl frame, screen fell off	ND	ND	ND
NOSSE 10	O-WVShw-10-R1	Very Small	Thermal deformation of vinyl frame, screen fell off	ND	ND	ND
NOSSE 11	O-WShw-15-R1 Door opening:180°	Small	ND	ND	ND	ND
NOSSE 12	O-WShw-10 Door opening: 180°	Small	Melting and charring of vinyl frame	Cracking of cement board	ND	ND
NOSSE 13	O-WVShw-10-R2	Very Small	Melting and charring of vinyl frame	Exterior wood ignited	Ignited	Failed

ND = No Damage

3.3.1. Wall Performance

The performance of the target wall constructed above the minimum requirements specified by the Chapter 7A of the California Building Code was assessed for various exposures in this experimental series. The usual damage that can occur due to thermal exposure is spalling of the exterior cement that protects the OSB from exposure to fire. For the outdoor experimental series, local damage to the cement board was observed for tests O-SChw-5 (NOSSE5) and O-WShw-10 (NOSSE12), which were characterized by low SSD and high fuel loading, respectively. The high exposures from the source structures in these tests resulted in cracking of the cement board, which can be attributed to high temperatures leading to thermal expansion and the buildup of large axial forces in restrained cement boards. Examples of cracked cement boards are shown in Fig. 46 below. For test O-SChw-5, the thermal exposure was high due to a small SSD of 5 ft, while in case of O-WShw-10, high thermal exposure was due to a higher amount of combustible fuel (larger shed size and higher number of wood cribs). In the previous shed burn experiments conducted indoors without wind [21], significant spalling of the cement board was also observed, as shown in Fig. 47. Greater damage to the cement board was noted for a wood Closet placed next to the wall (SSD=0 ft). The intensity of cracking and/or spalling is thus a function of shed construction, fuel loading, shed orientation and SSD.

Cracking of the cement board does not directly imply structure ignition. However, once the exterior cladding of the structure is compromised, the potential for ignition of the underlying materials increases. Failures associated with cladding can result in high exposures to the substrate (e.g., OSB) from direct flame exposures or indirectly from ember intrusions.

For test O-WVShw-10-R2 (NOSSE13), with similar exposure to O-WShw-10, the non-hardened exterior wall with exposed OSB ignited within 6 mins (see Fig. 48). The vulnerability associated with non-hardened construction resulted in a structure ignition, highlighting the value added from fire hardening of the structure in O-WShw-10, as outlined in CA Chapter 7A.
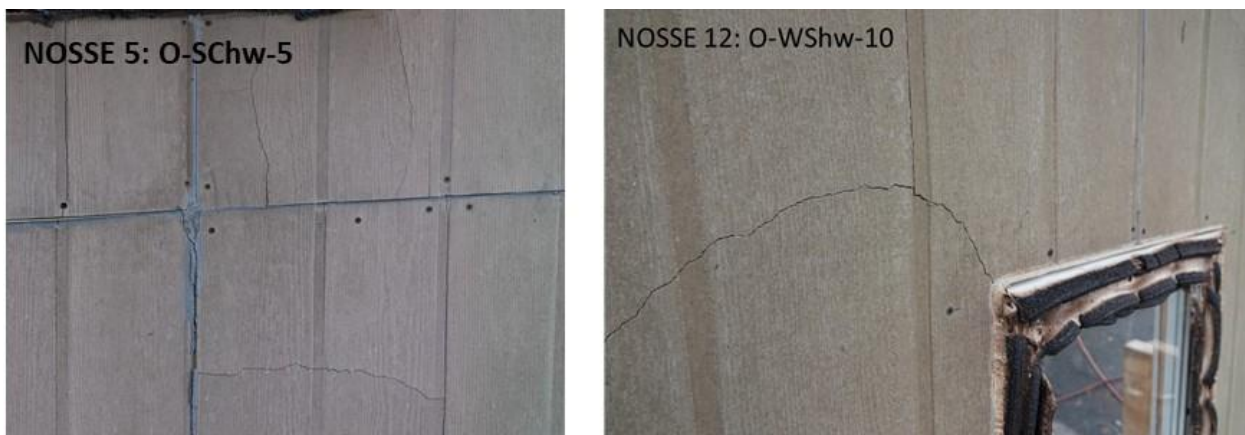
Fig. 46. Photograph showing cracking of cement board in tests NOSSE5: O-SChw-5 and NOSSE12: O-WShw-10.

Fig. 47. Photograph showing spalling of exterior layer (cement board) in indoor test 1B-WCl0-0.

Fig. 48. Photograph showing ignition of exposed OSB in Test NOSSE13: O-WVShw-10-R2.

3.3.2. Window Performance

Window performances for various radiant and convective heat exposures can be clearly noted from Fig. 49. The effect of wind on window performance can be seen from window images from test O-WVSh0-10 and test O-WVShw-10 in Fig. 49. While the window frames in both the tests were thermally deformed, the damage to the window in presence of wind in test O-WVShw-10 was slightly more than the window in test O-WVSh0-10 with no applied wind. This is clearly due to the wind that was instrumental in stretching and lengthening the flames and 'licking' the window.

Comparison of window performance in test O-WVShw-10-R1 (NOSSE10) and test O-WShw-10 (NOSSE12) on the second line of Fig. 49 shows that for combustible wood sheds with similar SSD, the amount of fuel loading significantly affects thermal exposure on the window. The window in test O-WVShw-10-R1 is exposed to radiant heat from the Very Small wood shed at an SSD of 10 ft while the window in test O-WShw-10 is exposed to both radiant and convective heating, with flames touching the window vinyl frame. Consequently, the window in test

O-WVShw-10-R1 shows some deformation due to radiant heating while the window in test O-WShw-10 shows significant thermal decomposition and charring of the vinyl frame. However, the tempered glass in both of these windows remained intact and no signs of cracking were seen. The window panes in both cases remained in place (in the frame).

In tests O-SChw-5 (NOSSE5) and O-WVShw-10-R2 (NOSSE13), shown at the bottom of Fig. 49, the flames from the source structure were in contact with the window frames for a longer duration due to the proximity of burning fuel (SSD = 5 ft for test O-SChw-5) and higher thermal exposure (six 1-A wood cribs in test O-WVShw-10-R2). The ignition of the vinyl frame and cracking of the glass occurred in both tests, and subsequently the broken glass was displaced by the wind, thereby forming an opening in the target structure. The embers and flames could enter the structure through this opening, thereby compromising the complete structure. An example of flame extending to the target structure and 'licking' the window, with subsequent ignition of the vinyl frame during test O-SChw-5, is shown in Fig. 50.

For the seven remaining tests, no visible damage to the windows was observed. This was primarily due to reduced exposures from the noncombustible sheds coupled with the SSD (O-SVSh0-10, O-SVShw-10, O-SShw-15, O-SVShw-10-90°), or higher SSDs for combustible wood sheds (O-WChw-10, O-WShw-15, O-WShw-15-R1).

Fig. 49. Photographs showing window damage for different exposures.

Fig. 50. Photographs showing (a) flame jetting from noncombustible steel Closet in test O-SChw-5 and (b) ignition of vinyl frame.

3.3.3. Eave Performance

The eave performance in this study was assessed by comparing heat fluxes in the eaves and the effects of various factors on thermal exposures at the eaves, as discussed in the sections above. Heat flux gauges were placed on the sides of the central bay where the eave vent was located. This was done so that the performance of the eave vent assembly was not affected. Since the heat flux data was collected on either side of the central bay, the measured heat flux values are likely lower than the incident peak heat fluxes at the centerline where the source fire (exposure) was centered for all the experiments with the shed door facing the target structure.

As summarized in Table 10, the eaves of the non-fire hardened target structure (NOSSE13) ignited following the ignition of the wall. From Table 9, a peak heat flux of 27 kW/m² was registered for test O-WShw-10 (NOSSE12), with a fire hardened target structure. Ignition of the eaves did not occur in this test because the peak heat flux registered at the eaves was transient and was not sufficient to cause ignition of the wood. The limited data from the indoor shed burn experiments with no applied wind field [21] suggested that heat fluxes at the eaves of approximately 15 kW/m² sustained for at least 5 min resulted in ignition. These conditions were observed with thermal exposure from: (i) a noncombustible Very Small shed with a fuel loading of six 1-A wood cribs (total combustible mass of 115 kg ± 1kg) and an SSD of 5 ft (1B-SVS0-5 and 1B-SVS0-5-R1), and (ii) a combustible wood Closet with a fuel loading of two 1-A wood cribs (total combustible mass of 90 kg) and an SSD of 0 ft (1B-WCl-0). However, for a wood Closet with an SSD of 0 ft and no fuel loading (combustible mass of shed = 56 kg), the heat fluxes in the eaves peaked at 20 kW/m² for a short duration of 5 s, which was not sufficient to cause ignition of the eaves (1B-WC00-0).

This data suggests that under applied wind conditions, eaves were not exposed to sufficient heat flux to cause ignition. However, in many cases flames were contacting the eaves, and any flame contact has potential to ignite leaves or debris in the gutter. To extend the findings to real situations, the fuel loading of the source structure and the size and orientation of the door can be very different from the configurations tested in this limited test series. Several other factors, including the duration of fire exposure, the environmental conditions, and the weathering of the target structure components, may lead to ignition of eaves in real-life situations. In order to characterize open eave performance for different thermal exposures, additional experiments will be performed in the future.

3.3.4. Vent Performance

This limited test series assessed the performance of eave vents when exposed to combustible and noncombustible Closets, Very Small, and Small sheds with high fuel loads under applied wind conditions. The maximum temperatures recorded at the vent for different exposure conditions are provided in Table 9. For tests O-SChw-5 (NOSSE5), O-WShw-10 (NOSSE12) (with door opening upwind), and O-WVShw-10-R2 (NOSSE13), the radiant and convective heat exposure was sufficient to raise the gas temperature at the vent above 176 ºC and activate the intumescent coating on the honeycomb core. The intumescent coating was effective in blocking the heat in test O-SChw-5 thereby keeping the temperatures on the interior side of the vent below 150 ºC as shown in Fig. 51 (a). However, the intumescent coating was not effective in blocking the heat in test O-WShw-10. The temperatures at the TCventR rapidly increased up to 250 ºC as shown in Fig. 51 (b).

Another important experimental observation was that the ember exposure at the vent was noticeably higher for combustible wood sheds compared to the tests including noncombustible steel sheds. The burning wood cribs became exposed when the combustible wood shed structure was consumed by the fire. Ember generation from the exposed wood cribs was visually noted to be significantly higher as compared to the confined burning of wood cribs inside the noncombustible steel sheds. This was likely due to the wind being able to dislodge parts of the shed structure and burning cribs. The ember exposure at the eave is visible in Fig. 52 (a), and embers passing through the vent into the interior of the structure are seen in Fig. 52 (b) during test O-WChw-10 (NOSSE6).
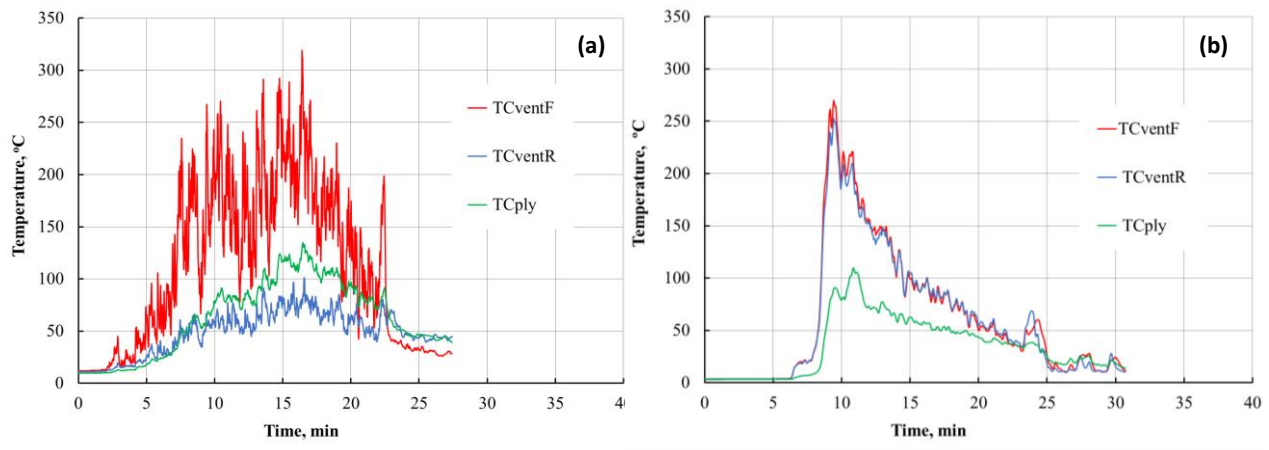
Fig. 51. Temperature-time profiles recorded by TCs in front of the vent (TCventF), behind the vent (TCventR), and on the plywood (TCply) behind the vent in test (a) O-SChw-5 and (b) O-WShw-10. Standard relative uncertainty is ± 0.75 %.
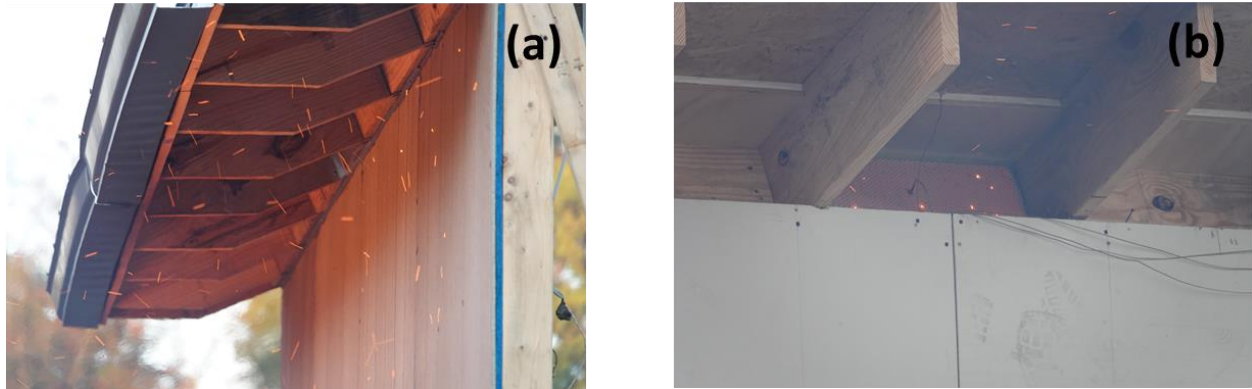
Fig. 52. Photographs showing (a) ember exposure in the eaves and (b) embers escaping through the vent in Test O-WChw-10.

Finally, the vent failed to perform when the eaves ignited following the ignition of exposed OSB in test O-WVShw-10-R2 (NOSSE13). The photograph in Fig. 53 shows flame penetration through the vent for this test.

Fig. 53. Photograph showing flames penetrating through the vent for test O-WVShw-10-R2.

A burn-through of the vent can become a path for flame spread under the roof or into the attic. Although the eave vent openings are small in the beginning, the roof can fall due to heating from fire and form a fire spread pathway that can ultimately compromise the entire structure. Flame ejected from a burn-through vent is considered as a major cause of fire spread in structure-to-structure fire spread, as such flames merge into a larger flame, magnifying the radiation intensity [18]. Failure of the roof may also depend on the extent of fire hardening applied to the underside of the roof rafters, as required by Chapter 7A of California Building Code for WUI construction.

3.4. Summary and Concluding Remarks

Based on the target structure performance discussed above, minimum structure separation distances for given sizes of combustible and noncombustible sheds were identified.

Initially, combustible and noncombustible Very Small sheds were tested with an SSD of 10 ft. This distance was chosen based on the findings from the indoor shed burn experiments [21]. An SSD of 5 ft for a noncombustible Very Small shed with no wind had resulted in ignition of eaves and the target structure. With 5 ft known to be too close, an SSD of 10 ft was selected for initial tests with Very Small sheds in the presence of an applied wind field. The result was that thermal exposures from both the combustible shed and noncombustible shed were found to be minimal with an SSD of 10 ft, and no thermal damage to the target structure was noted. An SSD_{min} of 10 ft was therefore assigned to these combustible and noncombustible Very Small sheds.

Next, since a noncombustible steel Closet had lower fuel loading, this source structure was tested with an SSD of 5 ft. In this test, the thermal exposure from the steel Closet was found to cause significant thermal damage to the target structure, and an SSD of 10 ft was identified as the next logical step for testing the noncombustible steel Closet. Due to the limited number of tests that could be carried out, however, this test was subsumed under a test of the more hazardous combustible wood Closet at an SSD of 10 ft. This test configuration resulted in no damage to the target structure. A minimum SSD of 10 ft was therefore ascertained for both combustible and noncombustible Closets with floor area < 16 ft². This is in accordance with the SSD_{min} of 10 ft found for the larger Very Small sheds.

Noncombustible and combustible Small sheds tested with SSD of 15 ft resulted in no signs of thermal damage to the target structure; a minimum SSD of 15 ft was therefore assigned for these source structures.

The estimated SSD_{min} for various sizes of combustible and noncombustible sheds are given in Table 11. The SSD_{min} listed in Table 11 are applicable to fire hardened structures compliant with Chapter 7A of the California Building Code. The limitations for the implementation of the SSD_{min} are provided in Section 3.5 below.

Table 11. Minimum SSD estimated from shed burn experiments with applied wind. (1ft = 0.305 m, 1 kg = 2.2 lbs)

Shed/SSD for hardened structure	0 ft	5 ft	10 ft	15 ft
Wood Closet and Very Small (up to 26 ft²)			Minimum SSD	
Wood Small shed (26 ft² to 64 ft²)				Minimum SSD
Steel Closet* and Very Small shed* (up to 20 ft²)			Minimum SSD	
Steel Small* shed (20 ft² to 64 ft²)				Minimum SSD

* Place door opening away from primary residence and neighboring residence.

Data from the outdoor shed burn experiments suggests adopting the SSD_{min} to prevent structure-to-structure flame spread. These SSD_{min} do not consider vegetation, other structures (decks, fences, etc), or variations in terrain and weather conditions, nor do they consider fire spread through embers. This suggests that the actual SSD_{min} between a residence and a structure should

be larger than those listed in Table 11 above to account for the above-mentioned conditions. Limitations of the NOSSE experiments and associated SSD data are summarized in the following section.

3.5. NOSSE Limitations

There are a number of limitations associated with the interpretation of the NOSSE SSD data listed in Table 11. These are listed below in two categories: limitations associated with the source structure (shed) and limitations associated with the target structure (exterior wall).

Source Structure Limitations

1. The sheds were tested with representative "high" equivalent fuel loading using standard 1-A wood cribs. Since fuel loading in the storage sheds cannot be regulated, "high" equivalent fuel loading representing "worst" case scenarios was tested to determine minimum structure separation distance. Explosive fuels such as gasoline containers or propane tanks were not included in the study to avoid explosive damage to the surroundings. Such explosive items typically stored in residential sheds are likely to cause window breakages at minimum.

2. All experiments were conducted on flat ground; effects of topography on flame spread or thermal exposures to the target structure were not considered in this study.

3. Only limited shed orientations with respect to target structure and wind direction were tested.

4. The presence of additional fuels between the source structure and the target structure, including ladder fuels[3] or vehicles, were not considered in this study.

5. Non-flame retarded plastic sheds that can melt and burn as pool fires have not been studied. Such source structures have potential to spread fires away from the source, as the polymer melt can flow and carry heat and flames with it [21].

6. These experiments do not reflect the ignition hazard associated with embers generated by the burning shed.

7. Only a few tests were repeated to confirm the minimum SSD_{min}.

Target Structure Limitations

1. Assumes structure hardened for ember exposures.

2. Fire hardened in compliance with Chapter 7A of the California Building Code requirement (for all but one experiment).

3. Single story target structure.

4. Normal to wind flow (limited data on various orientations).

5. Simplified geometry.

6. No weathering, cracking, or other deterioration of the target structure.

---

[3] Vertical fuels that help initiate and assure the continuation of fire.

Recognizing the limitations of the experiments in estimating the minimum SSDs, implementation guidance of the minimum SSD data generated from the outdoor shed burn experiments can be used for hazard assessment and for hazard mitigation.

3.6. Technical findings

The NOSSE experiments demonstrate that even a small combustible shed under 64 ft^2 can compromise a hardened residence from 10 ft away, highlighting the hazard of structure-to-structure fire spread in high density new residential construction. Given the above mentioned limitations, the technical findings based on thermal exposures to the target structure are listed below. While these findings are associated with the auxiliary structures, they can also provide guidance on structure separation distance for residential structures. Plausible implementation of these technical findings is discussed in Appendix D.

- **NOSSE TF1 –** A repeat experiment showed reproducibility of the measured quantities with the peak heat flux variation of 16 % in the eaves and variation of 45% at the rig. The variation in temperatures recorded at the eaves was in the range of 4 % to 6 %.

- **NOSSE TF2** – Increasing the SSD by 5 ft from 10 ft to 15 ft reduced the peak heat flux registered at HF1 in the eaves by roughly three times and reduced the temperatures measured at the eaves by more than a factor of two.

- **NOSSE TF3** - For combustible sheds the peak heat flux measured at the target structure:

  - corresponded with the total combustible fuel.

  - is not affected by orientation (i.e., door opening facing downwind or upwind).

- **NOSSE TF4** - The wind had complex effects on the burning behavior of combustible source structures causing turbulence and eddies. These affected flame lengths and enhanced convective heat transfer to the target structure, causing preheating with likely localized removal of moisture.

- **NOSSE TF5** - Combustible wood sheds were consumed in the fire, resulting in higher thermal exposure to the target structure as opposed to noncombustible sheds.

- **NOSSE TF6** - In the case of noncombustible sheds with door openings facing the target structure, the applied wind had minimal or no effect on thermal exposure to the target structure.

- **NOSSE TF7** - The noncombustible steel sheds contained the fire effectively, thus reducing, but not eliminating, the thermal exposure to the target structure.

- **NOSSE TF8** – For the noncombustible shed scenarios evaluated, peak heat flux at the target structure was reduced by half by changing the orientation of the door opening 90° away from the target structure.

- **NOSSE TF9** – The minimum SSD$_{min}$ for both combustible and noncombustible sheds with floor area < 26 ft^2 was determined to be 10 ft. For sheds with floor area between 26 ft^2 and 64 ft², the minimum SSD$_{min}$ was determined to be 15 ft. Because the local

winds during a WUI fire are unpredictable, SSD is omnidirectional, i.e., the same SSD in all directions.

- **NOSSE TF10** – A non-fire hardened target structure ignited within 6 mins when exposed to a Very Small wood shed with total combustible fuel of 467 lbs ± 20 lbs (212 kg ± 9 kg) and SSD of 10 ft. With similar combustible fuel, SSD, and thermal exposure, the fire hardened target structure exhibited minimal thermal damage and significant ignition resistance.

References

[1] M. Bennett, S. A. Fitzgerald, B. Parker, M. Main, A. Perleberg, C. C. Schnepf and R. Mahoney, "Reducing Fire Risk on Your Forest Property," PNW 618, A Pacific Northwest Extension Publication: Oregon State University, University of Idaho, Washington State University, 2010.

[2] D. Leavell, C. Berger, S. A. Fitzgerald and B. Parker, "Fire Science Core Curriculum," EM 9172, OSU Forestry & Natural Resources Extension Program, 2017.

[3] S. E. Caton, R. S. Hakes, D. J. Gorham, A. Zhou and M. J. Gollner, "Review of Pathways for Building Fire Spread in the Wildland Urban Interface Part I: Exposure Conditions," *Fire Technology,* vol. 53, no. 2, pp. 429-473, 2017.

[4] S. L. Manzello, "Structure Ignition Mechanisms in Wildland-Urban Interface (WUI) Fire and Associated California State Fire Marshal Standard Test Methods," in *Proceedings of the Japan Association for Fire Science and Engineering*, Hirosaki, 2020.

[5] S. Suzuki and S. L. Manzello, "Ignition Vulnerabilities of Combustibles around Houses to Firebrand Showers: Further Comparison of Experiments," *Sustainability,* vol. 13, no. 4, pp. 2136-2149, 2021.

[6] S. Nazaré, I. T. Leventon and R. Davis, "Ignitibility of Structural Wood Products Exposed to Embers During Wildland Fires: A Review of Literature," NIST Technical Note 2153, National Institute of Standards and Technology, Gaithersburg, Maryland, 2021.

[7] J. D. Cohen, "An Examination of the Summerhaven, Arizona Home Destruction Related to the Local Wildland Fire Behavior during the June 2003 Aspen Fire," U.S. Department of Agriculture Forest Service, Rocky Mountain Research Station, Missoula Fire Sciences LaboratoryMissoula Fire Sciences Laboratory, Missoula, MT, 2003.

[8] J. D. Cohen and R. D. Stratton, "Home Destruction Examination: Grass Valley Fire, Lake Arrowhead, CA," U.S. Department of Agriculture, Forest Service Report R5-TP-026b, 2008.

[9] A. Maranghides, E. D. Link, S. Hawks, J. McDougald, S. L. Quarles, D. J. Gorham and S. Nazare, "WUI Structure/Parcel/Community Fire Hazard Mitigation Methodology," NIST Technical Note 2205, National Institute of Standards and Technology, Gaithersburg, MD, 2022.

[10] A. Maranghides and D. McNamara, "2011 Wildland Urban Interface Amarillo Fires Report #2 – Assessment of Fire Behavior and WUI Measurement Science," NIST Technical Note 1909, National Institute of Standards and Technology, Gaithersburg, MD, 2016.

[11] A. Maranghides and W. Mell, "Framework for Addressing the National Wildland Urban Interface Fire Problem – Determining Fire and Ember Exposure Zones Using a WUI Hazard Scale," NIST Technical Note 1748, National Institute of Standards and Technology, Gaithersburg, MD, 2013.

[12] A. Maranghides, W. Mell, K. Ridenour and D. McNamara, "Initial Reconnaissance of the 2011 Wildland-Urban Interface Fires in Amarillo, Texas," NIST Technical Note 1708, National Institute of Standards and Technology, Gaithersburg, MD, 2011.

[13] E. D. Link, "Pre-fire and Post-fire Data Studies in the WUI," in *Manzello, S.L. (ed.) Encyclopedia of Wildfires and Wildland-Urban Interface (WUI) Fires*, Springer, Cham., 2020, pp. 845-852.

[14] A. Papalou and D. K. Baros, "Assessing Structural Damage after a Severe Wildfire: A Case Study," *Buildings,* vol. 9, pp. 171-192, 2019.

[15] A. Maranghides, D. McNamara, W. Mell, J. Trook and B. Toman, "A Case Study of a Community Affected by the Witch and Guejito Fires: Report #2 – Evaluating the Effects of Hazard Mitigation Actions on Structure Ignitions," NIST Technical Note 1796, National Institute of Standards and Technology, Gaithersburg, MD, 2013.

[16] A. Maranghides, D. McNamara, R. Vihnanek, J. Restaino and C. Leland, "A Case Study of a Community Affected by the Waldo Fire – Event Timeline and Defensive Actions," NIST Technical Note 1910, National Institute of Standards and Technology, Gaithersburg, MD, 2015.

[17] R. G. Rehm, A. Hamins, H. R. Baum, K. B. McGrattan and D. D. Evans, "Community-Scale Fire Spread," NISTIR 6891, National Institute of Standards and Technology, Gaithersburg, MD, 2002.

[18] K. Himoto, M. Shinohara, A. Sekizawa, K.-i. Takanashi and H. Saiki, "A field experiment on fire spread within a group of model houses," *Fire Safety Journal,* vol. 96, pp. 105-114, 2018.

[19] A. Edalati-nejad, M. Ghodrat, S. A. Fanaee and A. Simeoni, "Numerical Simulation of the Effect of Fire Intensity on Wind Driven Surface Fire and Its Impact on an Idealized Building," *Fire,* vol. 5, pp. 17-34, 2022.

[20] M. Ghodrat, F. Shakeriaski, D. J. Nelson and A. Simeoni, "Existing Improvements in Simulation of Fire-Wind Interaction and Its Effects on Structures," *Fire,* vol. 4, pp. 27-43, 2021.

[21] A. Maranghides, S. Nazare, F. Hedayati, D. Gorham, E. Link, M. Hoehler, M. Bundy, X. Monroy, M. Morrison, W. Mell, A. Bova, D. McNamara, T. Milac, S. Hawks, F. Bigelow, B. Raymer, F. Frievalt and W. Walton, "Structure Separation Experiments: Shed Burns without Wind," NIST Technical Note 2235, National Institute of Standards and Technology, Gaithersburg, MD, 2022.

[22] A. Maranghides, S. Nazare, E. Link, K. Prasad, M. Hoehler, M. Bundy, S. Hawks, F. Bigelow, W. Mell, A. Bova, D. McNamara, T. Milac, D. Gorham, F. Hedayati, B. Raymer, F. Frievalt and W. Walton, "Structure Separation Experiments: Phase 1 Preliminary Test Plan," NIST Technical Note 2161, National Institute of Standards and Technology, Gaithersburg, MD, 2021.

[23] B. J. McCaffrey and G. Heskestad, "A Robust Bidirectional Low-Velocity Probe for Flame and Fire Application," *Combustion and Flame,* vol. 26, pp. 125-127, 1976.

[24] R. M. Young Company, "Instructions-Ultrasonic Anemometer Model 86000,," PN: 86000-90, Revision G051820, Traverse City MI.

[25] R. A. Bryant and M. F. Bundy, "The NIST 20 MW Calorimetry Measurement System for Large-Fire Research," NIST Technical Note 2077, National Institute of Standards and Technology, Gaithersburg, MD, 2019.

[26] B. N. Taylor and C. E. Kuyatt, "Guidelines for Evaluating and Expressing the Uncertainty of NIST Measurement Results," NIST Technical Note 1297, 1994 Edition, National Institute of Standards and Technology, Gaithersburg, MD, 1994.

[27] K. M. Butler, E. L. Johnsson, A. Maranghides, S. Nazare, M. Fernandez, M. Zarzecki, W. Tang, E. Auth, R. McIntyre, M. Pryor, W. Saar and C. McLaughlin, "Wind-Driven Fire Spread to a Structure from Fences and Mulch," NIST Technical Note 2228, National Institute of Standards and Technology, Gaithersburg, MD, 2022.

[28] R. A. Bryant, "A comparison of gas velocity measurements in a full-scale enclosure fire," *Fire Safety Journal,* vol. 44, pp. 793-800, 2009.

[29] S. L. Quarles and M. Sindelar, "Wildfire Ignition Resistant Home Design (WIRHD) Program: Full-scale Testing and Demonstration Final Report," U.S. Department of Energy; USDOE EM Office of Program and Site Support (EM-50), DOE Contract Number AI09-00SR22188, Report Number 11-14-R, 2011.

[30] Delmhorst Europe, "Frequently Asked Questions about moisture measurement," 2023. [Online]. Available: http://www.moisturemetersdelmhorst.com/service-support/faqs.html.

[31] W. D. Walton, "Suppression of Wood Crib Fires With Sprinkler Sprays: Test Results," NBSIR 88-3696, National Institute of Standards and Technology, Gaithersburg, MD, 1988.

[32] F. Morandini and X. Silvani, "Experimental investigation of the physical mechanisms governing the spread of wildfires," *International Journal of Wildland Fire,* vol. 19, pp. 570-582, 2010.

[33] S. McAllister and M. Finney, "Burning Rates of Wood Cribs with Implications for Wildland Fires," *Fire Technology,* vol. 52, pp. 1755-1777, 2016.

[34] UL711, 8th Edition, January 5, 2023 - UL Standard for Safety Rating and Fire Testing of Fire Extinguishers.

Appendix A. Fuel Loading Specifications and Equivalence

To limit experimental variables, wood cribs are commonly used in large fire experiments, particularly because their combustion is well characterized [33] . Additionally, they are inexpensive, easy to construct, and burn at a relatively constant rate under fully ventilated conditions. In this study, wood cribs were substituted for combustible fuel typically stored in residential sheds. The burning rate of the crib is controlled by the internal surface, which directly scales with the number of wood cribs used [31].

The fuel loading in the shed experiments performed in this study consisted of wood cribs as described in ANSI/UL 711 for evaluating class 1-A fire extinguishers [34]. The wood crib used for 1-A evaluations is built from 72 pieces of dry wood, each with dimensions 38 mm × 38 mm × 500 mm. The crib consists of 12 layers of six evenly-spaced, parallel pieces of wood spanning 500 mm. The orientation of each successive layer of wood is perpendicular to the one below it. The final dimension of the test (1-A) crib is 500 mm × 500 mm × 456 mm.

The fuel-loading specifications for each shed size tested are provided in Table A-1. The predicted heat output from fuel loading (wood cribs) is determined by multiplying the mass of the wood by the heat of combustion for pine wood (ΔH =19.2 MJ/kg).

Table A-1. Fuel loading specifications for different shed sizes. (1ft = 0.305 m, 1 kg = 2.2 lbs)

Source Size	Number of 1-A Cribs	Total mass of cribs, kg	Total heat output, MJ	Fuel Loading, MJ/ft²
Closet (3 ft × 5 ft) 15 ft²	4	104	1.16	133
Very Small (4 ft × 5 ft) 20 ft²	6	156	1.74	166
Small (8 ft × 8 ft) 64 ft²	12	312	3.49	187

In this section, the fuel loads of the wood cribs used in the shed burn experiments are compared to fuel loads of typical contents found in residential sheds. This was done by examining the contents of several sheds and estimating the heat of combustion (HOC). The HOC represents the amount of heat generated by burning the object under ideal conditions and can be used as a measure of fire hazard. It is important to highlight that the HOC measures the amount of heat that is released upon combustion but is not indicative of the heat release rate. Two materials with similar HOC can burn very differently. A material with low heat release rate can burn slowly for a long period of time, while another material with high heat release rate can burn almost immediately.

A casual survey of several storage sheds in residential settings showed that a wide variety of materials were stored in the sheds. The shed contents were divided into several categories, including items made of wood, plastic, rubber, gasoline, and propane. Items made of metal or mostly metal were not included in this analysis since they are not expected to burn in a fire. Although commonly found in residential sheds, gasoline or battery powered tools such as lawn mowers were not included, since they would include substantial amounts of metal.

The mass of combustible items was measured with a hand-held scale. To simplify the calculation of the HOC of the items found in a typical storage shed, the mass of the item was multiplied by typical HOC values found in the literature. For many materials, the HOC in the literature covers a range of values. This is due to variations in the material and moisture content. To make the calculation even more complicated, most of the combustible material in residential sheds is made of plastic. There are many different plastics used in consumer products, and the determination of the exact plastic used in each item was beyond the scope of this study. To simplify the study, a single HOC was chosen for all plastics. Many of the items considered for the purpose of this study were made from either polyethylene or polypropylene. The HOC for polyethylene and polypropylene ranges from 43 MJ/kg to 47 MJ/kg (reference attached) so an average value of 45 MJ/kg was used. This section was intended to show the potential contents of sheds and is not a survey of actual sheds. It is also important to note that this section is not a study of fuel loads or HOC. The description, size, mass, HOC per kilogram, and total HOC for each of the items are provided in Table A-2.

Table A-2. Specifications of combustible items commonly found in residential storage sheds (1ft = 0.305 m, 1 kg = 2.2 lbs)

Description	Size	Mass (kg)	HOC (MJ/kg)	Total Heat (MJ)
Pine wood 2 × 4 per linear foot	38 mm × 89 mm × 305 mm	0.7	17.8	12
Plywood 3/8 in	3/8 in thick, 1 sq ft	0.4	18	7
4 Tier plastic shelving	711 mm × 381 mm × 1320 mm	4.5	45	200
Gasoline	1 gallon	3.0	46.8	133
Motor oil	1 quart	1.0	45	37
Automobile tire	P195/75R14	10	32.6	326
Propane cylinder	14.1 oz	0.4	50.33	20
Propane tank	20 lb	9.1	50.33	457
Rubber garden hose	25 ft long, 5/8 in inner diameter (ID), 7620 mm long × 15.9 mm ID	2.4	44	103
Plastic garden hose reel	51 mm × 56 mm × 61 mm	4.7	44	207
Plastic watering can	2 gal, 560 mm × 190 mm × 330 mm	0.3	45	11
Plastic rake (large)	660 mm × 500 mm × 1860 mm	1.2	45	53
Plastic rake (medium)	610 mm × 540 mm × 1610 mm	1	45	38
Plastic rake wooden handle only (medium)	1200 mm × 23.1 mm diameter	0.4	45	16
Plastic bucket w/Top	5 gal, 30 cm diam., 37 cm high	1.5	45	48

Garden tool wooden handle	1300 mm × 27 mm diam., 744000 mm³ volume – ash wood	0.3	20	7
Plastic flower pot base	260 mm diam. × 70 mm high	0.14	45	6
Plastic flower pot (medium)	225 mm diam. × 160 mm high	0.1	45	3
Plastic flower pot (small)	155 mm diam. × 180 mm high	0.1	45	2
Plastic flower pot (large)	285 mm diam. × 250 mm high	0.14	45	6
Plastic bucket	320 mm diam. × 275 mm high	0.13	45	6
Wooden croquet set	450 mm × 640 mm × 175 mm	4.4	19	84
Plastic milk crate	380 mm × 355 mm × 260 mm	1	45	37
Plastic frisbee	255 mm diam.	0.16	45	7
Black plastic tote w/top	27 gal (102 L), 726 mm × 497 mm × 381 mm	3	45	140
Small plastic lawn spreader w/metal handle	406 mm × 508 mm × 1150 mm high	5	45	218
Large plastic lawn spreader w/metal handle	558 mm × 558 mm × 1150 mm high	6	45	262
Large plastic flower pot	20 in 500 mm × 420 mm high	1.2	45	54
Small plastic flower pot	10 in 220 mm × 220 mm high, #5	0.2	45	9
Extra large plastic flower pot	540 mm × 410 mm high	1.7	45	77
Plastic planter	300 mm × 670 mm × 240 mm high	0.8	45	36
Plastic trash can w/lid	44 gal, 610 mm × 820 mm high	6	45	277
Plastic trash can w/lid	32 gal, 570 mm × 690 mm high, #4	3	45	128
Plastic trash can w/lid	32 gal, 560 mm × 730 mm high	4.05	45	182
Can liner	33 gal 50 package	2.3	45	104
Paper leaf bags	30 gal 5 package, each 406 mm × 305 mm × 889 mm, 0.0254 mm thick	1.1	17	19
Plastic recliner	584 mm × 627 mm × 813 mm	9.2	45	414
Plastic gas can	2 gal, 178 mm × 254 mm × 292 mm	0.7	45	32
Plastic kid's water table	229 mm × 991 mm × 737 mm	9	45	409
Plastic patio chair	584 mm × 627 mm × 813 mm high	2	45	94

The combustible items in each shed type were determined by adding items until the total HOC for all the items was approximately equal to total HOC for the wood cribs used in the shed. The thirteen experiments included crib fuel loading in three ranges as shown in Table A-3. Similar items were used for the sheds in each of the three ranges.

Table A-3. Crib Fuel Ranges. (1 kg = 2.2 lbs)

NOSSE Test Numbers	Crib Mass, Kg	Crib HOC, MJ
5,6	95-96	1824-1843
1,2,3,4,9,10,13	128-147	2458-2822
7,8,11,12	283-290	5434-5568

Appendix B. Shed Burn Specification

The experimental data for each experiment, including the test and shed specifications, are provided here. Images captured from video cameras were used to provide an overview of each shed burn experiment. The overview photograph shows the shed orientation with respect to the target structure at the time when peak heat fluxes were recorded. The experimental data includes temporal plots of heat fluxes at the eaves and on the free-standing heat flux gauge rig. Temporal plots of temperature data collected at the eaves and at the eave vent are also included.

Section 3.1.4 gives a summary of the set-up for each test. Section 3.1.6 discusses the data in more detail and compares the results among experiments.

NOSSE1
Test: O-WVSh0-10
9/28/2021

Shed Material: Wood
Shed Type: Very Small
Floor area, ft²: 26
Fuel Loading, 1-A wood cribs: 6
Combustible Mass, kg: 204
Wind speed: Ambient
SSD: 10 ft

t= 11 min
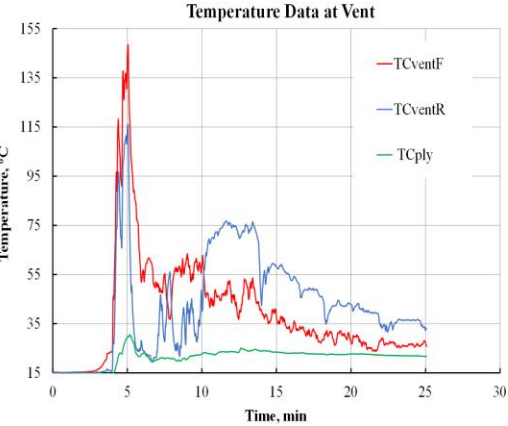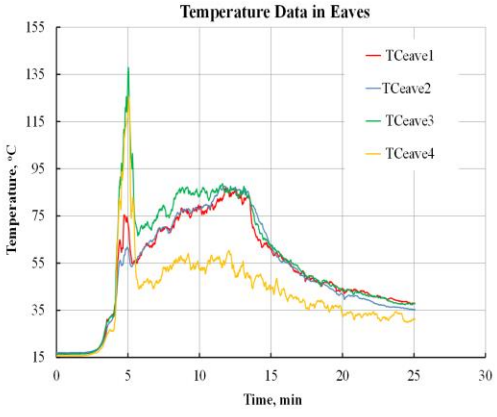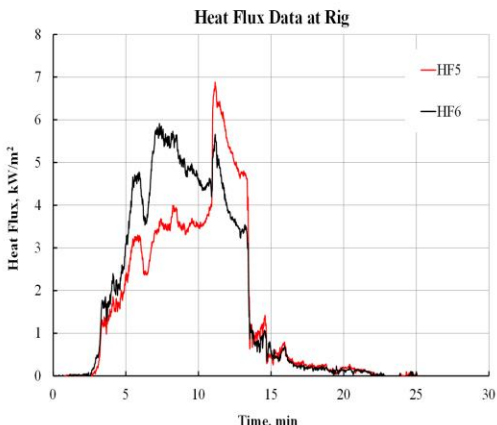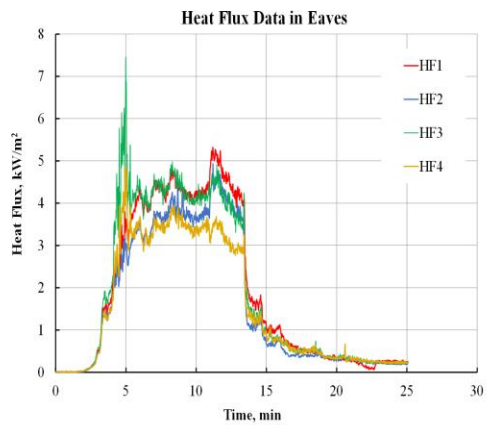
	Peak Temp., °C	Peak Heat Flux, kW/m²
HF1	87	5
HF2	88	5
HF3	138	7
HF4	125	5
HF5	-	7
HF6	-	6
	Peak Temp., °C	
TCventF	148	
TCventR	116	
TCventPly	31	

NOSSE2
Test: O-SVSh0-10
10/05/2021

Shed Material: Steel
Shed Type: Very Small
Floor area, ft²: 20
Fuel Loading, 1-A wood cribs: : 6
Combustible Mass, kg: 172
Wind speed: Ambient
SSD: 10 ft

t= 22 min

Heat Flux Data at Eaves

HF1
HF2
HF3
HF4

Heat Flux Data at Rig

HF5
HF6

Temperature Data at Eaves

TCeave1
TCeave2
TCeave3
TCeave4

Temperature Data at Vent

TCventF
TCventR
TCply
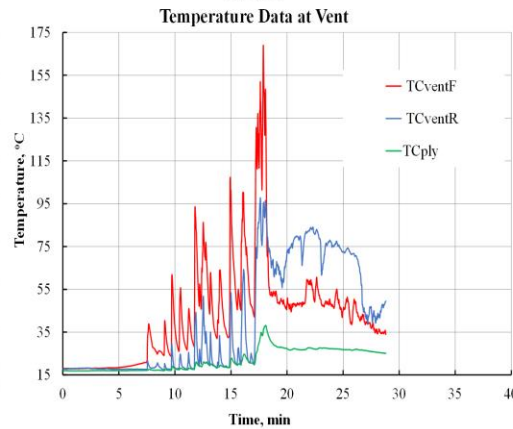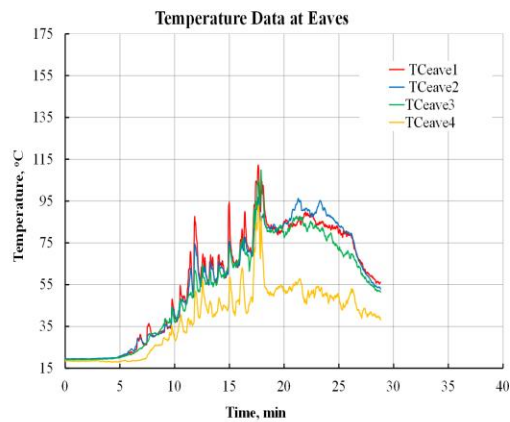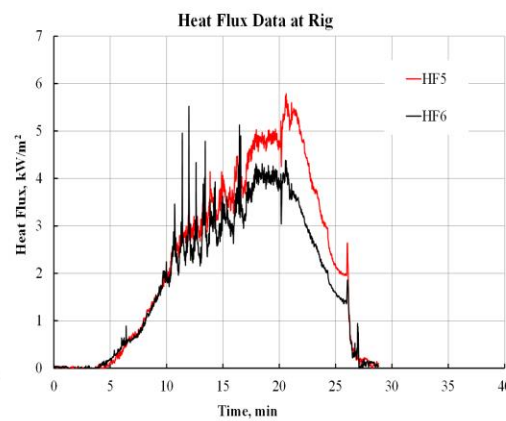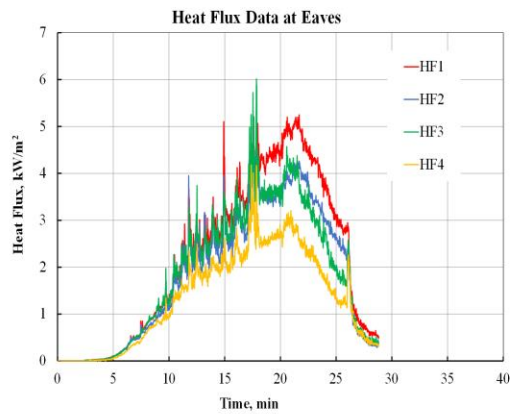
	Peak Temp., °C	Peak Heat Flux, kW/m²
HF1	112	5
HF2	97	5
HF3	110	6
HF4	93	4
HF5	-	6
HF6	-	4
	Peak Temp., °C	
TCventF	169	
TCventR	98	
TCventPly	38	

82

NOSSE3
Test ID: O-WVShw-10
10/14/2021

Shed Material: Wood
Shed Type: Very Small
Floor area, ft²: 26
Fuel Loading, 1-A wood cribs: 6
Combustible Mass, kg: 203
Wind speed: High
SSD: 10 ft

t= 9 min

Heat Flux Data at Eaves
(HF1, HF2, HF3, HF4)

Heat Flux Data at Rig
(HF5, HF6)

Temperature Data at Eaves
(TCeave1, TCeave2, TCeave3, TCeave4)

Temperature Data at Vent
(TCventF, TCventR, TCply)
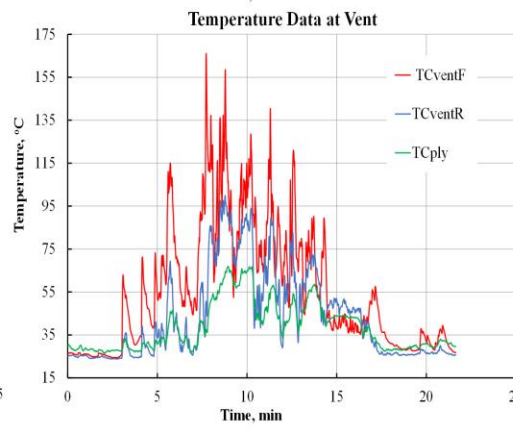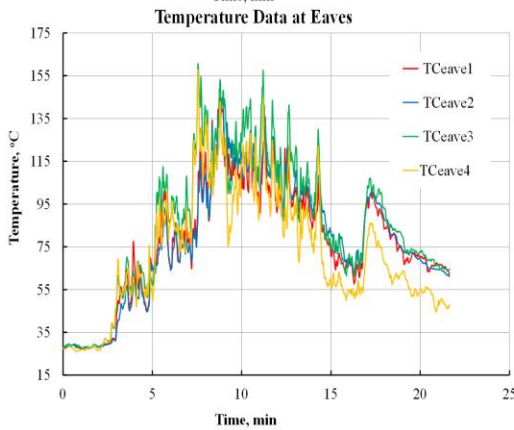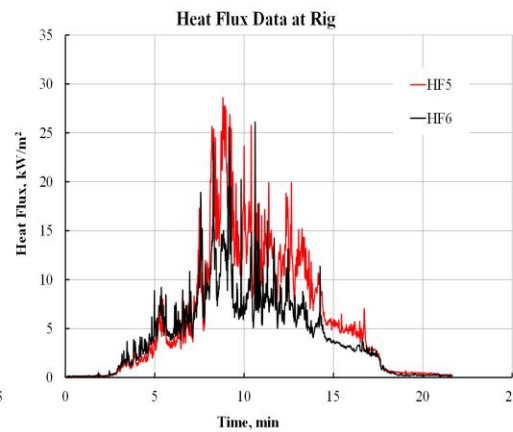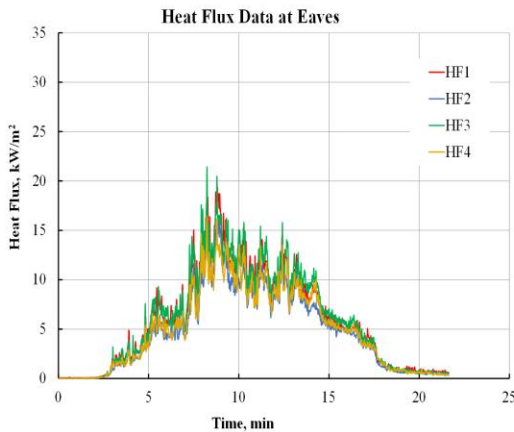
	Peak Temp., °C	Peak Heat Flux, kW/m²
HF1	144	19
HF2	145	16
HF3	161	21
HF4	158	16
HF5	-	29
HF6	-	26
	Peak Temp., °C	
TCventF	166	
TCventR	100	
TCventPly	67	

NOSSE4
Test ID: O-SVShw-10
10/19/2021

Shed Material: Steel
Shed Type: Very Small
Floor area, ft²: 20
Fuel Loading, 1-A wood cribs: 6
Combustible Mass, kg: 138
Wind speed: High
SSD: 10 ft
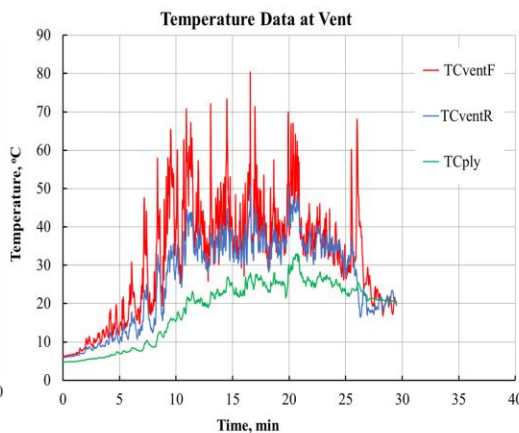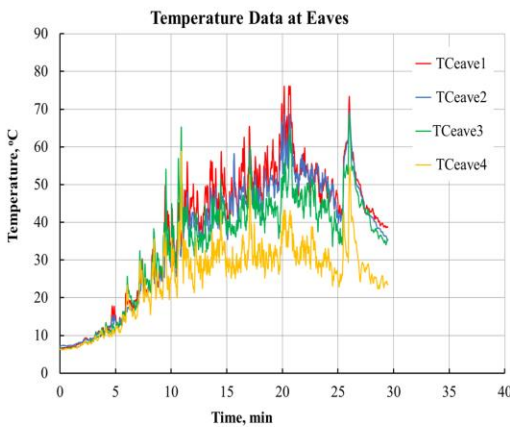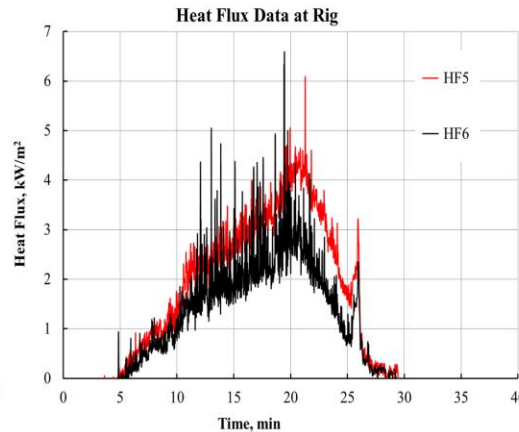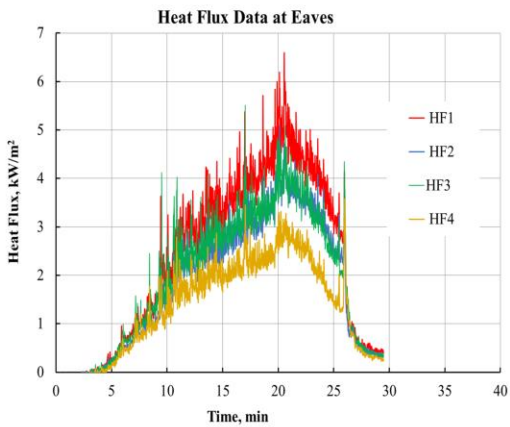
	Peak Temp., °C	Peak Heat Flux, kW/m²
HF1	59	6
HF2	58	4
HF3	65	4
HF4	59	3
HF5	-	5
HF6	-	4
	Peak Temp., °C	
TCventF	73	
TCventR	45	
TCventPly	27	

NOSSE5
Test ID: O-SChw-5
10/20/2021

Shed Material: Steel
Shed Type: Closet
Floor area, ft²: 15
Fuel Loading, 1-A wood cribs: 4
Combustible Mass, kg: 95
Wind speed: High
SSD: 5 ft

t= 15 min

Heat Flux Data in Eaves

Heat Flux Data at Rig

Temperature Data in Eaves

Temperature Data at Vent
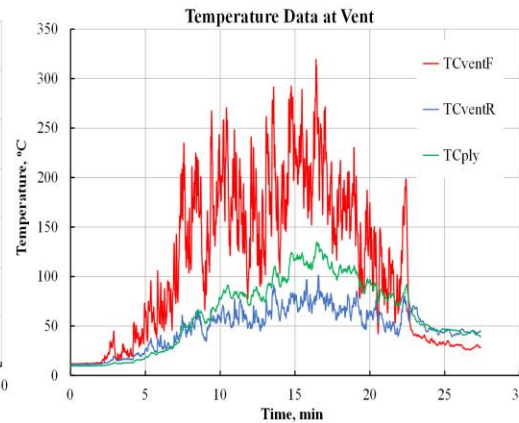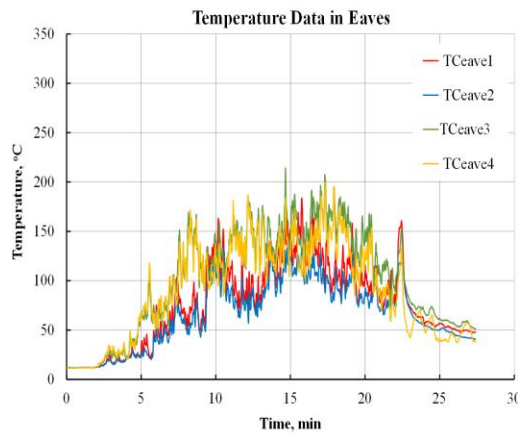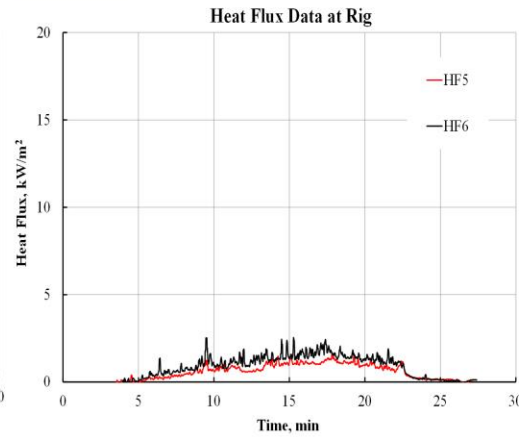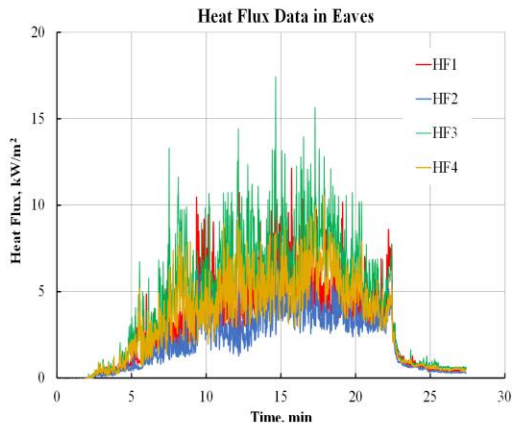
	Peak Temp., °C	Peak Heat Flux, kW/m²
HF1	184	9
HF2	136	6
HF3	214	12
HF4	200	9
HF5	-	2
HF6	-	2
	Peak Temp., °C	
TCventF	319	
TCventR	101	
TCventPly	135	

NOSSE6
Test ID: O-WChw-10
10/21/2021

Shed Material: Wood
Shed Type: Closet
Floor area, ft²: 16
Fuel Loading, 1-A wood cribs: 4
Combustible Mass, kg: 146
Wind speed: High
SSD: 10 ft

t= 14 min

Heat Flux Data at Eaves

Heat Flux Data at Rig

Temperature Data at Eaves

Temperature Data at Vent
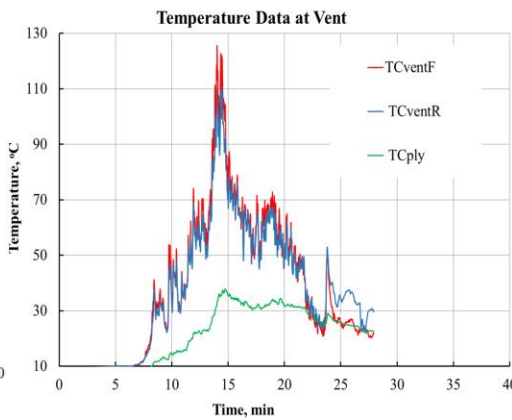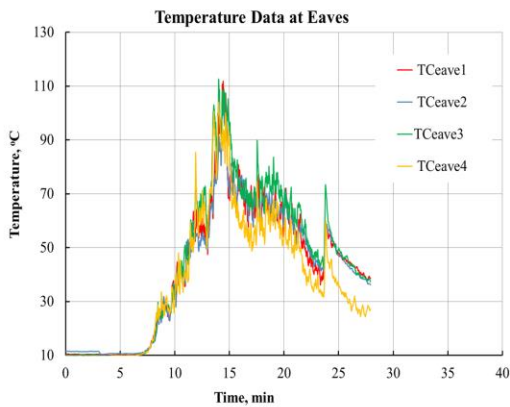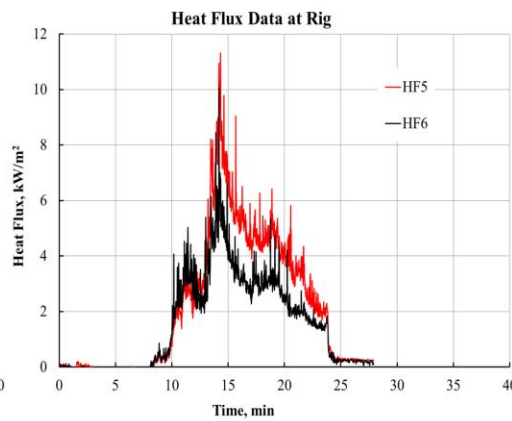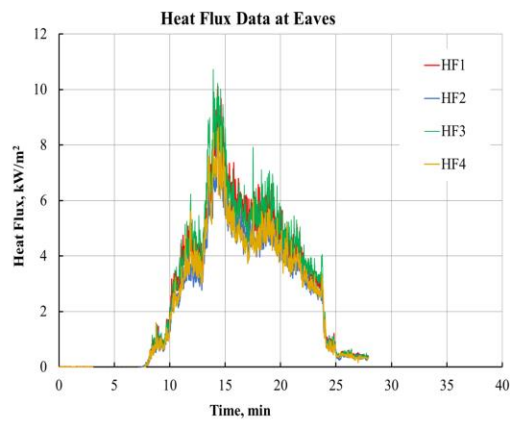
	Peak Temp., °C	Peak Heat Flux, kW/m²
HF1	112	10
HF2	105	8
HF3	113	11
HF4	104	9
HF5	-	11
HF6	-	10
	Peak Temp., °C	
TCventF	126	
TCventR	110	
TCventPly	38	

NOSSE7
Test ID: O-SShw-15
10/28/2021

Shed Material: Steel
Shed Type: Small
Floor area, ft²: 48
Fuel Loading, 1-A wood cribs: 12
Combustible Mass, kg: 287
Wind speed: High
SSD: 15 ft

t= 30 min

Heat Flux Data at Eaves

Heat Flux Data at Rig

Temperature Data at Eaves

Temperature Data at Vent
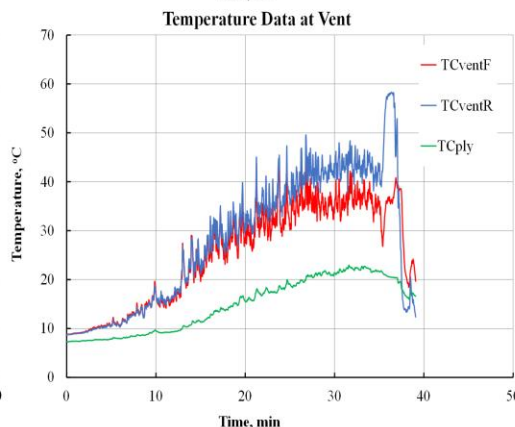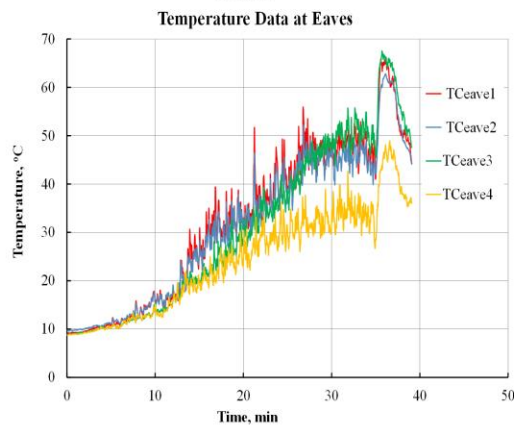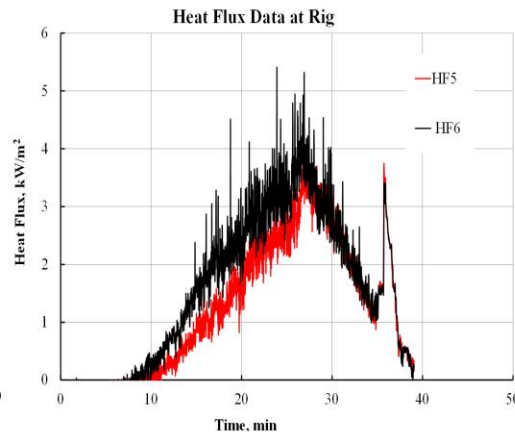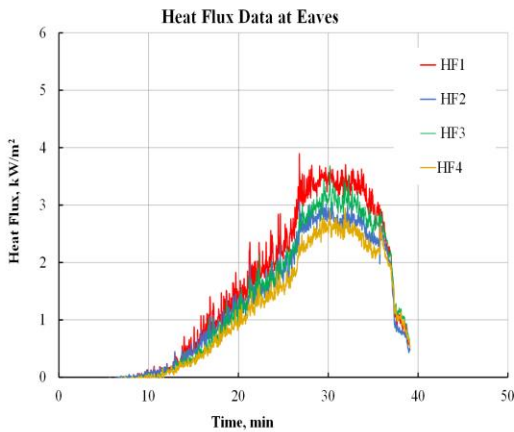
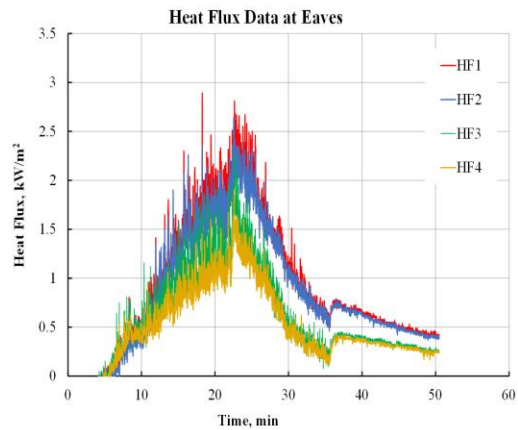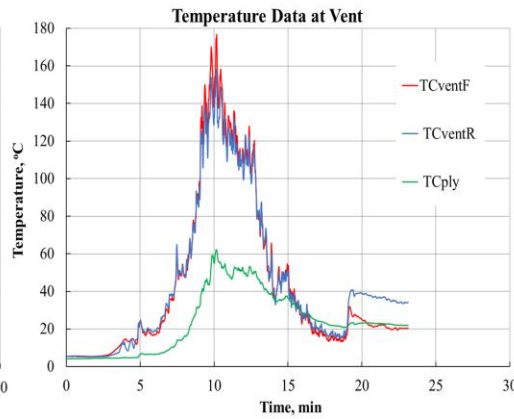|	Peak Temp., °C	Peak Heat Flux, kW/m²
HF1	66	3.5
HF2	63	3.5
HF3	68	3
HF4	49	3
HF5	-	4
HF6	-	5
	Peak Temp., °C	
TCventF	44	
TCventR	58	
TCventPly	23	

NOSSE8
Test ID: O-WShw-15
10/28/2021

Shed Material: Wood
Shed Type: Small
Floor area, ft²: 67
Fuel Loading, 1-A wood cribs: 12
Combustible Mass, kg: 544
Wind speed: High
SSD: 15 ft

t= 17 min
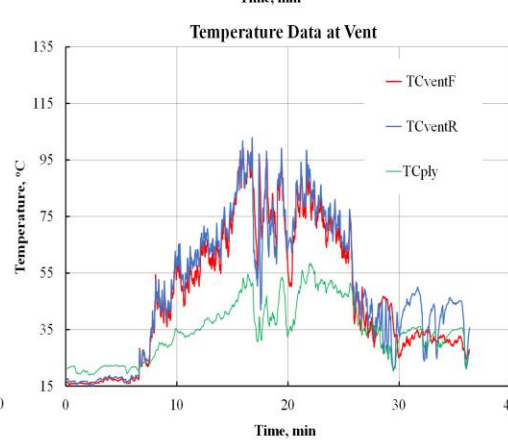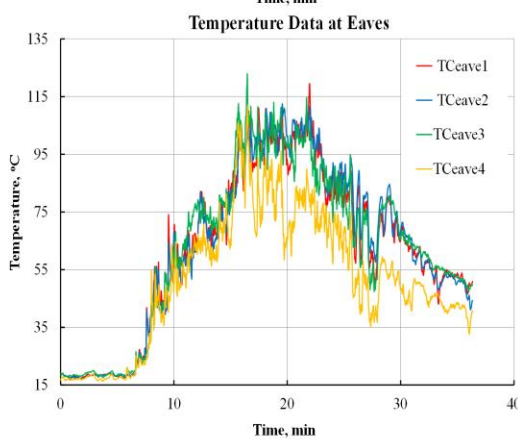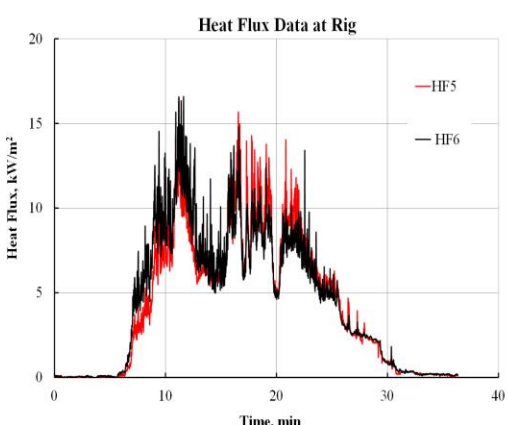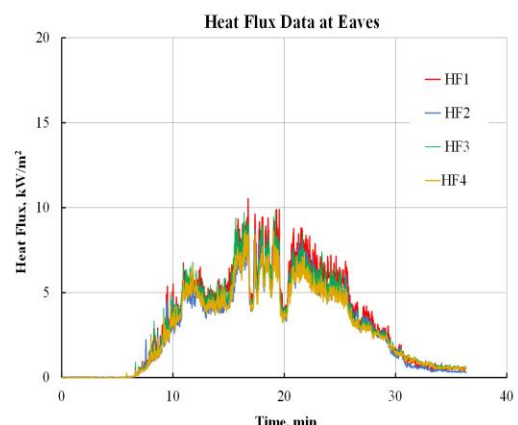
	Peak Temp., °C	Peak Heat Flux, kW/m²
HF1	120	10
HF2	113	9
HF3	123	10
HF4	112	9
HF5	-	12
HF6	-	15
	Peak Temp., °C	
TCventF	100	
TCventR	103	
TCventPly	59	

88

NOSSE9
Test: O-SVShw-10-
Door opening 90°
11/03/2021

Shed Material: Steel
Shed Type: Very Small
Floor area, ft²: 20
Fuel Loading, 1-A wood cribs: 6
Combustible Mass, kg: 140
Wind speed: High
SSD: 10 ft

t= 23 min

Heat Flux Data at Eaves

Heat Flux Data at Rig

Temperature Data at Eaves

Temperature Data at Vent
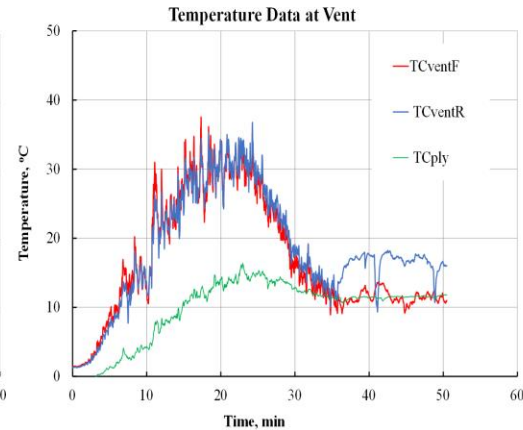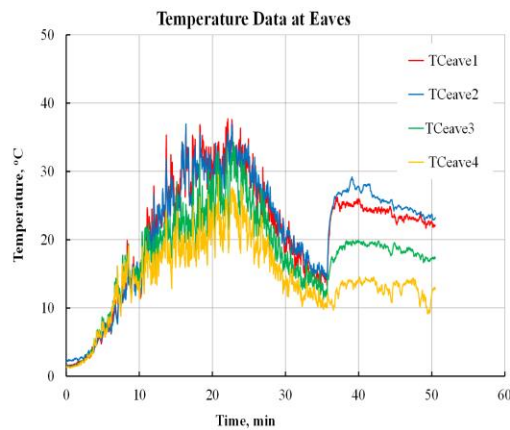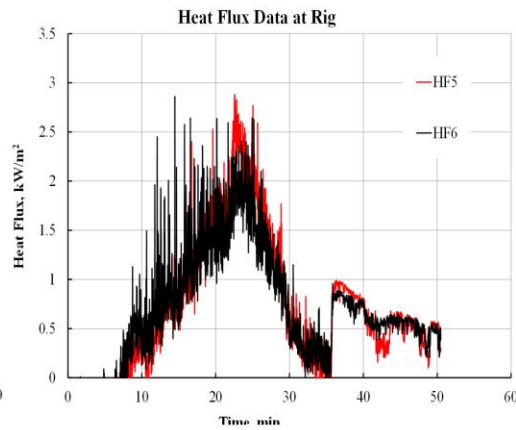
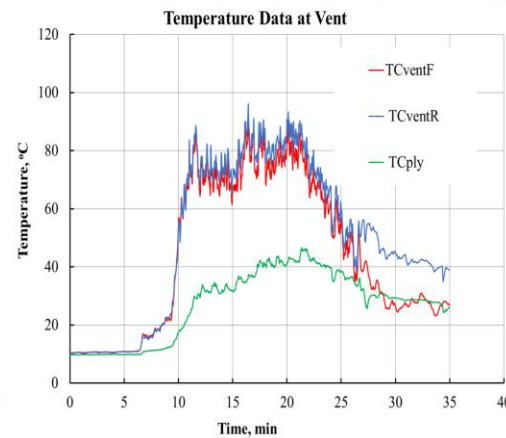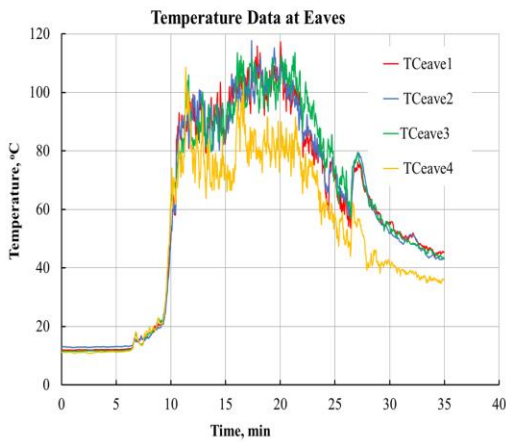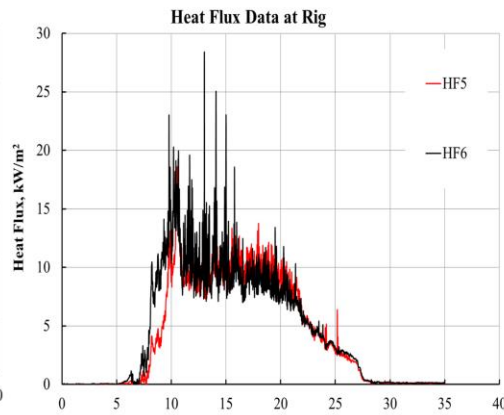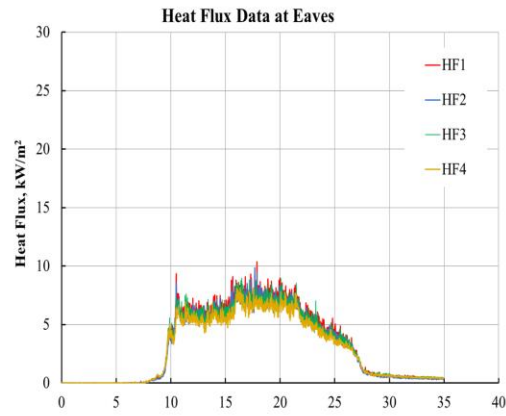|	Peak Temp., °C	Peak Heat Flux, kW/m²
HF1	38	3
HF2	37	3
HF3	34	2
HF4	30	2
HF5	-	2.5
HF6	-	2
	Peak Temp., °C	
TCventF	38	
TCventR	37	
TCventPly	16	

NOSSE10
Test ID: O-WVShw-10-R1
11/09/2021

Shed Material: Wood
Shed Type: Very Small
Floor area, ft²: 26
Fuel Loading, 1-A wood cribs: 6
Combustible Mass, kg: 190
Wind speed: High
SSD: 10 ft

t= 10 min
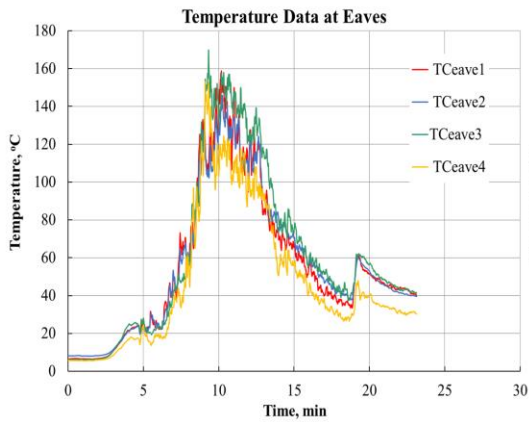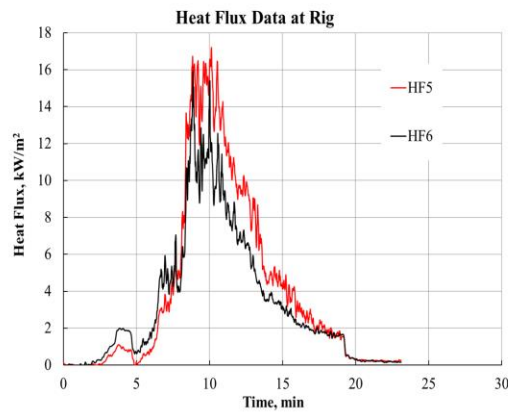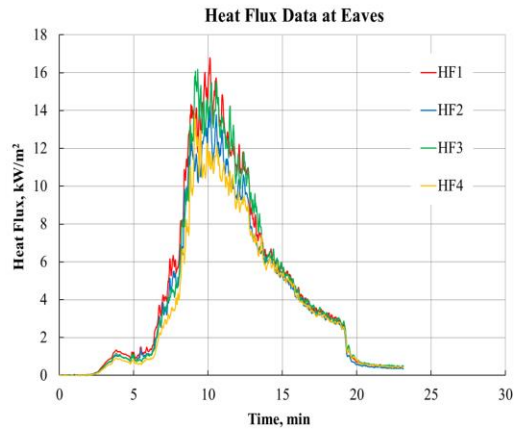
	Peak Temp., °C	Peak Heat Flux, kW/m²
HF1	159	18
HF2	146	15
HF3	170	18
HF4	153	16
HF5	-	17
HF6	-	16
	Peak Temp., °C	
TCventF	177	
TCventR	158	
TCventPly	62	

NOSSE11
Test ID: O-WShw-15-R1
11/10/2021

Shed Material: Wood
Shed Type: Small
Floor area, ft²: 67
Fuel Loading, 1-A wood cribs: 12
Combustible Mass, kg: 825
Wind speed: High
SSD: 10 ft

t= 15 min

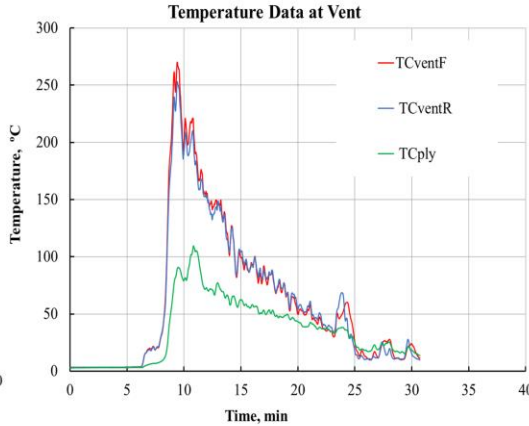|	Peak Temp., °C	Peak Heat Flux, kW/m²
HF1	117	10
HF2	118	10
HF3	114	9
HF4	109	8
HF5	-	19
HF6	-	28
	Peak Temp., °C	
TCventF	96	
TCventR	92	
TCventPly	47	

NOSSE12
Test ID: O-WShw-10
11/17/2021

Shed Material: Wood
Shed Type: Small
Floor area, ft²: 67
Fuel Loading, 1-A wood cribs: 12
Combustible Mass, kg: 825
Wind speed: High
SSD: 10 ft

t= 9 min
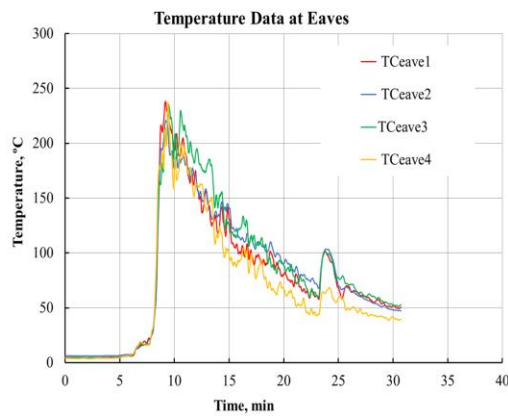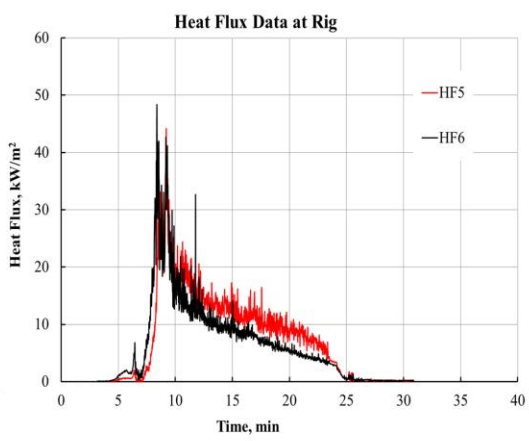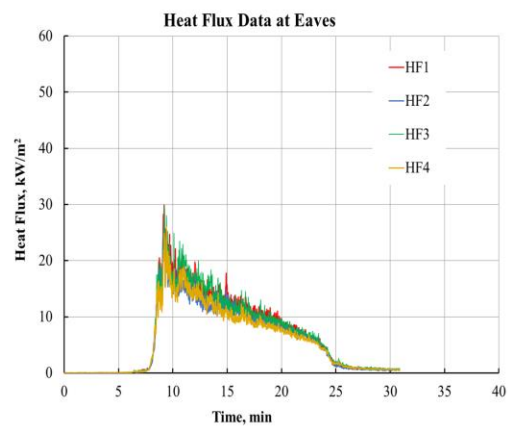
	Peak Temp., °C	Peak Heat Flux, kW/m²
HF1	251	30
HF2	226	27
HF3	243	30
HF4	256	26
HF5	-	44
HF6	-	48
	Peak Temp., °C	
TCventF	286	
TCventR	266	
TCventPly	111	

NOSSE13
Test ID: O-WVShw-10-R2
12/01/2021

Shed Material: Wood
Shed Type: Very Small
Floor area, ft²: 26
Fuel Loading, 1-A wood cribs: 6
Combustible Mass, kg: 240
Wind speed: High
SSD: 10 ft

t= 7 min

Heat Flux Data at Eaves

Heat Flux Data at Rig

Temperature Data at Eaves

Temperature Data at Vent
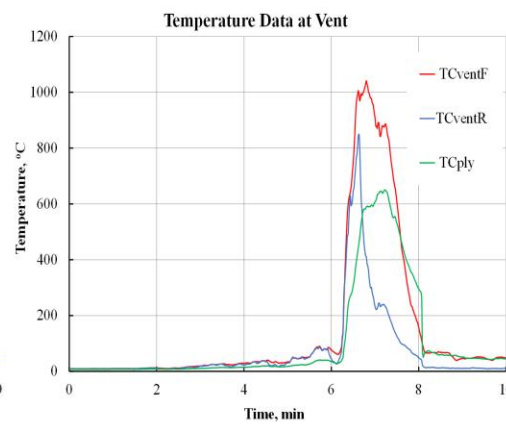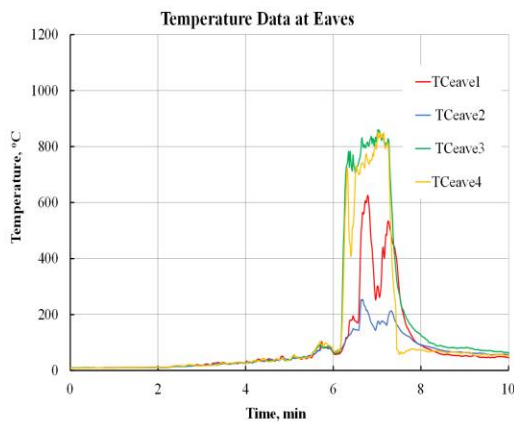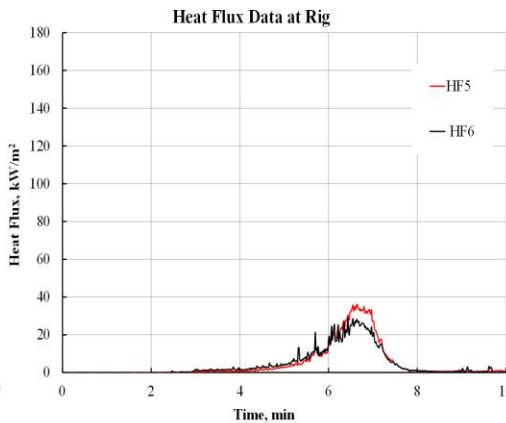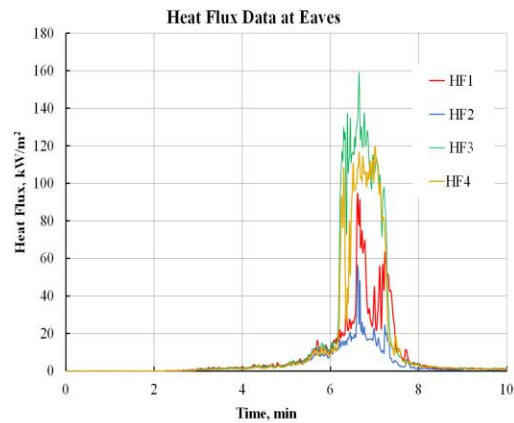
	Peak Temp., °C	Peak Heat Flux, kW/m²
HF1	626	95
HF2	254	56
HF3	860	159
HF4	853	120
HF5	-	36
HF6	-	29
	Peak Temp., °C	
TCventF	1041	
TCventR	849	
TCventPly	650	

NOSSE13
Test ID: O-WVShw-10-R2
12/01/2021

Shed Material: Wood
Shed Type: Very Small
Floor area, ft²: 20
Fuel Loading, 1-A wood cribs: 6
Combustible Mass, kg: 240
Wind speed: High
SSD: 10 ft

t= 7 min
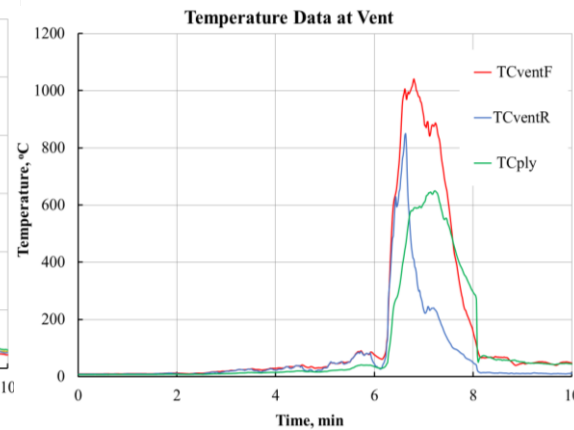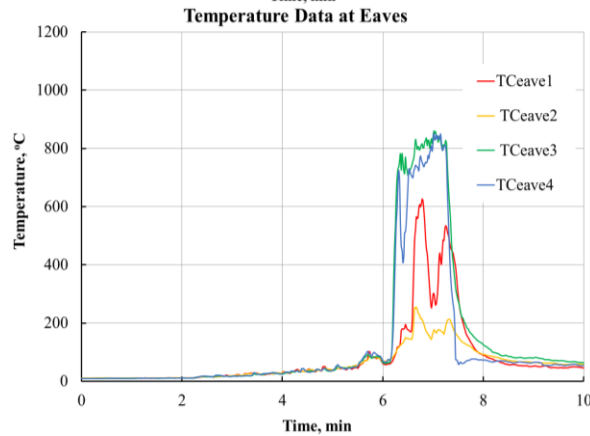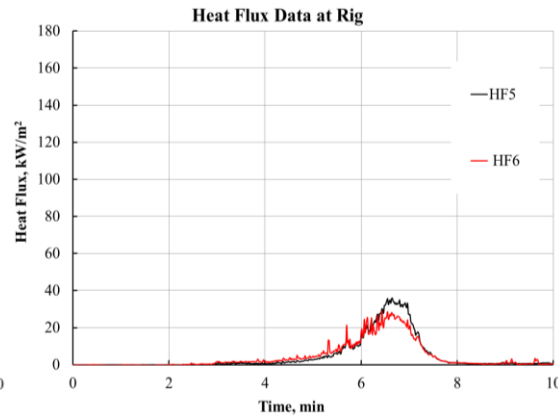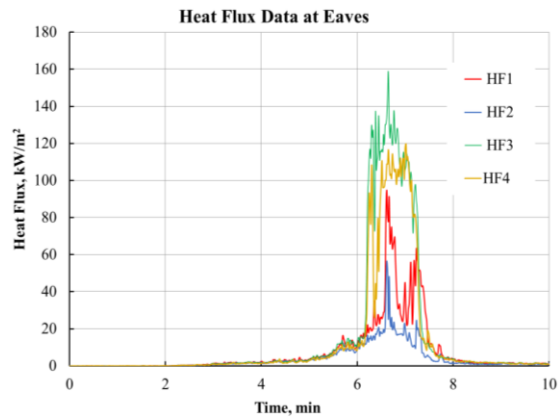
	Peak Temp., °C	Peak Heat Flux, kW/m²
HFG1	626	95
HFG2	254	56
HFG3	860	159
HFG4	853	120
HFG5	-	36
HFG6	-	29
	Peak Temp., °C	
TCventF	1041	
TCventR	849	
TCventPly	650	

Appendix C. Uncertainty Analysis

The measurements of heat fluxes, temperatures, times, wind flow, mass, and distances all involve uncertainties. Measurement uncertainties have several components that are typically grouped into two categories based on the method used to estimate their value. Type A uncertainties are evaluated by statistical methods, and Type B uncertainties are evaluated by other means, often based on scientific judgment using all available relevant information [26]. The component standard uncertainty includes resolution, calibration, installation, and random errors. The resolution is the minimum change in the data measurement the instrument can exhibit. Calibration error includes uncertainties from sensor calibration. Resolution and calibration uncertainties are derived from instrument specifications (Type B). Uncertainty due to the installation method was estimated based on engineering judgment (Type B) considering misalignment, quality of the sensor mounting method, and previous data.

Given the nature of experiments and hence the singular measurements in this study, the evaluation of Type A uncertainties was not feasible for the majority of measurements. Most uncertainties reported herein are Type B uncertainties, either estimated through scientific judgment or obtained from the literature.

Wind speed measurements: Uncertainty analysis of wind speed is provided in Section 2.1.5.2.

Temperature measurements: Type K thermocouples used in this test series have an inherent standard uncertainty in temperature measurements reported by the manufacturer was $\pm\ 0.75\ \%$.

Additional uncertainties in measured temperature are primarily due to radiative heating and cooling of the thermocouple bead that causes it to respond to phenomena other than the surrounding gas temperature. The thermal environment surrounding a given thermocouple is difficult to characterize, especially in the presence of wind. These uncertainties will overwhelm the inherent uncertainties in the thermocouple described earlier.

Heat flux measurements: The main sources of uncertainty about the total heat flux measurements are: (1) the uncertainty of the analog to digital (A/D) conversion, (2) uncertainty in the calibration, and (3) uncertainty due to soot deposition on the sensing surface of the gauge. (1) The uncertainty in A/D conversion is inherent to the data acquisition system. It is system-specific and is associated with the digitization of the analog signals from the gauge. This type of uncertainty is negligible. (2) The relative expanded uncertainty reported by the manufacturer is $\pm\ 3\ \%$ of the gauge sensitivity (the slope of the calibration curve) with a coverage factor of 2 (confidence level of 95 %). This would result in an uncertainty of about 4 kW/m² for a nominal reading of 140 kW/m². (3) The uncertainty due to soot deposition is more challenging to quantify. The amount of soot deposition depends on many parameters, such as the location of the gauge, the flow field and temperature fields near the gauge, the duration of an experiment, and the soot volume fraction. No attempt was made to quantify this soot effect for these experiments. Additional uncertainty due to flame impingement on the gauges is considered negligible.

Distance measurements: The structure separation distances (SSDs) between the target wall and the source structure and the distances between the source structure and instrumentation, including the heat flux gauge (HFG) rigs (surrogate target structures), were determined using a tape measure. Sources of uncertainty include the placement of the tape measure and the ability to adjust the positions of the source structure and the HFG rigs accurately. The expanded

uncertainty for engineering measurements with a confidence level of 95 % was estimated as ½ inch (1.2 cm). For tape measures 25 ft or longer, the expanded uncertainty was ±1 in (±2.54 cm).

The users of this report are advised to be informed that the experimental results presented in this report are either raw data or the statistics of raw data acquired by the measurement systems. Incorporating the measurement uncertainty reported here into the validation of predictive models is highly recommended.

Appendix D. Implementation of Technical Findings: Case Studies

Small auxiliary storage sheds can be ignited from flaming fire exposures and/or by embers. Once ignited, burning sheds readily become a source of additional fire spread, often igniting adjacent residential structures. This can lead to a cascade of ignitions, especially under high-wind conditions in high density housing communities. Such structure-to-structure fire spread can outpace fire control efforts, making it difficult to contain fires. In response to this, auxiliary storage sheds with footprints larger than 120 ft² are regulated under Chapter 7A of the California Building Code, as well as under the International Wildland-Urban Interface (IWUI) code. These codes require detached auxiliary structures that are located between 3 ft and 50 ft from the primary structure to be constructed of noncombustible materials or of ignition-resistant materials.

Recently, NIST introduced the WUI Fire Hazard Mitigation Methodology (HMM) [9] to reduce fire spread through communities based on spatial relationships between fuels, exposures, and fire hardening of both the structure and parcel. Implementation of minimum separation distances from a variety of structures common in residential plots (the SSD_{min}), in addition to the implementation of hazard mitigation tools described in the HMM (the three 'R's; **R**emove fuels, **R**educe fuels, and **R**elocate fuels), can improve community resilience to WUI and structure-to-structure fire exposures. The purpose of this report (NOSSE) is to estimate SSD_{min} through experimental measurements for some common structures in the presence of wind. It is important to note that the HMM assumes that the target structures are not hardened (typical of retrofit) whereas the work presented in this report and a report on previous shed burn experiments [21] were conducted primarily with fire-hardened target structures. Regardless, the value of this data informs actions that seek to provide the greatest value (risk reduction) for an investment. The intent of HMM is to create the highest risk reductions at the lowest cost in terms of time, modification, and monetary investment.

The outdoor shed experiments were performed to determine safe SSD to prevent fire spread in the presence of wind for various source sizes (Closet, Very Small shed, and Small shed) with high fuel loadings. The indoor shed burn experiments quantified and highlighted significant fire hazards from storage sheds to nearby residential structures under no-wind conditions. The experiments provide information on relative hazards associated with sheds of different construction materials, sizes, and fuel loadings. These outdoor and indoor shed burn experiments focused only on direct fire exposures.

Three prevalent cases from typical high-density WUI communities are discussed below in the context of hazard assessment and hazard mitigation. The HMM [9] divides high-density interface communities into Type 1 and Type 2. Type 1 communities are located at the perimeter of the community abutting a wildland area, and Type 2 are in the interior, defined as greater than 0.25 mi from the wildland. Unless otherwise specified, the hazard assessment is presented in the context of minimum SSDs. Adverse local conditions, including but not limited to lack of hardening of the residence, terrain, and the presence of other fuels (including linear and ladder fuels) in the vicinity of the shed, will increase the minimum SSDs described here.

D.1. Case 1: Reduce and Relocate Sheds

An example of high-density interface community is shown in the aerial imagery in Fig. D-1. The imagery shows that placement of storage sheds close to the primary structure (in yellow rectangles) is common. Such a case is representative of situations in high-density WUI communities. In the event of a WUI fire, a shed ignited by flames or embers presents a severe fire hazard to the entire community.
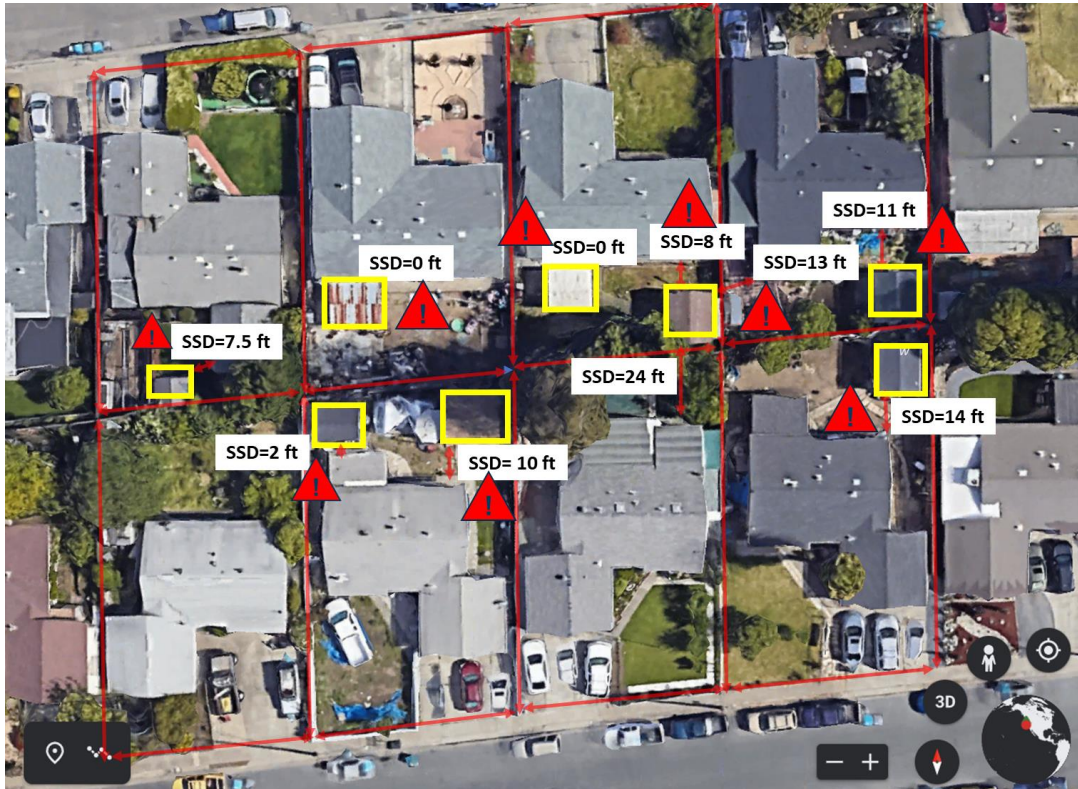
Fig. D-1. Case 1: High density community with 8 auxiliary structures (sheds) in 8 parcels. (1ft = 0.305 m)

A majority of the fuel fraction in high-density communities is in the form of residential structures and auxiliary structures. Residential structures represent a significant density of fuels that impact fire spread and, in many cases, directly contribute to the ignition of neighboring structures, propagating fire throughout the community. The primary residential structures are immobile and, therefore, pose a unique challenge in hazard management. While they can be hardened using the mitigation methodology described in HMM, they cannot be readily removed or displaced like many other WUI fuels, including auxiliary sheds.
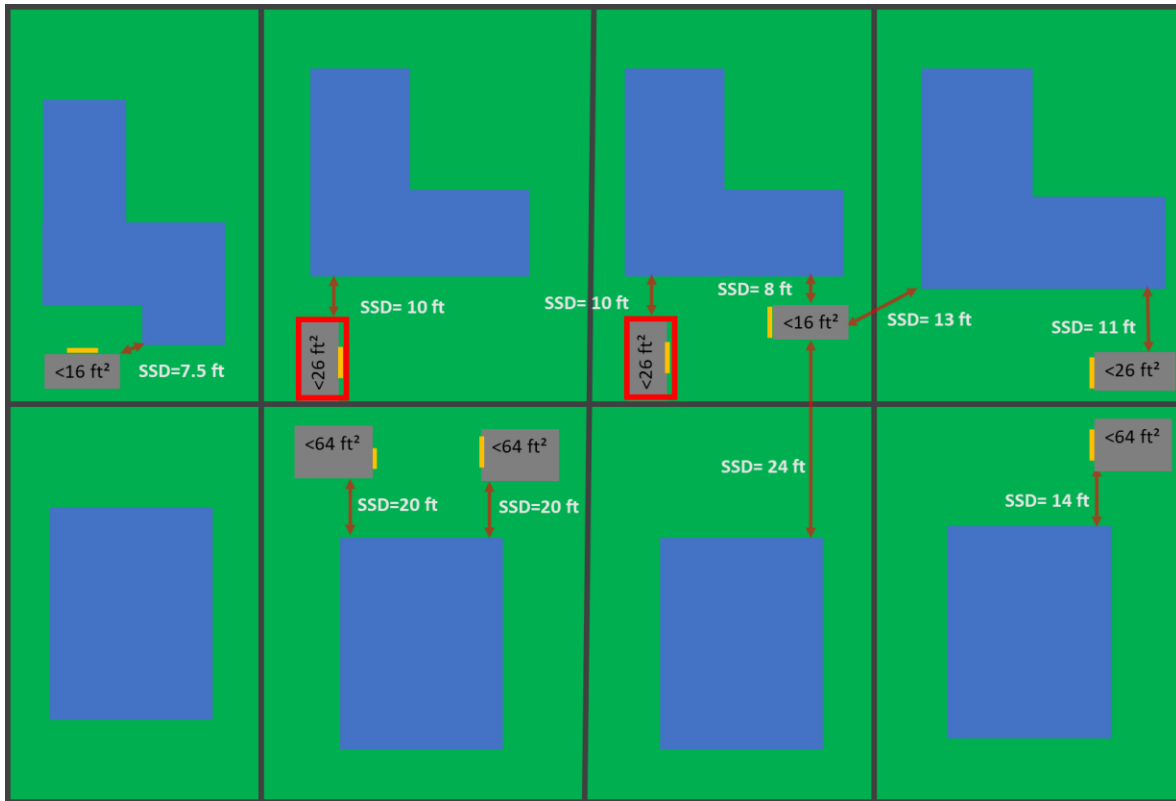
The high-density interface community shown in Fig. D-1 has parcel sizes of less than 0.13 ac, typical of such communities. The storage sheds on these parcels, outlined in yellow, have areas ranging from 80 ft² to 256 ft², as measured via GIS. Information about the construction materials for the storage sheds highlighted in Fig. D-1 is not available. Approximate SSDs estimated using GIS measurement tools are shown in an idealized schematic in Fig. D-2, highlighting approximate footprints of the primary residences and auxiliary structures. Additional fuels such as combustible fences and woodpiles are not illustrated in the idealized figure for clarity.
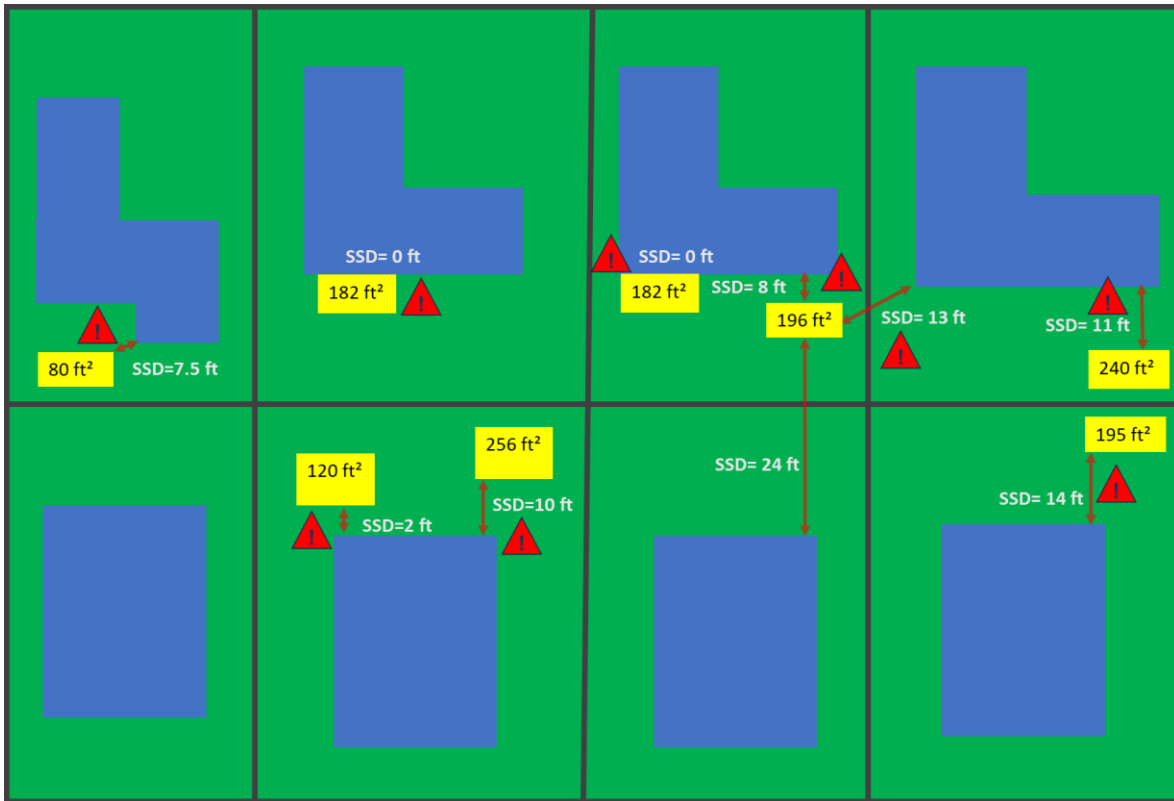
Fig. D-2. Case 1: Idealized schematic showing shed hazard to the primary residence based on estimated SSDs. (Figure not to scale) (1ft = 0.305 m)

The assessment of fire hazards in this community can be accomplished by using the minimum SSDs listed in this report. Assuming the sheds are made from combustible construction material and given the approximate floor area and the SSDs of these sheds, each shed is a potential fire hazard to this high-density community. The red caution signs in Fig. D-2 represent locations where a hazardous fire spread pathway or a structure ignition condition is likely.

The hazard mitigation approach for such a community would be to remove the sheds or to reduce the shed sizes, reduce the fuel loading by using noncombustible metal sheds, and/or relocate the sheds away from the primary or neighboring structures. In the event of ignition of contents of the shed, a noncombustible shed would contain the fire and prevent flame spread. Significant reduction in thermal exposures from this shed could be achieved with closed doors. However, since door closure cannot be guaranteed or regulated, the door opening of noncombustible steel sheds should be directed away from the primary structure, combustible fence, neighboring structure, or any other combustible objects. Figure D-3 shows hazard mitigation in Case 1 using the **R**educe and **R**elocate approaches. The gray boxes illustrate noncombustible steel sheds and the yellow lines represent door openings. The grey boxes with red outlines represent relocated sheds.

Fig. D-3. Case 1: Idealized schematic showing shed hazard mitigation tools applied to reduce fire hazard from storage sheds. (Figure not to scale) (1ft = 0.305 m)

D.2. Case 2: Remove Shed

Another example of a high-density interface community is shown in Fig. D-4. The highlighted shed in Fig. D-4 poses a fire spread hazard to the primary residence and the two neighboring residences. Using the minimum SSDs estimated in this study for noncombustible steel sheds, Fig. D-4 highlights the challenges of placing sheds with an appropriate SSD in a high-density community. Thus, in Case 2 the hazard mitigation tools of **R**educe and **R**elocate are not applicable. The only hazard mitigation tool that is available in Case 2 is to **R**emove the shed from the parcel.

Fig. D-4. Case 2: Small parcel with small SSD provides minimal SSD for storage shed. Shed poses hazard to both the primary residence and two neighboring residences. (1ft = 0.305 m)

D.3. Case 3: Fire Hazard for Neighboring Residence

Figure D-5 highlights the potential for parcel-to-parcel exposures from sheds placed on a larger parcel. A very large shed with an approximate floor area of 130 Sq. ft is at a safe SSD of approximately 34 ft from the primary residence but only 10 ft from the neighboring residence. An SSD of 10 ft from the neighboring residence clearly indicates a severe fire hazard from a 130 sq. ft shed. The hazard mitigation tools that can apply in Case 3 include **R**educe or **R**elocate the shed such that the thermal exposure to the neighboring residences is significantly reduced.

Fig. D-5. Case 3: Community showing shed hazard <u>only</u> for neighboring residence. (1ft = 0.305 m)

101